

# TREATISE ONLINE

Number 93

Part N, Revised, Volume 1, Chapter 3:  
Periostracum and Shell Formation in the Bivalvia

Antonio Checa and Carmen Salas

2017

**KU** PALEONTOLOGICAL  
INSTITUTE

---

The University of Kansas

Lawrence, Kansas, USA  
ISSN 2153-4012  
[paleo.ku.edu/treatiseonline](http://paleo.ku.edu/treatiseonline)



# PART N, REVISED, VOLUME 1, CHAPTER 3: PERIOSTRACUM AND SHELL FORMATION IN THE BIVALVIA

ANTONIO CHECA<sup>1</sup> and CARMEN SALAS<sup>2</sup>

[<sup>1</sup>Universidad de Granada, Granada, Spain, [achecca@ugr.es](mailto:achecca@ugr.es); <sup>2</sup>University of Málaga, Spain, [casanova@uma.es](mailto:casanova@uma.es)]

## INTRODUCTION

Biom mineralization in *Bivalvia* includes the periostracum and the major shell layers (outer, middle, inner), as well as deposits over the exterior of the shell (inductural deposits); adventitious structures such as accessory shell plates, callums, and calcareous tubes; and calcareous boring linings and mineralized rods within ctenidia. This chapter focuses on the formation of the periostracum and the major shell layers. It also summarizes what little is known about inductural, adventitious, and ctenidial mineralization in this group.

The bivalve shell consists of two calcareous valves connected by a partially mineralized ligament, covered by an outer, organic or sparsely mineralized layer called the periostracum. Shell secretion begins before gastrulation is complete, with the formation of the shell field, an area of ectodermal shells in the posterodorsal region of the developing embryo (MOOR, 1983). The shell field secretes a typically D-shaped shell (prodissoconch I), which progressively covers the soft parts (WALLER, 1981; WATABE, 1988). This primordial shell is divided into two valves that articulate through a protoligament. Later, prior to or at the initiation of the prodissoconch II (characterized by marginal growth lines), shell secretion activity is transferred to the mantle. Both the prodissoconch I and II are aragonitic (STENZEL, 1964; CARRIKER & PALMER, 1979), in some

with traces of calcite (MEDAKOVIC & others, 1989), although WEISS and others (2002) identified significant amounts of amorphous calcium carbonate in the larval shells of two bivalves that transformed subsequently into a crystalline phase (see discussion of precursor transient phases below). Together with proteins, chitin has been found to be an important component of the larval shell (CASTILHO & others, 1989; WEISS & SCHÖNITZER, 2006).

Shells are made of superimposed layers, each of which can be monomineralic or bimineralic. When calcite is present, it is typically restricted to the outer shell, to outer and innermost layers, or it may comprise all subperiostracal shell layers except for myostracal prisms and ligament fibers, which are invariably aragonitic. Rarely, an outermost shell layer can have both aragonitic and calcitic components, either as distinct sublayers as in some mytilids (CARTER & others, 1990) or as spatially isolated, calcitic, mineralogical aberrations—e.g., in some veneroids (CARTER, 1980a; CARTER, BARRERA, & TEVESZ, 1998). On these layers, shell-forming crystals organize according to different 3-D (three-dimensional) configurations and arrangements that define the different microstructures. Particular microstructures are characteristic of calcite (e.g., foliated, chalky) or aragonite (e.g., nacre, crossed lamellar), whereas others (e.g., prismatic) have both calcitic and aragonitic counterparts. The shell protects the animal

against certain environmental pressures and predators, and it provides a mechanism for burrowing, swimming, boring, or cementing to a hard substrate. Shell biomineralization in the Bivalvia is largely biologically controlled, rather than merely biologically mediated (LOWENSTAM, 1981; MANN, 1983).

Bivalve and other mollusk shells are organo-mineral biocomposites, in which the mineral part constitutes 95%–99% and the organic fraction makes up 0.1%–5% of the shell weight (HARE & ABELSON, 1965). Despite its small volumetric representation, the organic fraction is extremely complex, with hundreds of proteins, polysaccharides, and lipids, which can differ by molluscan group. The mineral part of the bivalve shell is typically made entirely of calcium carbonate, in particular of calcite and aragonite. Vaterite, a third anhydrous polymorph of calcium carbonate, is only found as part of pearls secreted by some freshwater unionids (MA & LEE, 2006; WEHRMEISTER & others, 2007) or as abnormal secretions in shells of *Corbicula fluminea* (O. F. MÜLLER, 1774 in 1773–1774) and *Laternula elliptica* (KING, 1832 in KING & BRODERIP, 1832) (SPANN, HARPER, & ALDRIDGE, 2010; NEHRKE & others, 2012). Amorphous calcium carbonate has been described within the shells of some bivalves (BARONNET & others, 2008; NUDELMAN & others, 2007), but it is regarded as a transient precursor phase. Some lithophagins deposit crystalline calcium phosphate (e.g., as fluorapatite) in their periostracum (CARTER & others, 1990).

Calcite has a trigonal, aragonite an orthorhombic, and vaterite a hexagonal structure (KAMHI, 1963; BEHRENS & others, 1995; WANG & BECKER, 2009). All can be grown *in vitro*, and the formation of the different polymorphs in abiogenic conditions is influenced by temperature (CARTER, BARRERA, & TEVESZ, 1998; VECHT & IRELAND, 2000), proteins (LAKSHMINARAYANAN & others, 2005), pCO<sub>2</sub>, certain ions (e.g., Mg or the Mg/Ca ratio; STANLEY, 2006; STANLEY & HARDIE, 1998), and organic acids (MELDRUM & HYDE, 2001).

## THE BIOMINERALIZATION COMPARTMENT

Formation of the shell is carried out by the adjacent mantle, which in most species has three marginal folds that YONGE (1957) called outer, middle, and inner, from exterior to interior (Fig. 1.1–1.2). In some Veneridae, four (ANSELL, 1961; NEFF, 1972b) and five mantle folds (PAILLARD & LE PENNEC, 1993; GARCÍA-GASCA & GARCÍA-DOMÍNGUEZ, 1995) have been observed (Fig. 1.3). The effective number of folds is sometimes reduced due to fusion of the mantle edges (YONGE, 1957; Fig. 1.4). Shell formation begins at the base of a groove between the outer and middle mantle folds, called the periostracal groove because it is where the periostracum is secreted. The calcified part of the shell is secreted by the outer epithelium of the outer mantle fold. Thus, periostracal mineralization, when present, is differentiated from biomineralization of the outer shell layer by secretion from the inner or outer surface of the outer mantle fold, respectively. The shell can also be repaired by the mantle. In many cases, the periostracum serves as a framework on which the outer shell layer is initiated. However, in bivalves with strongly reflected shell margins, such as many Veneroidea, new outer shell layer is deposited directly onto previously deposited outer shell layer, independently of the periostracum. In either case, the periostracum seals the biomineralization compartment between mantle and shell, and allows this compartment to attain ion concentrations sufficient for crystallization to occur.

Calcium ions are obtained from the organism's environment through the gills, gut, and epithelium, and transported by the haemolymph (blood) to the calcifying epithelium; the clearest evidence of this process comes from gastropods (WILBUR & SALEUDDIN, 1983). Calcium is stored as granules within or in between cells (NEFF, 1972a), ready to be dissolved and pumped into the site of shell production (i.e., the extrapallial space), when they are required (Fig. 2). The extrapal-

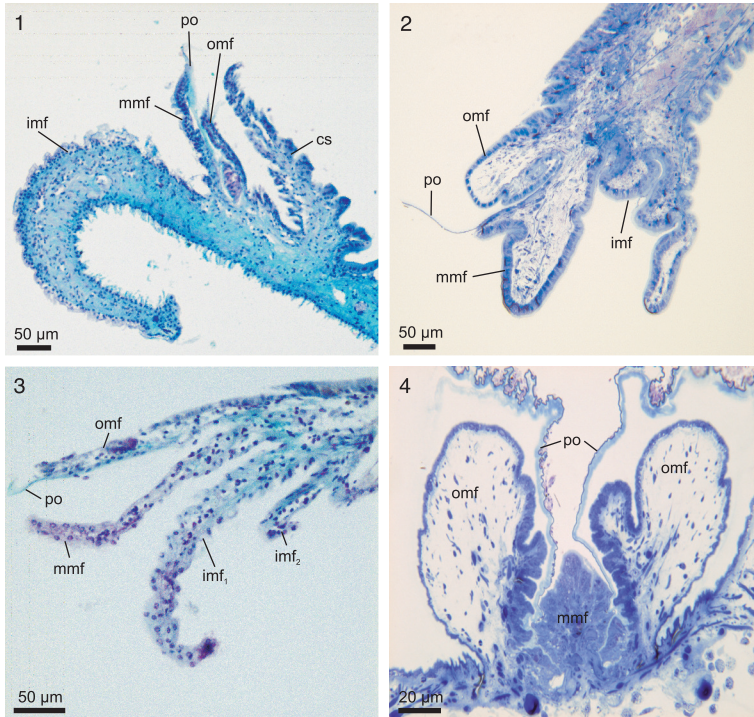


FIG. 1. Optical micrographs of the mantle margins in various species. 1, *Acanthocardia tuberculata* (LINNAEUS, 1758), with three folds; 2, *Neotrigonia margaritacea* (LAMARCK, 1804), with three folds; 3, *Gouldia minima* (MONTAGU, 1803), with four folds; 4, *Laternula valenciennesii* (REEVE, 1863 in 1860–1863), with fused folds; *cs*, corpus spinosus (the structure responsible for the formation of ribs and knobs); *imf*, *imf*<sub>1</sub>, *imf*<sub>2</sub>, inner mantle fold; *mmf*, middle mantle fold; *omf*, outer mantle fold; *po*, periostracum (1, 3, new; 2, 4, adapted from Checa, Salas, & others, 2014).

lial space is the thin, fluid film between the growing shell and the biomineralizing mantle epithelium. It is isolated from the environment by the waterproof periostracum. In this way, supersaturation conditions necessary for the initiation and growth of the shell can be achieved and maintained.

Shell formation occurs within the extrapallial space. Very little is known about the characteristics of the extrapallial space. Its dimensions are virtually unknown. The only relevant data in this respect are the exceptional transmission electron microscopy (TEM) sections of the shell-mantle complex in the nacre and in the calcitic prismatic layers of the pteriod *Pinctada radiata* (LEACH, 1814 in 1814–1817) (BEVELANDER & NAKAHARA, 1969; NAKAHARA & BEVELANDER, 1971; NAKAHARA, 1991) (Fig.

3.1). Adjacent to the nacre, the extrapallial space has a thickness of ~100 nm, whereas adjacent to the calcitic prismatic layer, the thickness is less precisely known, but also submicrometric. It is assumed that these dimensions of the extrapallial space were not altered as a result of sample preparation. The thickness of the extrapallial fluid (EPS) is more precisely known from TEM sections of the mineralized periostracal bosses of the bivalve *Neotrigonia* COSSMAN, 1912 (CHECA, SALAS, & others, 2014). These bosses begin as flat, aragonite platelets inside the initial periostracal dark layer, very deep within the spiral-shaped periostracal groove. At this position, the periostracal groove is a very narrow slit, where the periostracum is bounded by both the inner epithelium of the outer mantle fold and the outer

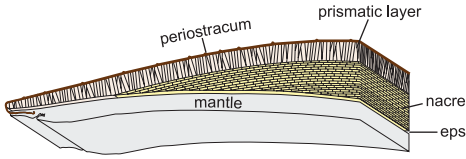


FIG. 2. The bivalve biomineralization system is composed of the mantle, extrapallial space, and shell (archetypical prismatic-nacreous shell is used for the illustration); the outermost organic layer, the periostracum, is secreted by the mantle margin. *eps*, extrapallial space (new).

epithelium of the middle mantle fold (see Fig. 7.1–7.2). The relative positions and dimensions of these structures were not affected during ultramicrotome sectioning for TEM. The observed thickness of the extrapallial space below the forming bosses is ~100 nm (Fig. 3.2–3.3), which agrees with the measurements derived from BEVELANDER and NAKAHARA's (1969) illustrations of nacre. It has yet to be demonstrated that this is also the situation during calcification by the external surface of the outer mantle fold—i.e., outside the periostracal groove. However, the fact that the boundaries between shell layers with different microstructures (and sometimes also with different mineralogies) are so well defined argues for a submicron-thick extrapallial space (CUIF & others, 2012), which imposes strict limits on the lateral diffusion of organic and inorganic components.

The fluid filling in the extrapallial space is the extrapallial fluid. Its composition has also attracted the attention of researchers, and, consequently, a number of studies were conducted on this issue, particularly during the 1960s to the 1980s (for a good summary, see WILBUR & SALEUDDIN, 1983). The extrapallial space contains  $\text{Na}^+$ ,  $\text{K}^+$ ,  $\text{Ca}^{2+}$  and  $\text{Mg}^{2+}$  as major cations and  $\text{HCO}_3^-$ ,  $\text{Cl}^-$ , and  $\text{SO}_4^{2-}$  as anions (CRENSHAW, 1972; MISOGIANES & CHASTEEN, 1979; LORENS & BENDER, 1980; LOPES-LIMA & others, 2012). In freshwater bivalves, the concentrations of these cations and anions are much smaller, although still greatly increased with respect to the external environment. The mean pH values vary between 7.4 and 8.3, with

freshwater species displaying the highest values (WILBUR, 1964; CRENSHAW, 1972; PIETRZAK, BATES, & SCOTT, 1973; WADA & FUJINUKI, 1976; MISOGIANES & CHASTEEN, 1979; RICHARDSON, CRISP, & RUNHAM, 1981). The extrapallial space also contains organic compounds, including amino acids (MISOGIANES & CHASTEEN, 1979), proteins (KOBAYASHI, 1964a, 1964b; PIETRZAK, BATES, & SCOTT, 1973; MISOGIANES & CHASTEEN, 1979), mucopolysaccharides (KOBAYASHI, 1964a; CRENSHAW, 1972; MISOGIANES & CHASTEEN, 1979), and organic acids (WILBUR & SIMKISS, 1968). This organic fraction is presumably incorporated into the shell as intracrystalline and extracrystalline organic fractions, to which essential roles in the nucleation, growth, cessation, and shaping of crystals have been attributed (see next section).

## THE PERIOSTRACUM

The periostracum is an entirely organic or discretely mineralized, thin, pliable, and fibrous layer composed of quinone-tanned proteins, mucopolysaccharides, and lipids. Fifteen amino acids were identified in the periostracum of each of twenty-seven species of marine and freshwater gastropods and bivalves by MEENAKSHI and others (1969). Glycine usually accounted for 40% or more of the amino acids, followed by tyrosin, which represents about 15%. There are also small amounts of inorganic ions, such as iron, lead, sulphur, or cadmium (RAITH & others, 1996; MARKICH, JEFFREE, & BURKE, 2002; KÁDÁR & COSTA, 2006), which are incorporated from the environment. Besides its usual role as a matrix for the deposition of calcium carbonate crystals, the periostracum also protects the shell from dissolution (TEVESZ & CARTER, 1980). Other functions attributed to the periostracum include chemical defense against fouling (BERS & others, 2006), camouflage against predators (SAVAZZI & SASAKI, 2013), and reduction of scour around the shell of shallow, burrowing bivalves in some arcoids with periostracal hairs (BOTTJER & CARTER, 1980).

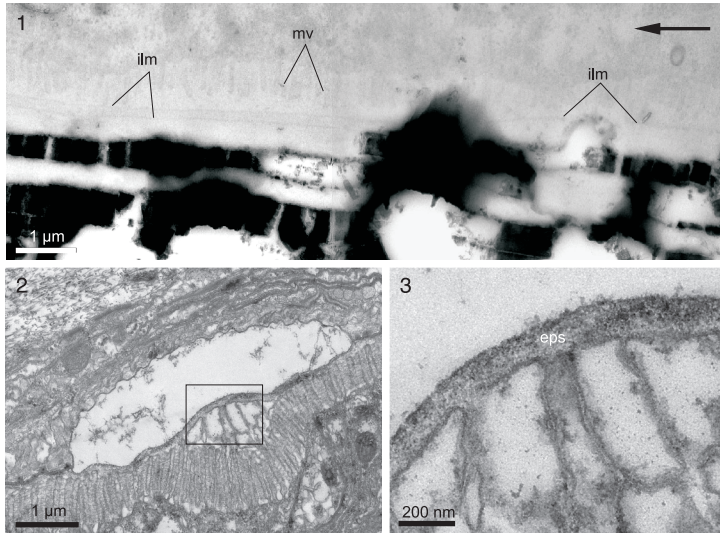


FIG. 3. Dimensions of the extrapallial space. 1, Section through the mantle and nacre of *Pinctada radiata* (LEACH, 1814 in 1814–1817); note the short distance between microvilli and the forming interlamellar membranes; arrow indicates growth direction (new; original material from H. Nakahara). 2–3, *Neotrigonia margaritacea* (LAMARCK, 1804); 2, section through an aragonite plaque forming inside periostracal groove; 3, detail of view 2 (framed), showing the dimension of the extrapallial space; *eps*, extrapallial space; *ilm*, interlamellar membrane; *mv*, microvilli (adapted from Checa, Salas, & others, 2014).

The term periostracum, from the Greek *peri-* (around) and *ostrakon* (shard, shell), was originally defined by GRAY (1825) as *periostraca* for a kind of web generally covering many mollusk shells. The correct, singular form, *periostracum*, was subsequently employed by GRAY (1833). There is some discussion as to whether the term should be restricted to the proteinaceous organic cover of mollusk shells or include any discrete calcified structures (e.g., spicules and spikes) that are simultaneously produced by the inner surface of the outer mantle fold, as defined by CARTER & ALLER (1975).

Secretion of the periostracum begins at the base of the periostracal groove from a row of innermost cells, called basal cells by KAWAGUTI & IKEMOTO (1962), of the outer mantle fold (KAWAKAMI & YASUZUMI, 1964; SALEUDDIN, 1974). Some authors have reported two rows of basal cells in some species—e.g., *Nucula sulcata* BRONN, 1831 (BUBEL, 1973) and *Cardium* (= *Cerastoderma*) *edule* (LINNAEUS, 1758) (RICHARDSON, RUNHAM, & CRISP, 1981)—a feature that we have observed in

several protobranchs (Fig. 4.1–4.2). The basal cells are characterized by the absence of microvilli at their free surface, a much infolded apical plasma membrane (Fig. 4.3), and many electron-dense vesicles (Fig. 4.4). BUBEL (1973) observed filamentous material inside similar vesicles in *Mytilus edulis* LINNAEUS, 1758, and stated that these microfilaments are later extruded to the periostracal groove, where they connect to form the beginning of the periostracum. Some authors have suggested that the middle mantle fold contributes to formation of the periostracum (FIELD, 1922; TSUJII, 1960; SALEUDDIN & PETIT, 1983), whereas others (KESSEL, 1944; YONGE, 1957; BEEDHAM, 1958a; BEVELANDER & NAKAHARA, 1967; WADA, 1968; RICHARDSON, RUNHAM, & CRISP, 1981; CARTER & others, 1990) have indicated that only the inner surface of the outer mantle fold is involved, even in species in which this clearly adheres to the outer surface of the middle mantle, as in the Astartidae (SALEUDDIN, 1974; SALAS & others, 2012) and *Macrocallista* MEEK, 1876 (BEVELANDER & NAKAHARA,

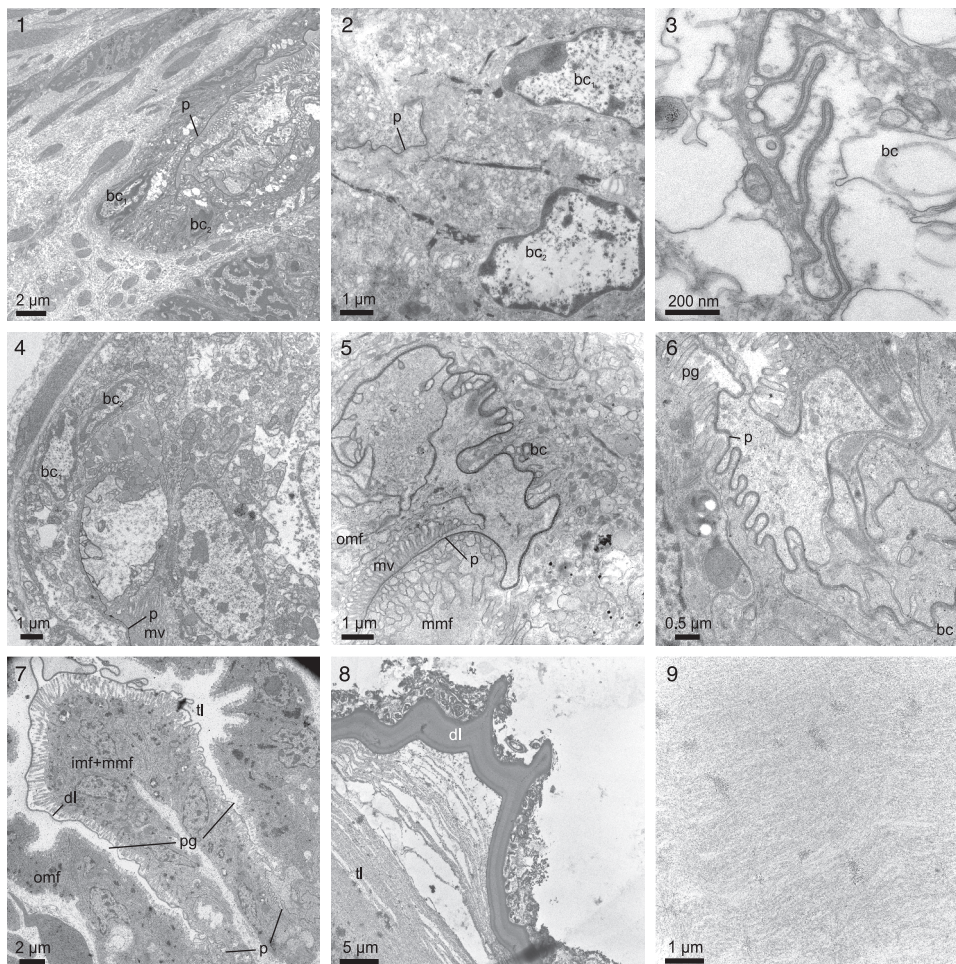


FIG. 4. Basal-cell area and initial periostracal groove in some bivalves. 1, *Nuculana soyoae* HABE, 1958, with two basal cells; 2, *Solemya elarraichensis* OLIVER, RODRIGUES, & CUNHA, 2011, with two basal cells; 3, *Nuculana pella* (LINNAEUS, 1767 in 1766–1768), apical infolded membrane of the basal cell; 4, *N. pella*, with two basal cells having abundant glandular vesicles; 5, *Digitaria digitaria* (LINNAEUS, 1758), with only one infolded basal cell; 6–7, *Laternula valenciennesii* (REEVE, 1863 in 1860–1863); 6, detail of the basal cell; 7, wide view of the periostracal groove and basal-cell area; all *Laternula* species studied have the inner and middle folds of both mantle sides fused; a dark and a translucent layer is visible between the outer and the fused inner and middle folds; 8, *L. rostrata* (G. B. SOWERBY II, 1839 in SOWERBY & SOWERBY, 1832–1841), detail of the layered dark layer and nanolaminated translucent layer; 9, *L. rostrata*, TEM view of the translucent layer, showing nanolamination; *bc*, *bc*<sub>1</sub>, *bc*<sub>2</sub>, basal cell; *dl*, dark layer; *imf* + *mmf*: fused inner and middle mantle folds; *mmf*: middle mantle fold; *mv*, microvilli; *omf*, outer mantle fold; *p*, pellicle; *pg*, periostracal groove; *tl*, translucent layer (1–4, 8, new; 5, adapted from Salas & others, 2012; 6–7, 9, adapted from Checa & Harper, 2010).

1967). More recently, TAYLOR, GLOVER, and WILLIAMS (2005) suggested that the middle mantle fold is responsible for additional thickening and tanning of the periostracum in the crassatellid *Eucrassatella donacina* (LAMARCK, 1818 in 1818–1822). The role of

the middle mantle fold in the formation of the periostracum needs further study.

A layered periostracum is the rule in marine and freshwater bivalves (SALEUDDIN & PETTIT, 1983). A thin (10–50 nm) membrane, termed the pellicle by BEVELANDER and NAKA-

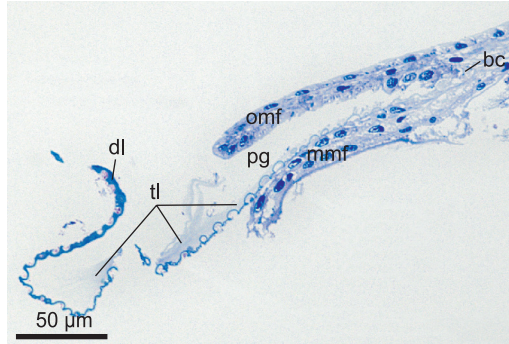


FIG. 5. Optical section through the mantle margin of *Digitaria digitaria* (LINNAEUS, 1758), showing how, with periostracum growth, the dark layer thickens as the translucent layer thins. *bc*, basal cell; *dl*, dark layer; *mmf*, middle mantle fold; *omf*, outer mantle fold; *pg*, periostracal groove; *tl*, translucent layer (adapted from Salas & others, 2012).

HARA (1967), is initially secreted at the intercellular space between the basal cells and the first cells of the outer mantle fold and the middle mantle fold (Fig. 4.5–4.6). Across and along the periostracal groove, secretions by usually columnar epithelial cells of the inner surface of the outer mantle fold are progressively added below the pellicle. These secretions form a dark, electron-dense layer immediately below the pellicle and a more internal, translucent layer (Fig. 4.7). In well-preserved specimens, under high magnification, however, both appear internally layered (Fig. 4.8–4.9). This is due to the fact that, during periostracum growth and thickening along the periostracal groove, the translucent layer polymerizes and transforms into dense layer. Transformation drastically reduces the thickness of the translucent layer (Fig. 5) and is attributed to quinone tanning (i.e., cross-linking by quinones) brought about by secretions of the inner surface of the outer mantle fold. Among the tanning secretions, 3-4-dihydroxyphenyl alanine (DOPA) is probably the main sclerotizing (i.e., hardening) agent (HILLMAN, 1961; SALEUDDIN & PETIT, 1983). WAITE, SALEUDDIN, and ANDERSEN (1979) identified a basic hydrophobic protein, called periostracin, in the periostracum of *Mytilus edulis*, that they considered to be later sclerotized by polymerization with DOPA, this being the precursor of the dense layer. Secretion of the

translucent layer and its transformation into dense layer continues up to the end of the periostracal groove, where the entire translucent layer is usually, though not always, transformed into dense layer (Fig. 5).

In the Protobranchia, the periostracum ranges in thickness from 3  $\mu\text{m}$  in some nuculids to over 100  $\mu\text{m}$  in some solemyids. The periostracum in this group is usually smooth, with no external ornamentation or indication of internal structures (HARPER, 1997). Two basal cells seem to be the general rule in this clade. Among the Nuculidae, two rows of basal cells are involved in the formation of the periostracum, as in *Nucula sulcata* BRONN, 1831 (BUBEL, 1973). According to BUBEL (1973), the pellicle is absent in this species, which could be the primitive condition of the nuculids. However, our electron microscopy observations of *Nucula nitidosa* WINCKWORTH, 1930, point to the presence of a pellicle layer (Fig. 6.1), albeit less defined than in many other bivalves. The dense layer and translucent layer are also present in these species. Two rows of basal cells, with large amounts of electron-dense vesicles, have been observed in the nuculanids *Nuculana pella* (LINNAEUS, 1767 in 1766–1768), *Nuculana soyoae* HABE, 1958 (Fig. 4.1), and *Saccella commutata* (PHILIPPI, 1844), which are involved in the formation of a well-defined pellicle (Fig. 6.2). Therefore, the periostracum in Protobranchia

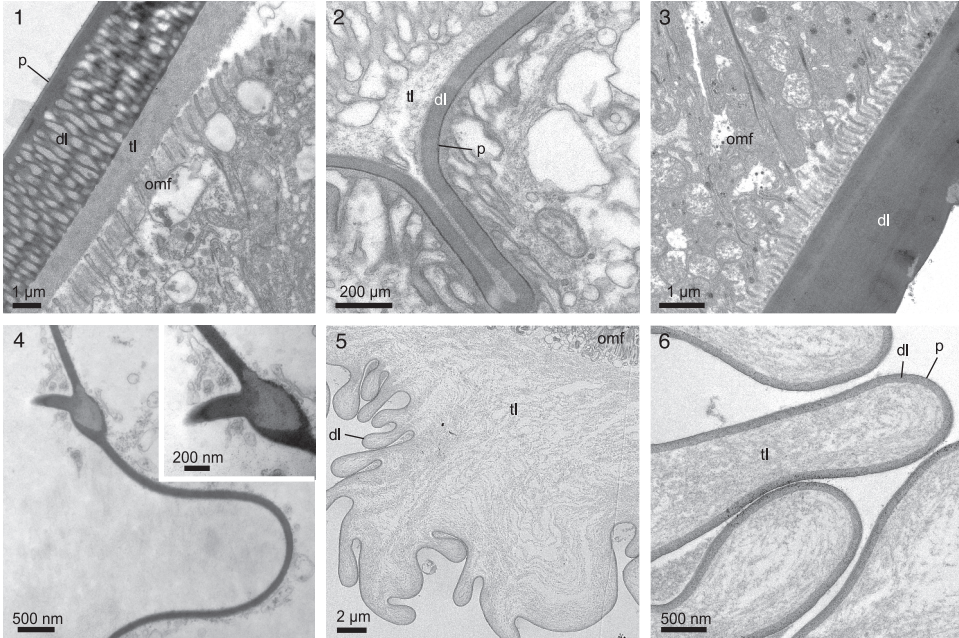


Fig. 6. 1, *Nucula nitidosa* WINCKWORTH, 1930, detail of the periostracum showing the slightly translucent pellicle and vacuolated dark layer. 2, *Nuculana pella* (LINNAEUS, 1767 in 1766–1768), periostracal fold within the periostracal groove, where the dark pellicle is evident. 3, *Solemya elarraichensis* OLIVER, RODRIGUES, & CUNHA, 2011, detail of the laminated dark layer; no translucent layer is seen at this level. 4, *S. elarraichensis*, forming free periostracum showing a prong-like process, the base of which encloses a patch of translucent material. 5, *Glycymeris nummaria* (LINNAEUS, 1758), view of the periostracum and mantle epithelium showing the extreme thickness of the laminated translucent layer. 6, *G. nummaria*, detail of the periostracum showing the presence of a dark pellicle. *dl*, dark layer; *omf*, outer mantle fold; *p*, pellicle; *tl*, translucent layer (new).

has three layers: pellicle, dense layer, and translucent layer.

In the Solemyidae, the shell of *Solemya* LAMARCK, 1818 in 1818–1822, exhibits considerable flexibility, which is further enhanced by the marked extension of the periostracum beyond the calcareous portions of the valves. We detected two rows of basal cells in *S. elarraichensis* OLIVER, RODRIGUES, & CUNHA, 2011, which form a pellicle with a constant width of ~50 nm (Fig. 4.2); later, the periostracum widens by secretions of the inner epithelium of the outer mantle fold, reaching a thickness of more than 2 μm when extruded from the periostracal groove (Fig. 6.3). BEEDHAM and OWEN (1965) identified four layers in the periostracum of *Solemya parkinsoni* E. A. SMITH, 1874. However, we have found only three layers in *S. elarraichensis*. Beneath the pellicle, the dense layer

thickens at the expense of the translucent layer; the latter disappears when the periostracum is projected beyond the periostracal groove. The dense layer has a multi-layered appearance due to periodicity of the tanning process. Transverse sections (light-microscopy and TEM examinations) of the periostracum of *S. elarraichensis* show small folds that are projected from the surface of the periostracum, producing microwrinkles (Fig. 6.4).

In the Pteriomorphia, the periostracum in arcoids is generally thick, persistent, and densely covered by hairs and/or shingles (HARPER, 1997). Hair formation in arcoids has been described by WALLER (1980), who argued that they are formed during maturation of the periostracal sheet and not under direct mantle control. The periostracum of *Glycymeris nummaria* (LINNAEUS, 1758) (Glycymerididae) is very thick and folded;

there is a thin pellicle (less than 50 nm in thickness), subjacent to which is a dark layer that has a constant width (~100 nm) along the periostracal groove (Fig. 6.5). In contrast to *Solemya*, the translucent layer is extremely thick, reaching up to 25  $\mu\text{m}$  (Fig. 6.5–6.6). *Barbatia cancellaria* (LAMARCK, 1819 in 1818–1822) has a periostracum with radial sculpture that seems to correspond to radial undulations of the epithelial surfaces within the periostracal groove (WALLER, 1980). Numerous commarginal pleats occur at the edge of the shell as the outer mantle fold extends and retracts, thus dragging the periostracal sheet. These pleats give the periostracum a thick, multilayered structure at the edge of the shell.

The periostracum of non-arcoid Pteriomorphia is extremely thin (<1  $\mu\text{m}$ ), except in the Anomiidae—e.g., *Anomia ephippium* LINNAEUS, 1758, and *Monia squama* (GMELIN, 1791 in 1791–1793) have periostraca ~10  $\mu\text{m}$  thick (HARPER, 1997)—and in many Mytiloidea. In the pteriid *Pinctada imbricata fucata* (GOULD, 1850), a synonym of *P. martensii* (DUNKER, 1880), the periostracum originates as a folded or branch-like structure at the bottom of the periostracal groove (KAWAKAMI & YASUZUMI, 1964). The latter authors indicated the presence of a dense layer and another made of homogeneous material of intermediate density. The latter layer is covered by the inner surface of the outer mantle fold. WADA (1968) restudied the formation of the periostracum in juveniles of *P. imbricata fucata*. He described a thick and pear-shaped basal cell—devoid of microvilli and with an electron-dense, folded, and concave free surface—that exhibits the presence of secretory substances. This basal cell secretes a dark pellicle, below which the other layers of the periostracum are secreted along the periostracal groove, to a total thickness of 60–100  $\mu\text{m}$ .

The periostracum of the Mytilida is generally thick and persistent, ranging in thickness from 5  $\mu\text{m}$  in *Cibotricula lunata* (HEDLEY, 1902) to 428  $\mu\text{m}$  in *Musculus laevigatus* (GRAY, 1824) (HARPER, 1997). *Mytilus edulis* has a three-layered periostracum. It originates from

a row of basal cells (BUBEL, 1973) that extrudes a pellicle into the periostracal groove. The middle dark layer is vacuolated and up to 80  $\mu\text{m}$  thick (BEEDHAM, 1958b; DUNACHIE, 1963). This layer is neither continuous nor homogeneous in aspect over the entire periostracum. In addition to *Mytilus*, vacuolated periostracum has been reported in *Perumytilus purpuratus* (LAMARCK, 1819) (CARTER, 1990; CARTER, LUTZ, & TEVESZ, 1990). CARTER (1990, p. 282) suggested that these vacuoles represent modifications of ancestral periostracal mineralization, and their replacement by fluid might help retain flexibility in the marginal periostracum for hermetic closure of the valves during desiccating, subaerial exposure. Different types of projections, called hairs, cover the external surface of the periostracum in a number of mytilids—e.g., *Modiolus modiolus* (LINNAEUS, 1758), *Modiolus barbatus* (LINNAEUS, 1758) (OCKELMANN, 1983). Different functions have been proposed for these hairs, such as stabilization, fouling, and epibiont avoidance. BOTTJER and CARTER (1980, p. 202) indicated that these “adventitious hairs” in mytilids are “probably not periostracal in origin.” OCKELMANN (1983) proposed that they represent secretions of the pedal byssal gland.

In the Palaeoheterodonta, TEM and optical microscopy of the trigonioid *Neotrigonia* COSSMANN, 1912 (Trigoniidae) reveal a spiral-shaped periostracal groove (Fig. 7.1; CHECA, SALAS, & others, 2014). The periostracum in *N. margaritacea* (LAMARCK, 1804) is initiated by a row of basal cells as a thin, dark pellicle. A dense layer is progressively added below the pellicle by the inner surface of the outer mantle fold. One whorl after the initiation along the spirally coiled periostracal groove, a clearly laminated translucent layer begins to be evident (Fig. 7.1–7.2). Transformation of the translucent layer into dense layer continues as discrete mineralization is added to the periostracum. Aragonitic crystals begin to form very early within the first half-turn of the periostracal groove, immediately below the initial dense layer, before the start of the translucent layer, directly in contact with the microvilli of the outer mantle fold

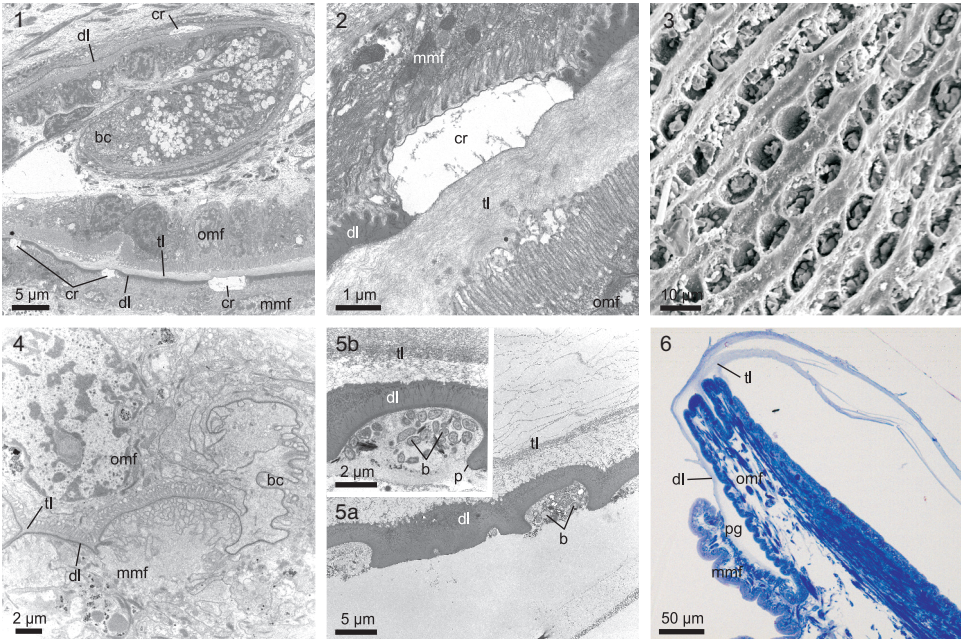


FIG. 7. 1, *Neotrigonia margaritacea* (LAMARCK, 1804), general view of the spiral periostracal groove; the translucent layer begins to be secreted one whorl after the initiation of the periostracum, and forming crystals can be seen as early as half a whorl after. 2, *N. margaritacea*, detail of a forming crystal; its growth surface is at the boundary between the dark and translucent layers. 3, *Astarte montagui* (DILLWYN, 1817); pitted external surface of the periostracum. 4, *Digitaria digitaria* (LINNAEUS, 1758), initial part of the periostracum; the pits are formed by the templating action of the cells of the middle mantle fold. 5a–b, *D. digitaria*; periostracal pits are filled with bacteria; 5b shows detailed view of one such pit. 6, *Cardita calyculata* (LINNAEUS, 1758), optical semi-thin section of the mantle edge, showing the periostracum layers. b, bacterium; bc, basal cell; cr, forming crystal; dl, dark layer; mmf, middle mantle fold; omf, outer mantle fold; p, pellicle; pg, periostracal groove; tl, translucent layer (1, adapted from Checa, Salas, & others, 2014; 2–3, 6, new; 4–5, adapted from Salas & others, 2012).

surface (see discussion of periostracal mineralization below).

The periostracum in the palaeoheterodont family Unionidae consists of two (CHECA, 2000b) or three (PETIT, DAVIS, & JONES, 1978, 1979, 1980; PETIT & others, 1980; PETIT, 1981) layers, of which the thin outer one is secreted within the periostracal groove, whereas the thicker, inner layer is secreted by the epithelium of the outer mantle fold (CHECA, 2000b). In *Unio elongatulus* PFEIFFER, 1825, and *Potomida littoralis* (CUVIER, 1798), the periostracum has an approximate thickness of 2–3 µm (CHECA, 2000b) and 25–50 µm in *Amblema* (SALEUDDIN & PETIT, 1983) upon extrusion from the periostracal groove. From this point, a new, non-tanned layer, composed of micron-thick sublayers, is secreted below the outer periostracum

(CHECA, 2000b). This latter layer corresponds with the middle periostracum of PETIT, DAVIS, & JONES (1978, 1979, 1980) and can reach 30–40 µm in thickness in *Unio elongatulus*.

The unionid periostracum contains discrete mineralization in the form of aragonitic radial-fibrous aggregates within its inner part (see discussion of periostracal mineralization, below). Below the periostracum, the outer surface of the outer mantle fold forms the underlying aragonitic composite prisms of the outer shell layer (LIU & LI, 2013). The existence of folds formed by the outer periostracum and reflected in the surface of the outer shell layer implies that calcification of the outer shell layer is a periodic activity, interrupted by refractory episodes in which only the periostracum is secreted, thus forming folds at the exit of the periostracal

groove and leaving major growth lines. Layers of inner periostracum are added occasionally to the outer part of the sub-periostracal shell during prolonged periods of inactivity in which the mantle is retracted (CHECA, 2000b).

Among the Archiheterodonta, the Astartidae are characterized by an externally pitted periostracum (Fig. 7.3), first described by OCKELMANN (1958), who used their morphology to discriminate species. The periostracum of several species of *Astarte* J. SOWERBY, 1816 (in SOWERBY & SOWERBY, 1812–1846) has been studied by SALEUDDIN (1965, 1974), although he did not address the formation of the pits. SALAS and others (2012) observed that the periostracal pits of the astartid *Digitaria digitaria* are templated by cells of the outer surface of the middle mantle fold at the bottom of the periostracal groove (Fig. 7.4). The pits are furnished with bacteria (Fig. 7.5). The periostraca of *Astarte castanea* (SAY, 1822) and *Astarte elliptica* (BROWN, 1827) appear to consist of two layers under light microscopy (SALEUDDIN, 1974), but three layers are visible under electron microscopy. Three layers have also been observed in *D. digitaria* (SALAS & others, 2012). In the carditid *Cardita calyculata* (LINNAEUS, 1758), the periostracum is not pitted as in the Astartidae, but it is similarly secreted by a single row of basal cells. The periostracum presents three layers: the pellicle, a thin dark layer, and a thick translucent layer. The latter continues onto and is conspicuous on the outer surface of the outer mantle fold (Fig. 7.6).

The periostracum of the Euheterodonta has received comparatively little study, despite the diversity of the group. In the Cardioidea, it is thin ( $\sim 1\text{--}2\ \mu\text{m}$ ) (HARPER, 1997). In *Cerastoderma edule* (LINNAEUS, 1758), the innermost part of the inner surface of the outer mantle fold is curved. Two rows of basal cells are present at the bottom of the periostracal groove (RICHARDSON, RUNHAM, & CRISP, 1981). A thin pellicle layer lies adjacent to the microvillous border of the middle mantle fold. Subjacent to the pellicle, two other layers are present:

an electron-dense dark layer and a fibrous translucent layer. In their study of the periostracum of the tellinid *Nitidotellina hokkaidoensis* (HABE, 1961), KAWAGUTI and IKEMOTO (1962) indicated the presence of a row of basal cells and two layers, a solid (dark) and a diffuse (translucent) layer; however, a pellicle can be identified in the figures (KAWAGUTI & IKEMOTO, 1962, fig. 3–4). In the tellinid *Macoma balthica* (LINNAEUS, 1758), two layers of different electron density have been recognized within the periostracum (BUBEL, 1973). Members of the Veneridae have four mantle folds as a general rule. The formation and structure of the periostracum in the venerids *Megapitaria* (formerly *Macrocallista*) *maculata* (LINNAEUS, 1758) (BEVELANDER & NAKAHARA, 1967), *Mercenaria mercenaria* (LINNAEUS, 1758) (NEFF, 1972b), and *Ruditapes philippinarum* (ADAMS & REEVE, 1850 in 1848–1850) (PAILLARD & LE PENNEC, 1993) is similar. It begins in a row of basal cells with large vacuoles, many cisternae, and an infolded free surface. BEVELANDER and NAKAHARA (1967) designated the term pellicle for the first time for the membrane secreted by the basal cells of *M. maculata*, beneath which a dark layer and a translucent layer are present. According to PAILLARD and LE PENNEC (1993), the periostracum of *R. philippinarum* is composed of three layers—two electron-dense granular layers separated by an electron-lucent homogeneous layer, which as a whole correspond to the dark layer of other bivalves. The electron-density differences found in this layer could be related to episodic tanning of the translucent layer. An additional fibrous (translucent) layer is present between the dark layer and the outer mantle fold.

The Anomalodesmata have a moderate to thick, persistent periostracum ranging from 2 to 80  $\mu\text{m}$  in thickness (HARPER, 1997). The formation of the periostracum has been studied only for *Laternula valenciennesii* (REEVE, 1863 in 1860–1863) (CHECA & HARPER, 2010). The periostracum and middle mantle fold show tissue-grade fusion, and the periostracal groove is located on both sides of the fused margins (Fig. 4.7).

The basal cells are located very close to the beginning of the two periostracal grooves and produce pellicles with an approximate thickness of 30 nm (Fig. 4.6). Each pellicle is later thickened by secretions from the inner surface of the outer mantle fold at the same time as it slides in a distal direction over the epithelium of the fused middle and inner mantle folds, while it adheres to the outer surface of the middle mantle fold (Fig. 4.7). As usual, the dark layer thickens by tanning of the translucent layer. The internal nanolamination of the translucent layer and the layering of the dark layer (produced by episodic tanning) have also been recognized in other species of *Laternula*—*L. recta* (REEVE, 1863 in 1860–1863) (Fig. 4.8–4.9). Members of this clade display a wide variety of noteworthy mineralized periostracal structures, such as spikes and plaques (CARTER & ALLER, 1975; CHECA & HARPER, 2014). They typically use the translucent layer as a calcifying medium to produce spikes and plaques, and in some cases they also use the translucent layer to initiate mineralization of the outer shell layer (see section on periostracal mineralization).

In summary, the basic structure of the periostracum of bivalves consists of a thin pellicle, produced by one or two rows of basal cells, that is underlain by a dark layer, which in turn is formed by the sclerotization of a transitory translucent layer. Differences, however, have been reported in the presence of the pellicle, the thickness of the layers, and the rate at which the translucent layer transforms into dark layer. A more in-depth study of the formation of the periostracum in a larger number of species of bivalves is needed in order to assess the role of the middle mantle fold in its formation.

#### PERIOSTRACAL MINERALIZATION

Mineralized periostracal structures are taxonomically widespread among non-protobranch bivalves. In all well-known examples, this mineralization begins within the translucent layer and is comparable to crystallization within a gel matrix. Due to

slow diffusion rates, intra-gel crystallization is a classic technique for the formation of large, euhedral crystals. Mineralized periostracal structures are cemented to or imbedded within the outer part of the outer shell layer in many trigonioids, unionoids, Archiheterodonta, Anomalodesmata, Hiattelloidea, Modiomorphoidea, Kalenteroidea, Gastrochaenoidea, and Veneroidea, as well as in a few Actinodontida, Arcticoidea, Cardioidea, and Lucinida—in the latter, even excluding the pseudoperiostracal mineralization in *Lucina pensylvanica* (LINNAEUS, 1758), which forms beneath the true periostracum, in the outer shell layer (see TAYLOR & others, 2004). Periostracal mineralization that is not attached to the outer shell layer and, therefore, unlikely to be preserved in fossils, is present in some Mytiloidea, Astartidae, and Veneridae (J. CARTER, personal communication, 2015; see also ALLER, 1974; CARTER & ALLER, 1975; CARTER, 1978, 1990; PREZANT, 1979; CALLIL & MANSUR, 2005; CHECA & HARPER, 2010; ZIERITZ & others, 2011). Considering this wide taxonomic distribution, the propensity for periostracal mineralization might be a synapomorphy for the Autobranchia or at least the Heteroconchia, although this has probably been realized convergently in various subgroups (see discussion in CHECA & HARPER, 2014). It is of particular interest that mineralized periostracal spikes are always associated with the inner translucent layer of the periostracum, which appears susceptible to calcification. Further research is required to establish whether the translucent layer is homologous among heterodont taxa.

Periostracal mineralization in the Pteriomorphia is apparently restricted to the Mytilida. A thin, mineralized, amorphous crust is deposited in antimarginal rays on the inner surface of the periostracum in the arcoid *Barbatia cancellaria*, but these are clearly products of the outer mantle fold and are, therefore, initiation sites of the outer shell layer (WALLER, 1980, p. 42, fig. 44). Aragonitic intraperiostracal granules and/or spikes are present in the periostracum

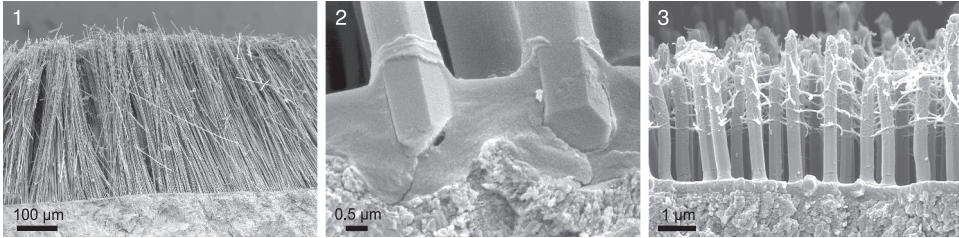


FIG. 8. Periostracal needles and pins. 1, Needles on the outer periostracal surface of *Lioconcha castrensis* (LINNAEUS, 1758). 2, Detail of the insertion of the needles within the periostracum of *Tivela lamyi* DAUTZENBERG, 1929. 3, Pins developed on the outer surface of the periostracum of *Pitar trevori* LAMPRELL & WHITEHEAD, 1990 (adapted from Glover & Taylor, 2010).

of several mytilid genera (CARTER, 1990, p. 281). Some species of *Lithophaga* RÖDING, 1798, have a densely mineralized periostracal sublayer with irregular or euhedral crystals of fluorapatite (WALLER, 1983; CARTER, 1990, fig. 53a, 54). As in the case of aragonitic periostracal needles in Veneridae, the mineralized sublayer in *Lithophaga* is connected with the inner surface of the periostracum by minute tubules (CARTER, 1990, p. 281; CARTER & others, 2012).

In the Palaeoheterodonta, the trigonioid *Neotrigonia* is unique in that the aragonitic periostracal plaques initiate at a very early stage of periostracum formation, within the particularly deep periostracal groove, immediately below the initial periostracal dark layer (CHECA, SALAS, & others, 2014; Fig. 7.1–7.2). During the crossing of the periostracum from the periostracal groove to the shell margin, the translucent layer becomes sclerotized into dark layer (similar to the process discussed above for anomalodesmatans). In coordination with the resulting thickening of the dark layer, the bosses first thicken and later extend towards the interior of the shell as incipient composite prisms with rounded cross sections. When they reach the mantle edge, periostracal mineralization is replaced by outer shell layer mineralization. In the inter-rib and internode spaces, this produces a much wider, polygonal composite prism directly beneath each boss, or a much different, granular microstructure in the ribs and nodes. In the outer part of the composite

prismatic portion of the outer shell layer, the composite prisms are separated by dark, pseudoperiostracal walls secreted by the outer surface of the outer mantle fold. The number and position of composite prisms in the outer shell layer is predetermined at the free periostracum stage. As noted above, periostracal mineralization also occurs in the Unionida.

In the Euheterodonta, aragonitic periostracal needles and pins have been described for several venerid genera (GLOVER & TAYLOR, 2010; Fig. 8). These structures are progressively extruded outward from the interior of the organic periostracum. Their proximal ends are intraperiostracal and commonly connect with the inner surface of the periostracum by narrow channels. Mineralized periostracal spikes are rare in the Veneroidea, but they occur in *Gafrarium divaricatum* (GMELIN, 1791 in 1791–1793) (GLOVER & TAYLOR, 2010, fig. 10E–G, as short pins), and they are not associated with periostracal channels.

In the Anomalodesmata and in many Hiatalloidea and Gastrochaenoidea, discrete periostracal mineralization, usually in the form of granules or spikes, rarely as plaques (Fig. 9.1–9.3), begins to be produced as the periostracum moves along the inner surface of the outer mantle fold, at the boundary between the dark layer and the translucent layer (Fig. 9.4–9.7). These aragonitic structures typically consist of prisms with their *c*-axis mainly oriented perpendicular to the periostracum surface. The elements may be

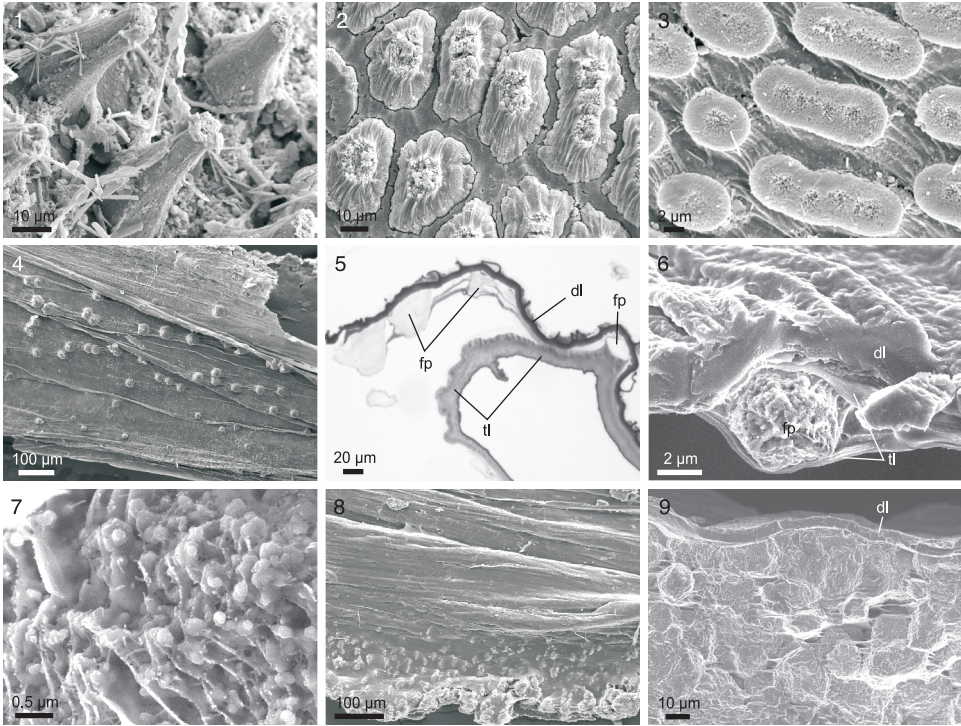


FIG. 9. Periostacal mineralization in Anomalodesmata; all SEM images, except for 5 (optical micrograph). 1, *Lyonsiella abyssicola* (G. O. SARS, 1872), spikes of the posterior area; 2, *Thraciopsis angustata* (ANGAS, 1868), wide spikes in the posterior area; 3, *T. angustata*, plaques in the anterior area; 4, *Laternula rostrata* (G. B. SOWERBY II, 1839 in SOWERBY & SOWERBY, 1832–1841), progressive formation of spikes within the free periostracum; 5, *L. rostrata*, thin section through decalcified free periostracum, showing growing prisms (note that the part of translucent layer that has not yet mineralized has split from the rest of periostracum); 6, *L. rostrata*, growing spike within the translucent layer; 7, *L. rostrata*, showing nanomembranes of the translucent layer incorporated within a forming spike (7) and progressive mineralization of the translucent layer towards lower part of the image, as seen from its internal surface (8) (new). 9, *L. rostrata*, appearance of the prismatic granular layer, with horizontal laminae; *dl*, dark layer; *fp*, forming prism; *tl*, translucent layer (1–2, 4–6, 9, adapted from Checa & Harper, 2010; 3, 7–8, new).

irregularly or regularly arranged. During further growth, the dark layer thickens at the expense of the translucent layer, at the same time that the structures progressively protrude and push the dark layer outward while its base continues to grow inwards towards the inner surface of the translucent layer. In many Anomalodesmata, when the periostracum reaches the shell margin, the remainder of the translucent layer is mineralized by the outer surface of the outer mantle fold (Fig. 9.8), thereby initiating the outer shell layer, which is commonly granular in Anomalodesmata (HARPER, CHECA, & RODRÍGUEZ-NAVARRO, 2009; CHECA & HARPER, 2010) (Fig. 9.9) or pris-

matic in *Spengleria* TRYON, 1861, and some Anomalodesmata (CARTER, 1978; CHECA & HARPER, 2010, 2014). In this way, the outer shell layers of these bivalves are formed and the previously formed spikes become imbedded within it. The complete process is summarized in Figure 10. This pattern of shell formation is also found in the anterior and ventral areas of *Spengleria*, but in the posterior area the spikes are separated from the rest of the calcified shell by a dark layer and by a substantial void (CARTER, 1978; CHECA & HARPER, 2014).

Mineralized periostacal structures might be considered cases of remote biomineralization when there is a translucent layer

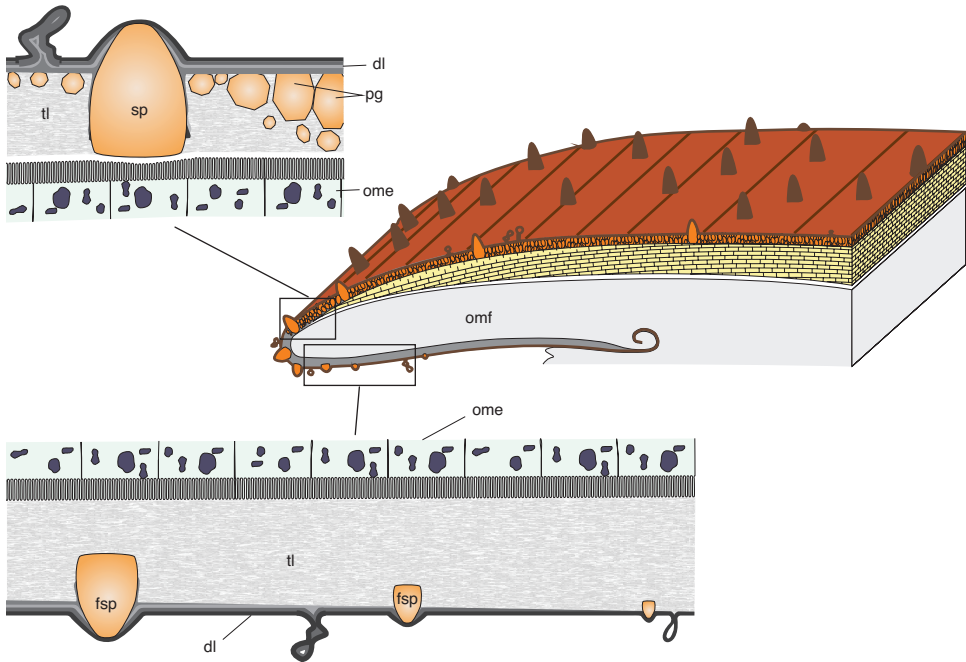


FIG. 10. Model for the formation of spikes and the outer granular prismatic shell layer in *Laternula* RÖDING, 1798. Spikes nucleate within the translucent periostracal layer, immediately below the dark layer. With growth, spikes protrude and push the dark layer outwards, at the same time as they extend towards the base of the periostracum. At the shell margin, an extensive mineralization of the translucent layer occurs, with the formation of many prismatic granules. In this way, the spikes become incorporated within the outer prismatic granular layer. *dl*, dark layer; *fsp*, forming spike; *ome*, outer mantle epithelium; *omf*, outer mantle fold; *pg*, prismatic granule; *sp*, spike; *tl*, translucent layer (adapted from Checa & Harper, 2010, fig. 12A).

between the mantle and the mineralized periostracal structure, which is usually the case. However, the term remote biomineralization was originally applied by CHINZEI and SEILACHER (1993) to situations in which the biomineralization does not occur within an organic layer secreted for this purpose. Such examples of remote biomineralization are rare in the Bivalvia. They include calcite crystals within the attached valves of several ostreoids after closure of intra-shell chambers; aragonitic pillar-like structures reported by GRÉGOIRE (1974) in analogous cavities of the unionoid *Etheria* LAMARCK, 1807, remote deposits in the valleys of the divaricate ribs of some tellinoideans, formed between the periostracum and the shell (CHECA, 2000a); external crusts on the shells of the venerids *Granicornium* HEDLEY, 1906, and *Samarangia* DALL, 1902, composed

of cemented sediment grains (TAYLOR, GLOVER, & BRAITHWAITE, 1999; BRAITHWAITE, TAYLOR, & GLOVER, 2000), formed within a mucus extruded by the outwardly reflected mantle margin; and acicular aragonite deposits below the posterior periostracum in *Spengleria* (CARTER, 1978; CHECA & HARPER, 2014).

## THE MAJOR SHELL LAYERS

### THE ORGANIC FRACTION

The organic fraction of the major shell layers is mainly proteins, acidic polysaccharides, and chitin (presumably the  $\beta$  polymorph) (LOWENSTAM & WEINER, 1989; LEVI-KALISMAN & others, 2001; PEREIRA-MOURIÉS & others, 2002). Some of the organic fraction assembles into a 3-D organic-matrix framework, which

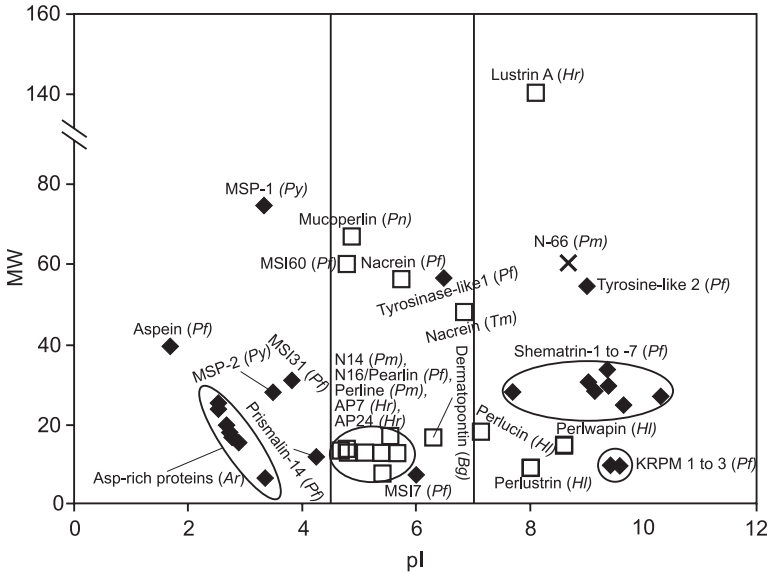


Fig. 11. Classification of proteins extracted from molluscan shells, according to their molecular weight ( $MW$ ) and isoelectric point ( $pI$ ); proteins associated with aragonite indicated with *square boxes* and those associated with calcite with *solid black diamonds*. *Ar*, *Atrina rigida* (LIGHTFOOT, 1786); *Bg*, *Biomphalaria glabrata* (SAY, 1818); *Hl*, *Haliotis laevigata* DONOVAN, 1808; *Hr*, *Haliotis rufescens* SWAINSON, 1822; *Pf*, *Pinctada fucata* (GOULD, 1850); *Pm*, *Pinctada maxima* (JAMESON, 1901); *Pn*, *Pinna nobilis* LINNAEUS, 1758; *Py*, *Patinopecten (=Mizuhopecten) yessoensis* (JAY, 1857); *Tm*, *Turbo marmoratus* LINNAEUS, 1758 (adapted from Marin & others, 2008, fig. 5).

provides the scaffold for mineral nucleation and growth (WEINER, TRAUB, & LOWENSTAM, 1983). Additionally, some macromolecules function as soluble additives and are absorbed by crystals during growth, forming an intracrystalline organic phase (BERMAN & others, 1993; WEINER & ADDADI, 1997) that is presumably involved in polymorph selection and in crystal nucleation, growth, and morphology (ADDADI & WEINER, 1985; ADDADI & others, 1987; FALINI & others, 1996). Isolation of macromolecules and regrowth of calcium carbonate in their presence has demonstrated selectivity for specific crystal planes (e.g., ADDADI & others, 1987). In 1996, two different research groups (BELCHER & others, 1996; FALINI & others, 1996) demonstrated that polymorph secretion is controlled by macromolecules associated with either calcitic or aragonitic shell layers. In particular, the first team, employing a variety of taxa

including four bivalve species, precipitated calcium carbonate in the presence of soluble proteins extracted from either calcitic or aragonitic shells preabsorbed on a substrate of squid chitin and silkworm fibroin. They consistently found that the precipitated polymorph coincided with that of the original shell. BELCHER and others (1996) extracted soluble polyanionic proteins from the nacre and prismatic calcite of the gastropod *Haliotis* LINNAEUS, 1758. Their results were similar to those of FALINI and others (1996), although their work also had implications regarding influence on crystal nucleation and orientation. They concluded that these aspects of shell formation do not require pre-organized organic arrays. Other studies also included the action of the ethylenediaminetetraacetic acid (EDTA)-insoluble fractions, with the conclusion that they can influence nucleation density and crystal size (FENG & others, 2000).

The organic fraction of the shell has traditionally been separated into soluble and insoluble, by using EDTA, acetic acid, or hydrochloric acid aqueous solutions to distinguish the acidic proteins from the hydrophobic glycine-alanine-rich molecules (HARE, 1963; HARE & ABELSON, 1965; WATABE, 1984; MANN, 1988; KONO, HAYASHI, & SAMATA, 2000). PEREIRA-MOURIÉS and others (2002) challenged this definition when they decalcified nacre with ultra-pure water and showed that there were significant differences in amino acid composition of the nacre EDTA-soluble fractions. According to them, the property-related difference between both fractions is not so straightforward.

Due to the important functions attributed to molluscan shell proteins and despite the fact that they are present in small amounts (0.03–0.5% by weight in the soluble fraction), efforts have been made to isolate and characterize them (for an account on the repertoires of proteins and their functions, see reviews by CUSACK & FREER, 2008; MARIN & others, 2008). Most proteins have been extracted from bivalves, mainly from the calcite of members of *Pinctada* RÖDING, 1798, and *Atrina* GRAY, 1842, and from the nacre of *Pinctada*. Regarding gastropods, most proteins that have been extracted and identified come from the nacre of *Haliotis*.

Molluscan shell proteins have been classified by MARIN and others (2008) according to isoelectric point (pI) and molecular weight (MW) (Fig. 11). Three groups can be distinguished according to pI: highly acidic (pI < 4.5), moderately acidic (pI = 4.5–7) and basic (pI > 7) proteins. Highly acidic proteins are exclusive to calcitic shells and, due to the preponderance of negatively charged Asp-rich residues, are Ca-binding proteins. They are particularly suited for control over crystal growth and interaction with crystal faces. The second group forms a disparate collection, with most being associated to aragonite and some to nacre. Some nacreins have a diversity of functions, from Ca-binding to carbonic anhydrase activity.

Pearlins inhibit calcium carbonate precipitation and induce the formation of platy aragonite platelets. Others (e.g., caspartin) induce changes in crystal shape. Basic proteins have been extracted both from calcitic and aragonitic layers. Some of them have been extracted from the nacre of abalone and display interesting *in vitro* activities, like the nucleation of calcium carbonate (perlucin) or its inhibition (perlwappin); perlinhibin inhibits the growth of calcite and induces the formation of flat platelets of aragonite. However, the molecular aspects of the shell-building process are still far from fully understood because soluble and insoluble organic molecules synergistically control the nucleation, growth, polymorphism, and orientation of biomineral deposition. For this reason, it is difficult to mimic the biomineralization process and to distinguish the precise roles played by these soluble and insoluble organic phases.

In the past decade, attention has been paid to the relationship between bivalve genomics and shell biomineralization. The interest is to identify transcripts (i.e., RNA molecules transcribed from DNA) encoding secreted shell proteins, proteins specific to the pallial space, and proteins implicated in calcium regulation in mantle cells, as well as transcription factors responsible for the regulation of the process. Only a few such studies have been performed on bivalves and gastropods (DUPLAT & others, 2006; JACKSON & others, 2006, 2010; JOUBERT & others, 2010), which have yielded general conclusions about the high complexity of the calcifying mantle transcriptome (i.e., the collection of all the transcripts present in a given cell, and which reflects the genes that are being actively expressed at any given time) and the substantial differences between major molluscan groups. Despite the small amount of genomic data presently available, this line of research is particularly promising since it opens the door for future genomic manipulation with the aim of obtaining biomaterials with desired mechanical and biomedical properties.

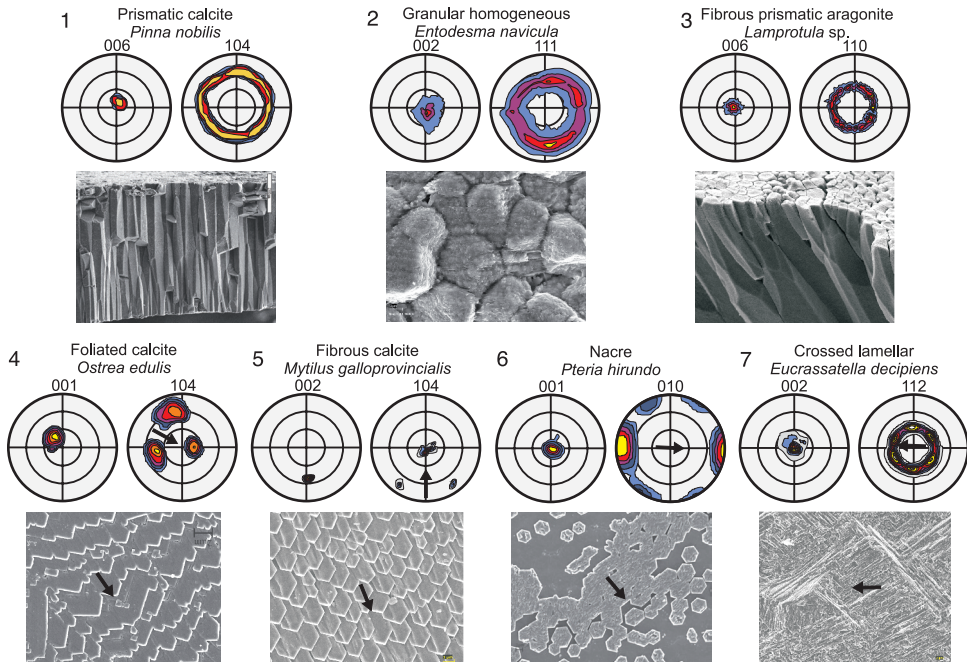


FIG. 12. Bivalve microstructures displaying fiber (1–3) and sheet textures (4–7). In each, the left (001, 002, or 006) pole figures represent the orientation of the  $c$ -axes, whereas the right (104 of calcite, and 111, 010, and 112 of aragonite) pole figures represent the orientation of the axes perpendicular to the  $c$ -axis ( $a$ -axes of calcite or  $a$ - and  $b$ -axes of aragonite). In all, there is a single, discrete maximum for the left pole figures, implying that the  $c$ -axes of crystals are co-oriented. Fiber textures (1–3) are characterized by a ringlike distribution in the right pole figures, implying that the axes perpendicular to the  $c$ -axis are disoriented. Sheet textures (4–7), on the other hand, have discrete maxima for the same pole figures, implying that those axes are co-oriented. An apparent ringlike distribution (in view 7) for the 112 pole figure of *Eucrassatella decipiens* (REEVE, 1842) is, in fact, a six-rayed distribution of the  $a$ - and  $b$ -axes of aragonite, typical of {110} twinning. This is clearly also the case of the 010 pole figure of *Pteria hirundo* (LINNAEUS, 1758), with a predominance of the orientations parallel to the local growth direction (arrow).  
1–3, 5, 7, XRD data; 4, 6, EBSD data; arrows indicate local growth directions of the shells (new).

### SHELL MICROSTRUCTURES AS CRYSTAL AGGREGATES

Shell microstructures are aggregates of crystals that have defined, recurrent morphologies and mutual relationships. Probably due to mineral-organic constraints, not every morphology (or arrangement) is possible, and there is a limited number of microstructures (CARTER & others, 2012). At the same time, homeomorphic microstructures (e.g., nacre, crossed-lamellar, foliated) have developed independently in and within the different classes. The most extreme example of convergence is crossed lamellar microstructure, which developed independently in all extant molluscan classes with the exception of the Cephalopoda and Aplousobranchia. Crossed lamellar microstruc-

ture probably also developed independently in certain extinct groups (i.e., the Bellerophonida) in the extinct molluscan class Rostroconchia and in the Hyolitha.

One of the most distinctive features of microstructures is their high degree of crystallographic ordering. The best way to show this is through the construction of pole figures derived from diffraction methods: X-ray diffraction (XRD) and electron backscatter diffraction (EBSD). Pole figures plot the distribution (usually as density curves) of the poles of particular faces or crystallographic directions in stereographic projection. When most values are concentrated in one or several (depending on the symmetry of the crystal) reduced areas (each called a

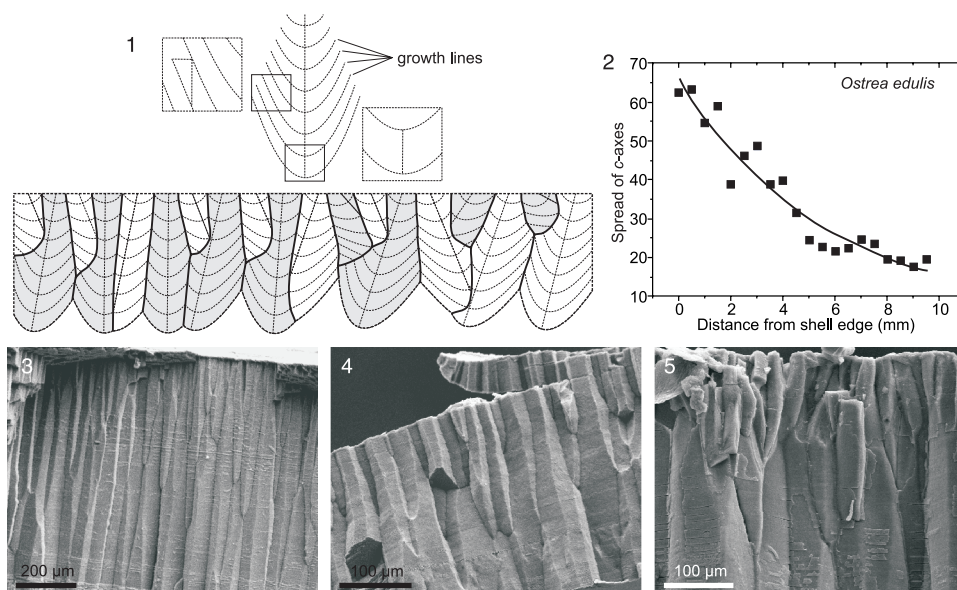


FIG. 13. 1, Theoretical model of competition between prismatic units, which have their highest growth rate along the central axis; in this model, the units having axes at a high angle to the main growth direction of the aggregate (perpendicular to the substrate) progressively disappear. 2, In *Ostrea edulis* LINNAEUS, 1758, the spread of the *c*-axes (measured by the relative width of the 006 maximum) becomes increasingly reduced with the thickness of the outer calcitic prismatic layer; this implies that the *c*-axes of the prisms become progressively aligned. 3–5, Fractures in the calcitic prismatic layers, showing progressive disappearance of units during growth (growth direction is towards the bottom in all); 3, *Pinctada margaritifera* (LINNAEUS, 1758); 4, *Isoognomon legumen* (GMELIN, 1791 in 1791–1793); 5, *Pinna nobilis* LINNAEUS, 1758 (new).

maximum), the different crystals within the analyzed area have a common orientation for that crystallographic direction. The degree of alignment is inversely related to the spread of the maxima.

All analyzed microstructures show a more or less defined maximum for the *c*-axis of either calcite or aragonite, which indicates that the *c*-axes of crystals are relatively co-oriented (Fig. 12). In some the maxima for the rest of the axes is ringlike (Fig. 12.1–12.3). This pattern is the so-called fiber texture, with the *c*-axis as the fiber axis. This texture is displayed by aragonitic and calcitic prismatic microstructures and aragonitic granular prismatic microstructures; outside bivalves, the nacre of gastropods is arranged likewise. Other microstructures display a higher degree of ordering, with all axes co-oriented. This is called a sheet texture and is found in bivalve and *Nautilus* LINNAEUS, 1758, nacre, the crossed lamellar layers of

all extant molluscan classes, the foliated aragonite of monoplacophorans, the foliated calcite of bivalves, and the fibrous calcite of Mytilidae (Fig. 12.4–12.7).

Discussion of crystal orientation have traditionally focused on nacre, which is the classical example of a biomineral comprised of 3D-oriented crystals. The mechanism was originally described as an epitaxial relationship between crystals and a preformed organic matrix (WEINER & TRAUB, 1980, 1984). Nevertheless, NASSIF and others (2005) found an ACC cortex (3–5 nm) around nacre tablets, which would make the epitaxial explanation impossible. Alternatively, selection of specific nucleation faces could be achieved by charge interaction with the organic substrate (i.e., negatively charged proteins sheets) across the thin ACC cortex, as proposed by NASSIF and others (2005). However, we know that nacre tablets communicate across the lamellae through

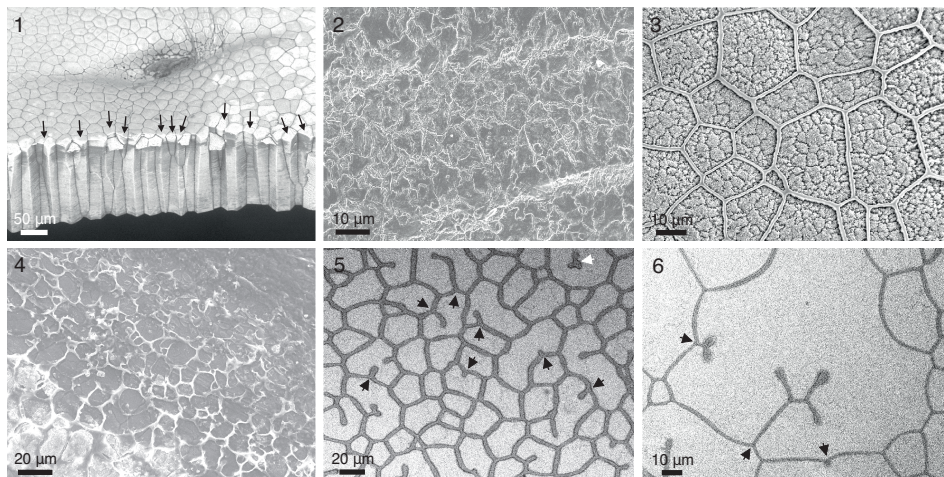


FIG. 14. Prism features and evolution in pteriomorph bivalve species. 1, *Pinctada margaritifera* (LINNAEUS, 1758); oblique view of a fracture through a prismatic lamella, with prisms growing towards bottom of image; prisms that disappear or are close to disappearing (black arrows) have fewer sides (new). 2, *Chama arcana* F. R. BERNARD, 1976; internal surface of the calcitic prismatic layer; prisms are devoid of organic membranes, and their outlines are complex pseudodendritic (new). 3, *Isognomon legumen* (GMELIN, 1791 in 1791–1793); external surface of the calcitic prismatic layer; calcitic units are polycrystalline, and boundaries between crystals are evident upon slight etching (adapted from Checa & others, 2016). 4, *Ostrea edulis* LINNAEUS, 1758; internal surface of the prismatic layer of a specimen kept in artificial seawater with a high magnesium content; the new, abnormal shell consists solely of an organic network (new). 5–6, *P. margaritifera*; internal surface of the calcitic prismatic layer of *P. margaritifera*, showing multiple instances of receding organic walls; every three complete walls meet at  $120^\circ$  (as in view 3), only at the junction with incomplete walls do the angles tend to be much wider (black arrows); note the trifid organic wall (white arrow) that remains isolated within one prism upon recession of its formerly complete organic walls (new).

mineral bridges (see section on nacre growth through mineral bridges), so that nucleation is not necessary for the initiation of nacre tablets.

The reasons for co-orientation of microstructural elements are not clear in all cases. In the prismatic calcite of perionids (UBUKATA, 1994) and the prismatic aragonite of unionids (UBUKATA, 1994; CHECA & RODRÍGUEZ-NAVARRO, 2001), the foliated calcite of bivalves (CHECA, ESTEBAN-DELGADO, & RODRÍGUEZ-NAVARRO, 2007), the foliated aragonite of monoplacophorans (CHECA, SÁNCHEZ-NAVAS, & RODRÍGUEZ-NAVARRO, 2009), and the fibrous calcite of mytilids (CHECA, PINA, & others, 2014), crystal selection by competition has been invoked. This happens when an aggregate of elongate crystals grows with a well-defined growth front. Those crystals within the aggregate with their fastest growth axis perpendicular to the growth front will

intercept those growing oblique and will outcompete them (Fig. 13.1). In this way the survivors will have their fastest growth-axes progressively co-oriented in the growth direction of the aggregate (Fig. 13.1–13.2). Crystal selection may account for cases in which crystals are elongate (fibers, prisms) and grow with their long axes perpendicular or at a high angle to the common growth front (Fig. 13.3–13.5). As a result, only the axis of elongation becomes co-oriented and a fiber texture is finally obtained. If crystals are lath-like and distribute into lamellae, a sheet texture will develop.

Recently, BAYERLEIN and others (2014) provided good evidence that prism evolution (including prism extinction; Fig. 13.3–13.5) during growth of the external layer of *Pinna nobilis* LINNAEUS, 1758, can be interpreted on the basis of the normal grain-growth theory (VON NEUMANN, 1952; MULLINS, 1956), which predicts that those elements with a

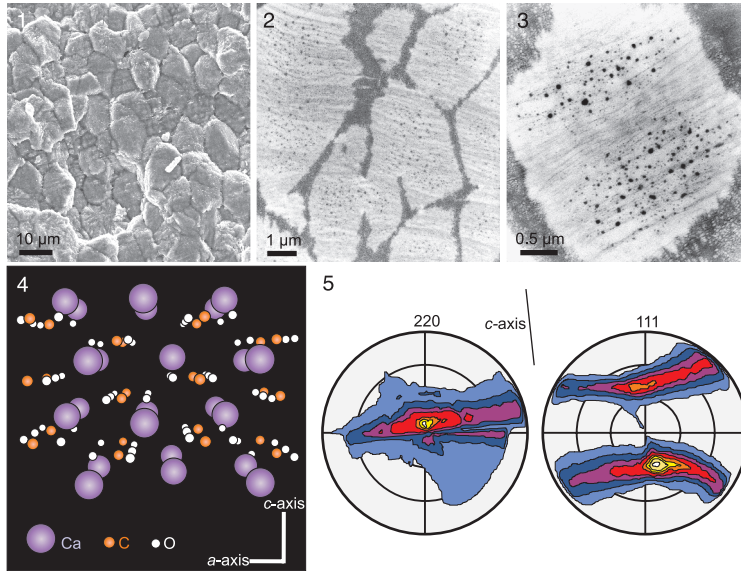


FIG. 15. Hypothetical interaction between organic membranes and growing aragonite crystals in the granular prismatic layer of *Entodesma navicula* (ADAMS & REEVE, 1850 in 1848–1850); 1, SEM view of the layer in vertical fracture; 2–3, two TEM views of the decalcified layer, showing the internal horizontal membranes; 4, atomic structure of aragonite viewed from the *b*-axis; note calcium planes perpendicular to the *c*-axis; 5, XRD pole figures for the granular, homogeneous layer, made on a surface similar to that shown in view 1; the *c*-axis shown is approximately perpendicular to the shell surface (horizontal direction) (1–3, 5, adapted from Harper, Checa, & Rodríguez-Navarro, 2009; 4, new).

number of sides greater than six will grow at the expense of those that have fewer than six sides (Fig. 14.1). In theory, for surface tension to remain constant through the aggregate, the angles between prisms are  $120^\circ$  at triple junctions (Plateau's law). Alternatively, we proposed that these dynamics can be attributed to the organic envelopes of the prisms typical of these layers. This organic network would evolve with time as an emulsion, in which the fluid precursor of the organic web would constitute the continuous phase (CHECA, RODRÍGUEZ-NAVARRO, & ESTEBAN-DELGADO, 2005; CHECA & others, 2016). Emulsions belong to the same kind of phenomena that include foams and grains, and to which the von Neumann-Mullins topological law can be applied. The control of prism evolution by the organic phase is supported by the facts that (1) the outlines of biogenic calcite crystals are not simple polygons, but much more complex in the absence of organic membranes (Fig. 14.2); (2)

in many instances, calcite units enclosed in single cavities are polycrystalline (Fig. 14.3); (3) cavities can exist in the absence of mineral infilling (Fig. 14.4); and (4) the outlines of the prismatic units change with growth or disappearance of organic walls (Fig. 14.5–6).

The instances in which short prismatic crystals develop into a fiber texture or fibers develop into a sheet texture, however, argue for a different explanation. The granular prismatic units of the outer shell layer of *Entodesma* (Fig. 15.1) grow within the translucent layer of the periostracum, which is composed of parallel nanolaminae. Upon growth, they absorb the nanolaminae, which is revealed upon decalcification of the granular units (Fig. 15.2–15.3). The granular prisms are oriented with their *c*-axes perpendicular to the periostracum (i.e., the shell surface; Fig. 15.5). This orientation is most probably determined by the interaction of the negatively charged protein sheets making up the laminae with the positively charged

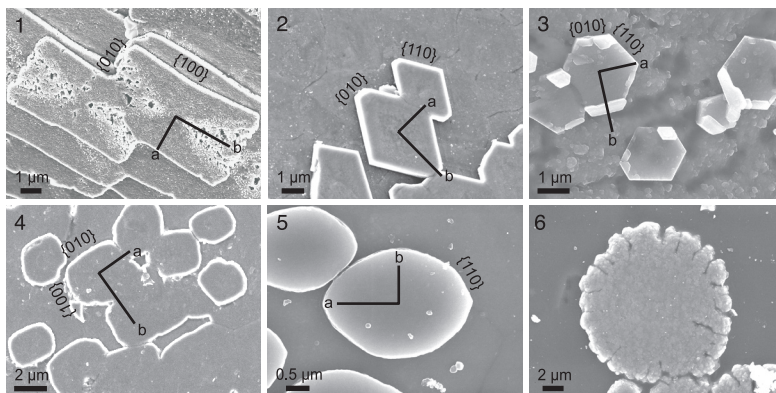


FIG. 16. Morphologies of nacre platelets under SEM and their inferred crystallographies; the  $c$ -axis is approximately parallel to the viewing direction; main faces have been indexed. 1, *Pinna nobilis* LINNAEUS, 1758; rectangular platelets elongated along the  $b$ -axis. 2, *Pteria hirundo* (LINNAEUS, 1758); rhombic, truncated platelets elongated along the  $b$ -axis. 3, *Atrina pectinata* (LINNAEUS, 1767 in 1766–1768); pseudo-hexagonal platelets. 4, *Isognomon legumen* (GMELIN, 1791 in 1791–1793); rectangular platelets elongated along the  $a$ -axis. 5–6, *Pinctada martensii* (DUNKER, 1880); 5, oval platelets elongated along the  $a$ -axis, with incipient  $\{110\}$  faces; 6, round, pseudo-dendritic platelet with crystallography unknown (new).

calcium planes of the aragonite structure (which are perpendicular to the crystallographic  $c$ -axis; Fig. 15.4) (HARPER, CHECA, & RODRÍGUEZ-NAVARRO, 2009). The same applies to mineralized spikes and plaques that form intraperiostracally in many anomalodesmatans (see section on periostracal mineralization) and always grow with their  $c$ -axes perpendicular to the periostracum surface (CHECA & HARPER, 2010).

The mineralization compartment of the outer, anvil-type, calcitic, fibrous shell layer of *Mytilus* LINNAEUS, 1758, is covered by a proteinaceous layer called the surface membrane. This membrane is internally nanolaminated. Experiments with precipitation of synthetic calcite both on the unaltered material and after decalcification have demonstrated that (1) the surface membrane is transparent to ions and (2) synthetic calcite crystals nucleate on the underside of the membrane on their  $\{104\}$  faces. Additionally, the calcite fibers of *Mytilus* have been shown to be able to twist and bend. When, during growth, a twisting/bending fiber places one of its  $\{104\}$  rhombohedral faces parallel to the surface membrane, the horizontal proteinaceous nanolaminae are able to lock that

face during further growth. In this way, the aggregate of fibers finally acquires a sheet texture through a combination of interaction between crystals (competition) and between these crystals and the surface membrane (CHECA, PINA, & others, 2014).

In many instances, a coherent explanation cannot be provided for the high degree of microstructural ordering. For example, the nacre of many bivalves, unlike that of gastropods, has a sheet arrangement, with the  $b$ -axes of tablets co-oriented in the local growth direction of the shell (WADA, 1960, 1961, 1972; WISE, 1970; WEINER & TRAUB, 1981, 1984; CHECA & RODRÍGUEZ-NAVARRO, 2005) (Fig. 12.6). Co-ordering appears gradually with the accumulation of nacre lamellae (CHECA, OKAMOTO, & RAMÍREZ, 2006). A model of co-orientation by competition was proposed by the latter authors, but it might only hold for tablets elongated in the  $b$ -axis direction and not for the most common case of equidimensional (e.g., pseudo-hexagonal) platelets (Fig. 16.3) or for those which elongate in the direction of the  $a$ -axis (Fig. 16.4–16.5). How the most common microstructure, crossed lamellar, can be so well organized crystallographically

(Fig. 12.7) is still a mystery, particularly due to the incomplete understanding of its genesis (HEDEGAARD & WENK, 1998; CHATEIGNER, HEDEGAARD, & WENK, 2000; CHATEIGNER & others, 2010; RODRÍGUEZ-NAVARRO & others, 2012).

### CRYSTALLOGRAPHY OF INDIVIDUAL CRYSTALLITES

Present day high resolution techniques, like EBSD, allow us to map sections or surfaces of individual crystals, and thus, to unveil their crystallography. Many microstructure-constituent crystals have been mapped with EBSD. Additionally, it is interesting to know the relationship of individual crystals with their neighbors. This is particularly relevant when one microstructure grades into another.

The most well known microstructural units, nacre tablets, may be composed of one or several crystals—bivalve nacre being an example of the former and polycrystalline gastropod nacre tablets an example of the latter (MUTVEI, 1978). The first crystallographic data on nacre tablets comes from SCHMIDT (1922), who concluded with optical microscopy that the *c*-axes of aragonite were perpendicular to the main surfaces of the nacre platelets. OLSON, BLONSKY, and others (2013) have recently shown that the *c*-axis is not exactly perpendicular, though situated at a high angle. The different tablet morphologies are obtained by the relative abundance and development of particular crystal faces (SCHMIDT, 1924a, 1924b; WADA, 1972) (Fig. 16.1–16.5), although no crystal faces appear at all in some (Fig. 16.6).

Prismatic crystals tend to elongate along the *c*-axis, in both calcite and aragonite. In aragonite, pseudo-hexagonal prisms may consist of monocrystalline fibers that tend to diverge from a central axis (CHECA & RODRÍGUEZ-NAVARRO, 2001). Calcite crystals also grow along the *c*-axis and are sometimes terminated in typical {104} rhombohedral faces—i.e., fibrous calcite of mytilids (CHECA, PINA, & others, 2014). They are

similar to their inorganic equivalents, but in other cases the crystallography is unexpected. For example, the foliated calcite of *Ostreina* and *Pectinina* is constituted of laths with pointed terminations. Their main surfaces have been found to be {108} rhombohedral faces (CHECA, ESTEBAN-DELGADO, & RODRÍGUEZ-NAVARRO, 2007), which are unknown in inorganic calcite. POKROY and others (2007) identified a new {108} twin in the prismatic calcite of *Pinna nobilis* LINNAEUS, 1758, which is also never found in inorganic calcite. Their existence in bivalves is probably due to the action of organic molecules, which stabilize such unusual faces and planes.

In some instances, the relationships between neighboring crystals may be informative. In bivalve nacre, the lamellae generally grow in a stair-like manner. TEM, EBSD, and polarization-dependent imaging contrast (PIC) maps show that there are sets of staggered tablets that are in exactly the same orientation (DALBECK & others, 2006; OLSON, BLONSKY, & others, 2013) (Fig. 17), which argues for a crystallographic connection between them (see section on nacre growth through mineral bridges).

EBSD analysis of the boundary between an outer aragonitic prismatic shell layer and nacre shows that the fibers comprising the composite prisms in the unionid *Anodonta* LAMARCK, 1799, are crystallographically continuous with the underlying nacre tablets (FREER & others, 2010), the only difference being the initiation of the interlamellar membranes typical of nacre. Using XRD, ESTEBAN-DELGADO and others (2008) showed how outer, calcitic, prismatic layers are structurally and crystallographically continuous with the underlying foliated layer in pectinoids and ostreoids.

Some crystals display particular behaviors. The calcitic, prismatic units of *Pinctada* are (as in most pteriomorphs) enclosed within thick organic sheaths. Several studies have shown that the orientations of those units are not constant and change during growth

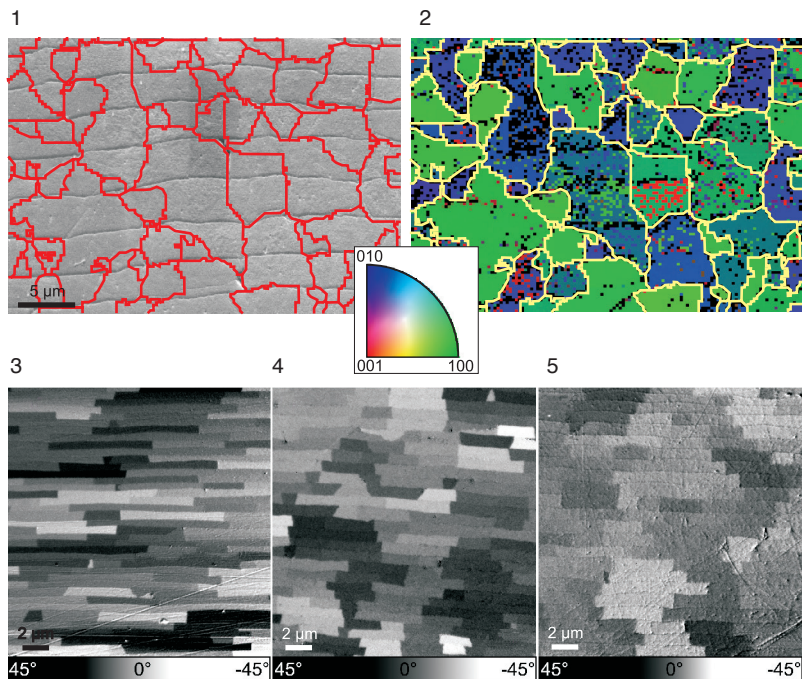


FIG. 17. 1–2, *Neotrigonia margaritacea* (LAMARCK, 1804); Polished section (1) and corresponding EBSD map (2) of the nacre; the section is approximately at  $40^\circ$  to the  $c$ -axis; the crystallographic domains uninterrupted cross the interlamellar boundaries and are delineated on both the section and orientation map; the orientation reference triangle is also shown (*bottom right*) (new). 3–5, Polarization-dependent imaging contrast (PIC) maps of the naces of *Atrina rigida* (LIGHTFOOT, 1786) (3), *Lasmigona complanata* (BARNES, 1823) (4), and *Mytilus californianus* CONRAD, 1837 (5); the gray levels represent the orientations of the  $c$ -axes of nacre platelets; note that groups of evenly oriented platelets consist of superposed and commonly offset platelets (adapted from Olson & others, 2012; reprinted with permission, copyright © 2012, American Chemical Society).

of the units (OKUMURA & others, 2010; CHECA, BONARSKI, & others, 2013; OLSON, METZLER, & others, 2013) (Fig. 18.1). In addition, at some growth stages, crystals may split into independent crystalline domains, so that what was initially a single calcite crystal progressively becomes a dendritic entity, with the branches being independent crystalline domains (CHECA, BONARSKI, & others, 2013) (Fig. 18.1). In contrast, the prisms of *Pinna* LINNAEUS, 1758, which may be several hundreds of microns long, do not show any degree of misorientation or splitting, thus being crystallographically invariant (Fig. 18.2). This may be related to the fact that the crystals of *Pinctada* are patterned into nanodomains delineated by high contrast

lines (OKUMURA & others, 2010, 2012, 2013; CHECA, BONARSKI, & others 2013), which are absent in *Atrina* (OKUMURA & others, 2012, 2013) (which together with *Pinna*, belongs to the Pinnoidea) (Fig. 18.3). It has been suggested that the recorded misorientations in *Pinctada* are produced by dislocations or distortions of the calcite lattice due to the incorporation of organic molecules (OKUMURA & others, 2010; CHECA, BONARSKI, & others, 2013). But the explanation is not so simple because pinnoideans and pterioideans have similar amounts of intracrystalline organic molecules (OKUMURA & others, 2012), although the distortion of the crystal lattice is much higher in the latter (Fig. 18.4). Significantly, the intracrystalline

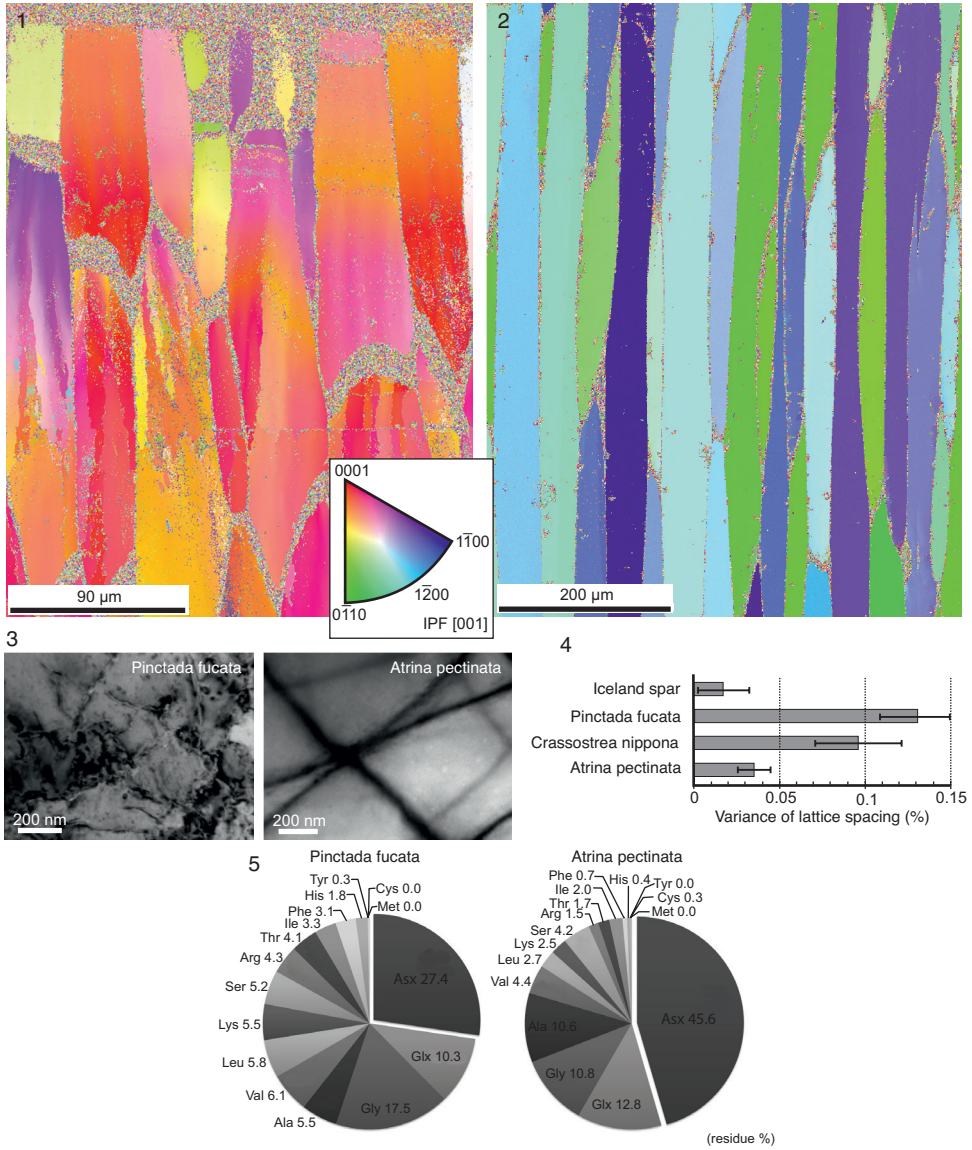


FIG. 18. 1–2, EBSD maps of the calcitic prismatic layers in two bivalve species (outer shell surface at the top); 1, *Pinctada margaritifera* (LINNAEUS, 1758); the changing colors within prismatic units imply changing crystallographic orientations, with prismatic units sometimes splitting into sub-grain crystallographic domains; 2, *Pinna nobilis* LINNAEUS, 1758; the crystallographic orientations are constant throughout and splitting processes absent (adapted from Checa, Bonarski, & others, 2013). 3, Bright-field TEM image with contrast diffraction for *Pinctada fucata* (GOULD, 1850) and *Atrina pectinata* (LINNAEUS, 1767 in 1766–1768); crystallographic nanodomains are delineated in *P. fucata* (though not in *A. pectinata*) by black contrast lines (Okumura & others, 2013; copyright © 2013, with permission from Elsevier). 4, Variance of lattice spacing for the prismatic calcitic layers of the aforementioned species and Iceland spar (adapted from Okumura & others, 2012; reprinted with permission; copyright © 2012, American Chemical Society). 5, Amino-acid composition of the intracrystalline organic matrices of *P. fucata* and *A. pectinata* (Okumura & others, 2013; copyright © 2013, with permission from Elsevier).

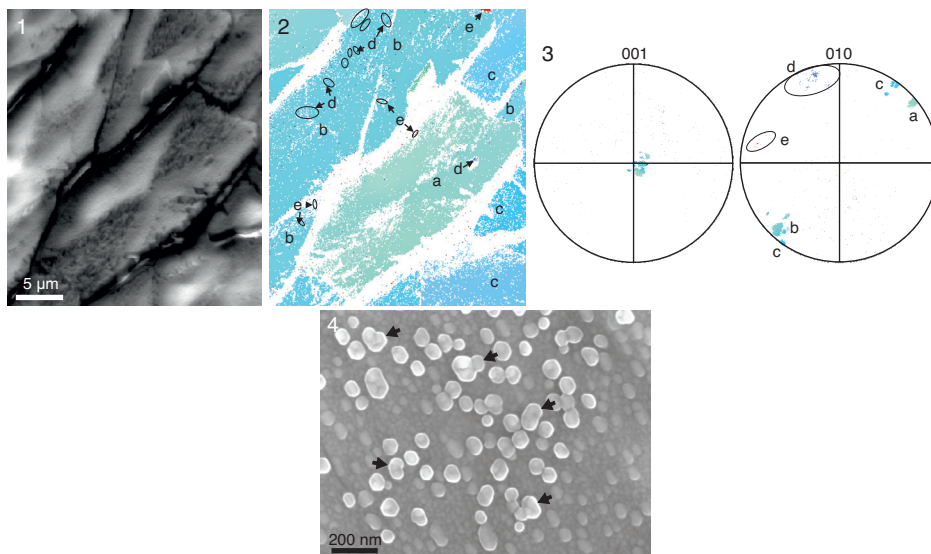


FIG. 19. 1–2, EBSD analysis of rectangular nacre platelets in *Pinna nobilis* LINNAEUS, 1758; 1, secondary electron image of the mapped area; 2, orientation map, with indication of the main crystallographic microdomains (platelets, *a–c*) and nanodomains (scattered dots, *d–e*) recognized (adapted from Checa, Mutvei, & others, 2013). 3, 001 and 010 pole figures with the positions of domains indicated; the *c*-axis in the 001 pole figure is common for all domains, irrespective of their size and position; in the 010 pole figure, nanodomain poles (*d–e*) are at 60° of those of the platelets onto which they settle, which is indicative of {110} twinning (adapted from Checa, Mutvei, & others, 2013; copyright © 2013, with permission from Elsevier). 4, Nanotwins (arrows) recognized with SEM on the surface of nacre platelets of *Pinctada margaritifera* (LINNAEUS, 1758) (adapted from Checa, Cartwright, & Willinger, 2011).

proteins in pinnoideans contain a much higher percent of acidic aminoacids (glutamic and aspartic acids) (OKUMURA & others, 2013) (Fig. 18.5). Therefore, the difference can probably be traced to how organic molecules are initially incorporated within the crystal lattice.

Misorientations have also been found in aragonite. OLSON, BLONSKY, and others (2013) found, by PIC-mapping, changes in the *c*-axis of nacre columns in gastropods, and CHECA, MUTVEI, and others (2013) found misorientations in single tablets of *Pinna* nacre, as well as in the fibers constituting the prisms of the external layer of *Neotrigonia*.

EBSD data indicate the existence of nanocrystals twinned on {110} which appear scattered both on the surface and within the interior of nacre tablets (Fig. 19.1–19.3). Nanocrystals of the external surface of tablets with the aspect of being twinned have been recognized in the bleached nacre

of *Nautilus pompilius* LINNAEUS, 1758, and *Pinctada margaritifera* (LINNAEUS, 1758) under scanning electron microscopy (SEM) (Fig. 19.4). Nacre tablets, and biocrystals in general, are made of crystallographically oriented nanoparticles. LI and HUANG (2009), HUANG and LI (2012), and ZHANG and LI (2012) identified nanoparticles using TEM and observed that, despite the fact that tablets of nacre diffract as single crystals, the constituent nanoparticles (which they implied are aggregation units) showed noticeable degrees of mutual misorientation (pseudo-single-crystal effect).

The nanostructure of nacre and of biocrystals in general has been typically identified as corresponding to a mesocrystal—that is, a composite crystal in which small units are embedded in a matrix of noncrystalline material. It is a form of oriented aggregation, in which the nanocrystals are mutually aligned crystallographically but are spatially separated (CÖLFEN & ANTONIETTI, 2005).

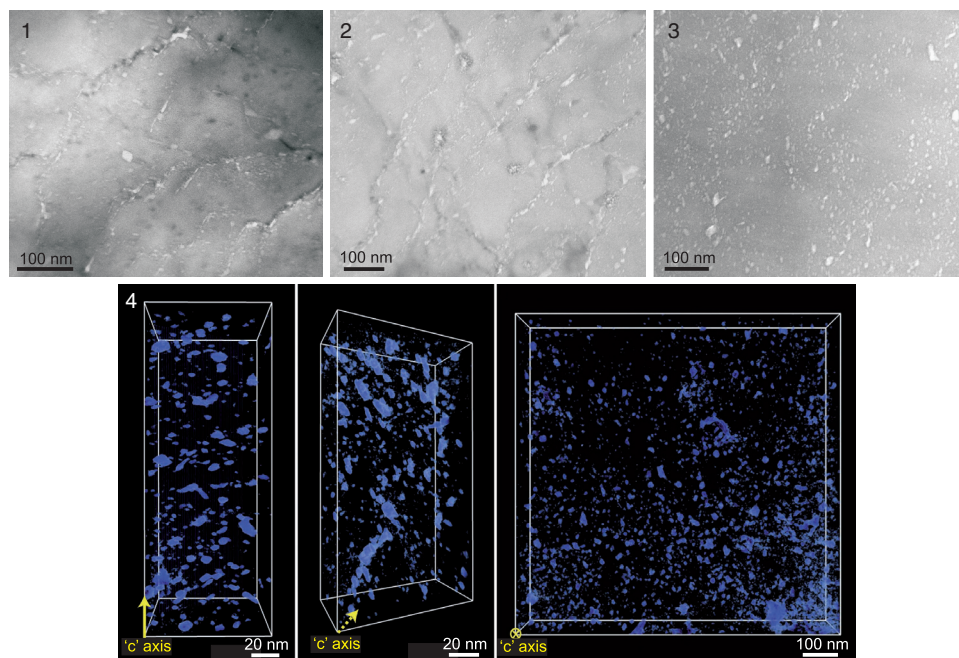


FIG. 20. 1–3, Bright-field TEM images of calcite prisms of *Pinctada fucata* (GOULD, 1850) (1), *Crassostrea nippona* (SEKI, 1934) (2), and *Atrina pectinata* (LINNAEUS, 1767 in 1766–1768) (3); spherule-like contrasts are interpreted as intracrystalline organic molecules (adapted from Okumura & others, 2012). 4, Tomographic reconstruction (three different views) of biomolecules occluded within the calcitic prisms of *Atrina rigida* (LIGHTFOOT, 1786); the nanopatches are disklike, with their maximum dimensions approximately perpendicular to the *c*-axis, and arranged in planes roughly perpendicular to the same axis (adapted from Li & others, 2011; reprinted with permission, copyright © 2011, WILEY-VCH Verlag GmbH & Co. KGaA, Weinheim).

According to SONG and CÖLFEN (2010), the sole criterion for recognizing a material as a mesocrystal is its unique crystallographic hierarchical structure, not its formation mechanism. The recognition of nanotwins between component nanounits in biogenic aragonite suggests that this criterion has to be modified if we want to define them as mesocrystals.

#### NANOSTRUCTURE OF BIOCRYSTALS

The nanostructure of biocrystals secreted by bivalves differs widely according to the techniques of observation used—SEM, TEM, atomic force microscopy (AFM)—so it is not always easy to reconcile differing sources of information. Nevertheless, the available evidence shows that biocrystals are nano-patterned, although the size and shape

of the nano-units differs according to the technique employed.

OKUMURA and others (2012), by means of TEM, showed that the prismatic calcite of *Pinctada fucata* (GOULD, 1850) and *Crassostrea nippona* (SEKI, 1934) is composed of nanodomains (several hundred nm in length) separated by diffraction contrast lines (Fig. 20.1–2). This implies that the nanodomains are slightly disoriented with respect to each other. This pattern was not found in *Atrina pectinata* (LINNAEUS, 1767 in 1766–1768) (Fig. 20.3). These authors interpreted the boundaries between nanodomains as the sites of occlusion of organic molecules, which would cause dislocations, leading to misorientations between nanodomains (see section on crystallography of individual crystallites). The 3-D distribution of such occluded molecules has been

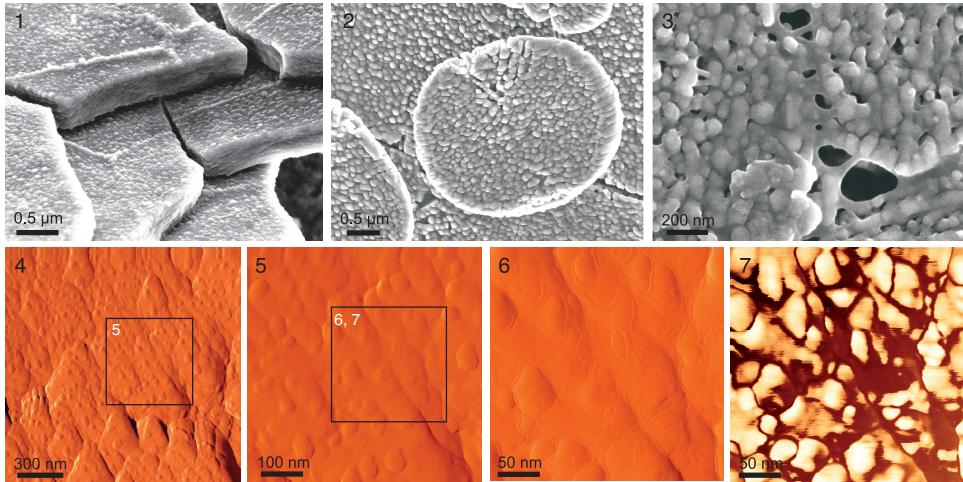


FIG. 21. Nanogranular substructure of nacre platelets, as seen in SEM (1–3) and AFM (4–6). 1, *Pinctada margaritifera* (LINNAEUS, 1758), oblique view of fractured platelets. 2–3, *Pteria hirundo* (LINNAEUS, 1758), platelets deproteinized with Protease (0.2 g/ml.1h). 4–7, Platelet surfaces of *P. hirundo*; amplitude (4–6) and phase (7) images show the pellicles surrounding the nanogranules; boxes indicate enlarged areas; note dark brown pellicles in view 7 (1, 3, new; 2, 4–7, adapted from Checa, Mutvei, & others, 2013).

recently imaged by LI and others (2011) (Fig. 20.4). This fits in with the fact that the calcite of pterioideans (*Pinctada*) and ostreoides (*Ostrea* LINNAEUS, 1758) displays misorientations and splitting processes (Fig. 18.1), whereas that of pinnoideans (*Pinna*) does not (Fig. 18.2) (CHECA, BONARSKI, & others, 2013).

A different nanostructural picture is revealed by examination with SEM (Fig. 21.1–21.3) and AFM (Fig. 21.4–21.7), which provides only surface views. AFM observations show that in all biocrystals examined so far there is a nanostructure composed of amalgamated granules (50–150 nm in diameter); this feature is easily confirmed with SEM, although the resolution achieved with AFM is far higher. Another feature, which can be observed only with AFM, is that the nanogranules are in turn surrounded by nanometer-sized pellicles (Fig. 21.6–7). This substructure was revealed for the first time by DAUPHIN (2001) in the nacre of *Nautilus*, and these AFM results were later confirmed with the same technique on the nacre of bivalves and gastropods (LI, ZHU, & WANG, 2006;

LI & others, 2004; BRUET & others, 2005; ROUSSEAU & others, 2005; WOLF & others, 2012). DAUPHIN (2008) found this to be a general property of calcitic and aragonitic materials secreted by mollusks, and this was later recognized in a variety of other invertebrate animals, including sponges (SETHMANN & others, 2006), corals (PRZENIOSŁO & others, 2008), echinoderms (SETO & others, 2012), and even in fish otoliths (DAUPHIN & DUFOUR, 2008). The great contrast in AFM tapping mode (phase imaging) between the calcium-carbonate granules and the enveloping pellicles has led some authors to hypothesize that the former are organic in nature (e.g., DAUPHIN, 2001, 2006; BRUET & others, 2005; ROUSSEAU & others, 2005; LI, ZHU, & WANG, 2006; BARONNET & others, 2008) (Fig. 21.7). LI, ZHU, and WANG (2006) even showed how rotation of nanoparticles in the nacre of *Haliothis* LINNAEUS, 1758, was favored by the intervening polymer biofilms when the material was subjected to tension. Based on previous TEM data for nacre by NASSIF and others (2005), SETO and others (2012) alternatively proposed that similar pellicles in the sea

urchin test might consist of ACC. Results of bleaching experiments (A. Checa & C. M. Pina, unpublished observations) conducted with AFM are consistent with the, at least partly, organic nature of pellicles.

In many examples of biogenic aragonite, the nanogranules tend to be preferentially aligned, thus forming vermiculations several  $\mu\text{m}$  in length (CHECA, MUTVEI, & others, 2013) (Fig. 21.5–21.6). Analyses of nacre tablets by EBSD (CHECA, MUTVEI, & others, 2013) and TEM (WANG & others, 2013) imply that the vermiculations consistently align with the  $a$ -axis of aragonite. According to the former authors, the vermiculations appear because, during growth of the tablet, organic molecules are expelled from the  $a$ -axis, where the  $\text{Ca}-\text{CO}_3^-$  bonds are the shortest and absorbed preferentially along the  $b$ -axis. In this way, the subunits forming nacre and other bioaragonites—similar etching lineations along the  $a$ -axis have also been reported in foliated and prismatic aragonite (CHECA, SÁNCHEZ-NAVAS, & RODRÍGUEZ-NAVARRO, 2009)—merge uninterrupted and form chains parallel to the  $a$ -axis, whereas the organic molecules are expelled to the sides of these chains.

#### PRECURSOR AND TRANSIENT MINERAL PHASES

Since the pioneer work of TOWE and LOWENSTAM (1967), who described the first transient amorphous phase in chiton teeth, increasing evidence indicates that biominerals, both in vertebrates and invertebrates, form from amorphous precursors (see reviews by GOWER, 2008; WEINER & others, 2009). In particular, amorphous calcium carbonate has been recognized in many groups of organisms (see review by ADDADI, RAZ, & WEINER, 2003). In some groups it may serve as a structural component (e.g., plant cystoliths, calcitic sponge spicules, ascidian spicules) or as a reservoir for calcium carbonate availability (e.g., earthworms, arthropods; ZIEGLER, 1994; RAZ & others, 2002; DILLAMAN, HEQUEMBOURG, & GAY, 2005; ZIEGLER, FABRITIUS, & HAGE-

DORN, 2005; AKIVA-TAL & others, 2011). In many cases, amorphous calcium carbonate is used as a precursor for the formation of crystalline calcium carbonate: for example, in mollusks (HASSE & others, 2000; WEISS & others, 2002; MARXEN & others, 2003; NASSIF & others, 2005; BARONNET & others, 2008; JACOB & others, 2008, 2011) and in sea urchins (BENIASH & others, 1997; BENIASH, ADDADI, & WEINER, 1999; WILT, 2002; RAZ & others, 2003; POLITI & others, 2004, 2006, 2008; MA, WEINER, & ADDADI, 2007; KILLIAN & others, 2009).

The transformation of amorphous calcium carbonate into a crystalline calcium carbonate phase (high-Mg calcite) was first proposed for the larval spicules of sea urchins (BENIASH & others, 1997). This was later verified by the detection of granules of amorphous calcium carbonate in spiculogenic cells, which could subsequently be transported to the mineralization site (BENIASH, ADDADI, & WEINER, 1999).

#### Subsequent Studies

The transformation of amorphous calcium carbonate into aragonite was implied by HASSE and others (2000) and MARXEN and others (2003) for the gastropod *Biomphalaria*, PRESTON, 1910; WEISS and others (2002) for larval bivalve shells (although KUDO & others, 2010, did not find amorphous calcium carbonate in the larval shell of a *Crassostrea*), and JACOB and others (2008) for cultured pearls in freshwater mussels. These authors observed that, during growth, the ratio of crystalline calcium carbonate to amorphous calcium carbonate increased. This, however, does not necessarily indicate transformation of amorphous calcium carbonate into crystalline calcium carbonate, because direct deposition of crystalline calcium carbonate might occur in more advanced growth stages.

The first direct evidence of amorphous calcium carbonate transformation into crystalline calcium carbonate came from the study of sea urchins and mollusks. POLITI and others (2004) found that amorphous

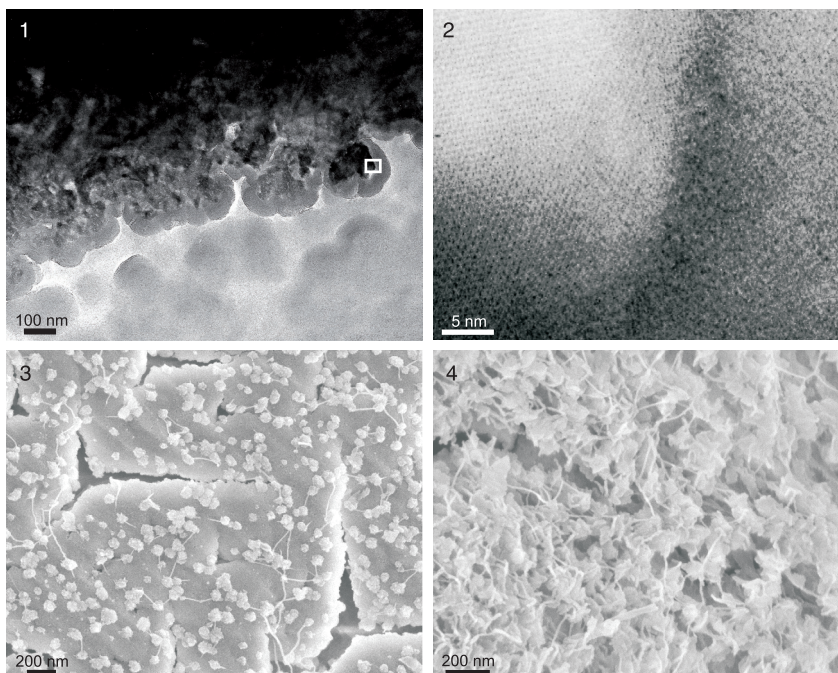


FIG. 22. 1–2, TEM views of the growing front of a prism of the outer calcitic layer of *Pinctada margaritifera* (LINNAEUS, 1758), showing an outer amorphous cortex; 2, detail of framed area in view 1, showing the contact between the calcite lattice and amorphous cortex (adapted from Baronnet & others, 2008). 3–4, SEM views of growth surfaces of the calcitic prisms of *Atrina rigida* (LIGHTFOOT, 1786), showing presumed amorphous calcium carbonate particles (note increased density in view 4), together with organic fibers, deposited on a previous mineral layer (adapted from Nudelman & others 2007).

calcium carbonate of regenerating sea urchin spines occurs in a 100–200 nm-thick outer layer (see also GILBERT & WILT, 2011; SETO & others, 2012). These authors also triggered the transformation of amorphous calcium carbonate into calcite through irradiation under the TEM. NASSIF and others (2005) found a 3–5 nm amorphous calcium carbonate layer coating the surface of mature nacre tablets in *Haliotis*. A similar, though thicker (25–75 nm) and more continuous, amorphous front was found in the prismatic calcitic layer of the pearl oyster *Pinctada margaritifera* (BARONNET & others, 2008) (Fig. 22.1–22.2). Since all these structures grow by the addition of material at the growth front, the only possibility is that the amorphous calcium carbonate cortex transforms into the corresponding crystalline phase. According to ADDADI, RAZ, and

WEINER (2003), transformation of amorphous calcium carbonate into crystalline calcium carbonate would proceed in three stages: (1) formation of hydrated amorphous calcium carbonate, which rapidly transforms into (2) short-lived anhydrous amorphous calcium carbonate, which changes into (3) calcite or aragonite (see review by CARTWRIGHT & others, 2012b). According to experimental data (RADHA & others, 2010), this sequence is energetically downhill.

Contrary to classical models of crystallization, which imply nucleation and growth by the assembly of ions from solution, there is experimental evidence that nucleation and growth proceeds via pre-nucleation clusters. GEBAUER, VÖLKEL, and CÖLFEN (2008) and POUGET and others (2009) observed the formation in solution of clusters of amor-

phous calcium carbonate, which varied in size from >1 nm to 4 nm, depending on the maturation stage. POUGET and others (2009) observed that these nano-clusters later assembled to form amorphous calcium carbonate particles up to 30 nm in diameter. These subsequently crystallized into different mineral species. NUDELMAN and others (2007) observed the presence of amorphous calcium carbonate granules (50–100 nm in diameter) attaching to the surface of the calcitic prisms of the bivalve *Atrina rigida* (LIGHTFOOT, 1786) (Fig. 22.3–22.4). In combination with the experimental evidence described above, these authors suggested that the calcitic prisms of *Atrina* grow by precipitation of amorphous calcium carbonate particles, which subsequently crystallize epitaxially upon contact with the crystalline surface. POLITI and others (2008) were the first to propose that the short-lived anhydrous amorphous calcium carbonate of sea urchin larvae transforms into calcite by secondary nucleation, in which crystallization of amorphous calcium carbonate stimulates the crystallization of the domains in contact. In this process, the two phases (ordered and disordered) are both solid and in contact with each other, and the transformation involves solid-state transformation (WEINER & ADDADI, 2011). The crystallographic orientation is determined by the central initial crystal of the larval skeleton. The secondary nucleation hypothesis has experimental support (PICHON & others, 2008).

Based on all the available evidence, WEINER and ADDADI (2011) proposed a synthetic model for calcification in molluscs and other organisms by which ions or seawater droplets extracted from the environment are transported into specialized vesicles, where the formation of an initial disordered phase (amorphous calcium carbonate) occurs. The amorphous calcium carbonate clusters (either free or encapsulated within their vesicles) are later expelled to the extrapallial fluid and move and adhere to the crystallization front, where they later change to an ordered phase (calcite or aragonite). This

process is summarized in Figure 23 for a forming molluscan biomineral. The growth process by cluster aggregation fits in with the granular aspect of biocrystals under AFM (see Fig. 21). An issue still under debate is whether the granules making up the biocrystals are crystallization units (as implied by NOUET, BARONNET, & HOWARD, 2012). If nanoclusters have to traverse the small spaces between the fibers making up the interlamellar membranes, whether they are empty (as in gastropods) or not (bivalves) (CHECA, CARTWRIGHT, & WILLINGER, 2011, fig. 6), they should be significantly smaller than the constituent nanogranules (as depicted in Fig. 23), but this still requires confirmation. Likewise, they cannot exceed the dimensions of the extrapallial space (see section on the biomineralization compartment).

These exceedingly small sizes contrast with the findings of MOUNT and others (2004), who reported the presence of granulocytes containing calcite crystals at the mineralization front in *Crassostrea virginica* (GMELIN, 1791 in 1791–1793), following experimentally induced shell regeneration. Some cells were observed releasing crystals that were subsequently remodeled. Nevertheless, KÁDÁR, GUERRA-TSCHUSCHKE, and CHECA (2008) found that shell repair in *Bathymodiolus azoricus* COSEL & COMTET, 1999 in COSEL, COMTET, & KRYLOVA, 1999, involved the presence of calcium-bearing haemocytes, whose density decreased with repair time; therefore, this is not the mechanism during normal (non-induced) shell calcification.

Distinct, short-range order has been observed in amorphous calcium carbonate. The amorphous calcium carbonate of the aragonitic freshwater snail *Biomphalaria glabrata* (SAY, 1818) was found to have a short-range order similar to aragonite (HASSE & others, 2000; MARXEN & others, 2003). Other orders relating, respectively, to aragonite and calcite were found in aragonitic larval mollusk shells and in calcitic sea urchin structures (ADDADI, RAZ, & WEINER, 2003; RAZ & others, 2003). Therefore, as

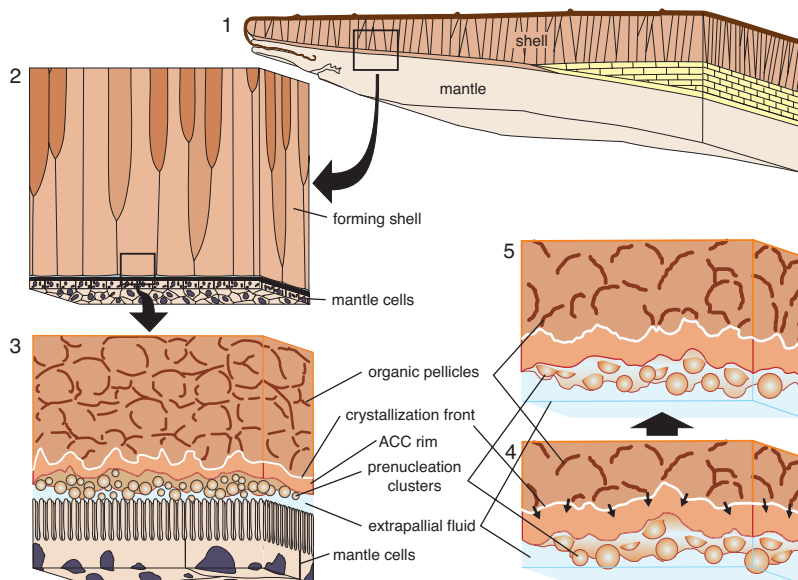


FIG. 23. Diagram of the growth process of molluscan biocrystals from an amorphous precursor. 1–3, Progressive close-up views of the shell-mantle system; in the closer view (3) amorphous calcium carbonate (ACC) prenucleation clusters are formed within the extrapallial fluid and, with time, attach to the surface of the forming biocrystal, producing an amorphous calcium carbonate cortex; slightly deeper within the forming unit, the amorphous calcium carbonate transforms into a mineral phase (aragonite or calcite), typically consisting of nanogranules surrounded by organic pellicles (diagram assumes that organic pellicles form by exsolution from the amorphous calcium carbonate upon crystallization). A detailed view (4–5) of two consecutive stages of the growth process shows amorphous calcium carbonate particles attaching and fusing to the amorphous calcium carbonate cortex; *small arrows* in view 4 indicate the progress of the crystallization front (new).

stated by ADDADI, RAZ, and WEINER (2003), biogenic amorphous calcium carbonate is structurally not one mineral phase, but a family of phases—that is, a case of polymorphism (CARTWRIGHT & others, 2012b).

#### SELF-ORGANIZATION: THE NACRE MODEL

##### Formation of Interlamellar Membranes

The shells of mollusks are created across the extrapallial space. Therefore, all the basic components of crystals and the associated organic matter have to be assembled outside the soft body—that is, they have to be self-organized materials.

The importance of self-organization processes can be seen in nacre. Nacre commonly has a brickwall-tablet stacking mode in which the bricks are aragonitic tablets and the mortar is horizontal, interlamellar membranes and vertical, inter-

tabular membranes. The interlamellar membranes consist of a feltlike arrangement of chitin (probably  $\beta$ -chitin) crystals in the form of nanorods of fibrils, surrounded by protein (LEVI-KALISMAN & others, 2001). In bivalves, before tablets in a given lamella begin to form, an interlamellar membrane is laid down on the body side. In excellent TEM sections across the shell and mantle of *Pinctada radiata* (LEACH, 1814 in 1814–1817), BEVELANDER and NAKAHARA (1969) and NAKAHARA (1991) showed how at the distal end, every new interlamellar membrane is at a very reduced distance from the preceding interlamellar membrane, estimated at  $\sim 100$  nm (CARTWRIGHT & CHECA, 2007) (Fig. 3.1). Towards the interior, this distance increases progressively to the usual distance in mature nacre (300–500 nm). Later, nacre platelets begin to emerge

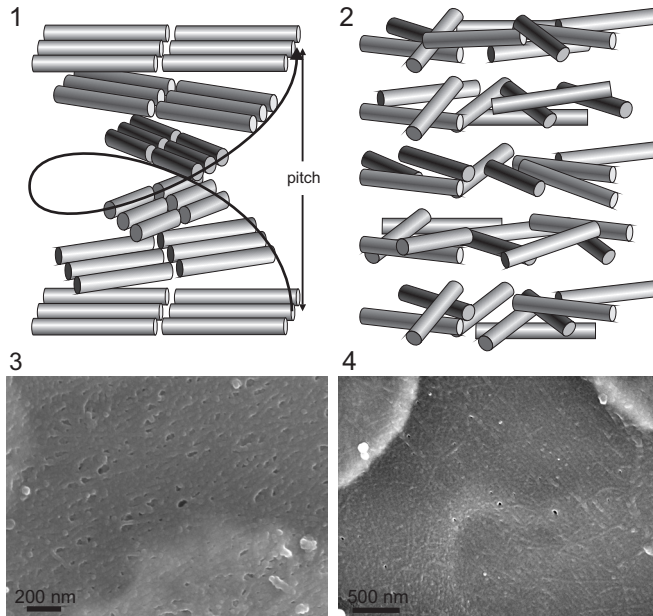


FIG. 24. Fibrous interlamellar membranes. 1, Ideal helical distribution of nanoparticles or molecules in a cholesteric (chiral-nematic) phase of a liquid crystal. 2, Proposed model for the distribution of fibrillar particles in the interlamellar membranes of nacre; the particles are distributed into layers, but they are not arranged in parallel within each membrane. 3–4, Fibrous disordered aspect of the interlamellar layers; 3, *Pteria hirundo* (LINNAEUS, 1758); 4, *Anodonta cygnea* (LINNAEUS, 1758) (new).

and grow at the interspace of the two interlamellar membranes.

How the animal is able to precisely control the distance between interlamellar membranes at such a nanometric scale is difficult to comprehend, unless we look for a physical process operating at a molecular or nanoparticle level. In particular, such behavior occurs during the formation of liquid crystals. In liquid crystals, polar fibers or molecules align due to electrostatic interactions. Of the several possible configurations, a common one is the so-called cholesteric or chiral-nematic phase in which fibers or molecules are arranged in planes, with the fibers in each plane being parallel to each other and slightly rotated with respect to those of the preceding plane. After a certain distance or pitch, the orientation of the fibers is exactly the same (Fig. 24.1).

Liquid-crystal self-organization has been postulated to explain the plywood structures

of many fibrous biocomposites ranging from plant cell walls to bone, including invertebrate skeletons (NEVILLE, 1993). A well-known example is that of the arthropod exoskeleton, which is made of  $\alpha$ -chitin fibers, occasionally impregnated with calcium carbonate (BOULIGAND, 1972). In mollusks, patterns typical of cholesteric phases have been recognized in the periostracum of some gastropods (NEVILLE, 1993), the squid pen (LEVI-KALISMAN & others, 2001), and shells of the cephalopods *Spirula* LAMARCK, 1799 (e.g., lamello-fibrillar microstructure; ERBEN, 1972, p. 28) and *Sepia* LINNAEUS, 1758 (CHECA & others, 2015). Lamello-fibrillar microstructure is approximated by the stepwise texture of certain Early Cambrian, stenotheleid tergomyan monoplacophorans (KOUCHINSKY, 1999, p. 177).

In liquid crystals formed *in vitro*, all layers develop at once from a suspension, provided that enough time is allowed for formation. In nacre, we face the case of a layer-by-layer

liquid crystal, in which new layers are added during growth at the same time as the preexisting layers extend at their edges. The process would be as follows. A new layer is initiated at ~100 nm from the top of the preceding membrane. At this stage it should consist of just the chitin core. Contrary to the typical cholesteric phase, the fibers in a layer are disorganized (Fig. 24.2). This may happen because either they have not had sufficient time to assemble in parallel or the observed length of the fibers (tens of microns; Fig. 24.3–24.4) hinders a parallel arrangement. With time, acidic proteins should adhere on both sides of the chitin framework (to form the structure hypothesized by LEVI-KALISMAN & others, 2001). The repulsive forces between the forming protein covers and those of the preceding layer would progressively increase the separation between layers to the distance of 300–500 nm usually observed in fully mineralized nacre. A certain distance back from the growth front of the interlamellar membrane, estimated at ~20  $\mu\text{m}$  in one specimen of *Pinctada radiata* by CARTWRIGHT and CHECA (2007), nacre crystals begin to grow in the interlamellar spaces. The cells of the mantle surface are never in contact with the forming nacre platelets because there is always an interlamellar membrane in between (Fig. 3.1). This process implies that the interlamellar membranes necessarily have to be transparent to the aggregation units (either ions or nanoclusters); see previous discussion of precursor transient phases.

The liquid-crystal hypothesis for the formation of the interlamellar membranes is an easy way to understand how such a complex structure is secreted via a simple physical mechanism and explains some features of nacre for which there is not presently an alternative explanation. For example, how can nacre tablets grow when they are never in contact with the soft body? This is particularly striking in gastropod nacre, in which the soft body is also separated from the forming interlamellar membranes by the intermediate surface membrane (CHECA, CARTWRIGHT,

& WILLINGER, 2009). This calls to mind the persistent, extremely thin, organic membrane closely adhering to the inner surface of the outer shell layer in arcoid bivalves, apparently during growth of the underlying crossed lamellar shell layer (WALLER, 1980).

As with crystals, defects are also common in liquid crystals. Screw and edge dislocations are both typically developed in cholesteric liquid crystals (KLÉMAN, 1989), with layers of crystallites or molecules being analogous to atomic or molecular terraces in crystals. Comparable features are also found in the interlamellar membranes of bivalve nacre. Screw dislocations manifest themselves as the typical spiral patterns seen in the nacre of bivalves (Fig. 25.1–25.2) and some gastropods, which are resolved at their very axis in a single tablet with screw growth (Fig. 25.3). Bivalve nacre also forms target patterns on its growth surface (Fig. 25.4). This is comparable to the typical nucleation and growth process by two-dimensional nucleation (CHERNOV, 2003), in which the formation of growth hillocks and islands during the formation of new atom planes is the common pattern. Accordingly, the formation of target patterns in nacre is the way in which the nucleation and growth of new interlamellar membranes proceeds. Spiral and target patterns have been modeled theoretically by assuming that the nacre formation system is an excitable medium which conforms to a layer-by-layer liquid crystal (CARTWRIGHT & others, 2012a). The template function of the surface membrane described in gastropods, which protects the nacre biomineralization compartment (CHECA, CARTWRIGHT, & WILLINGER, 2009), most probably reduces the incidence of defects in gastropod nacre.

However, for this hypothesis to be fully accepted, some additional information is needed. For example, the chitin nanocrystals reported by LEVI-KALISMAN and others (2001), were not observed in situ, and the detailed structure of the fibers shown to form the chitin core (OSUNA-MASCARÓ &

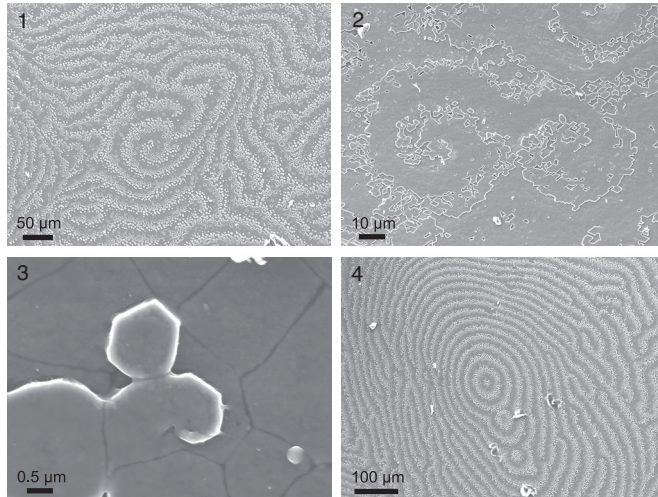


FIG. 25. Morphological patterns on the growth surfaces of bivalve nacre. 1, Digitiform pattern developed on the internal nacre surface of *Pteria avicular* (HOLTEN, 1802); 2, double-spiral pattern developed on the internal nacre surface of *Pteria hirundo* (LINNAEUS, 1758), 3, Initiation of a spiral growth front in *P. hirundo*, with a platelet that extends on two levels by producing a spiral dislocation. 4, Target-like patterns on the internal nacre surface of *P. avicular* (1–2, 4, adapted from Cartwright & Checa, 2007; 3, new).

others, 2015) and their 3-D arrangement are unknown.

### Nacre Growth Through Mineral Bridges

The concept of mineral bridges was originally developed by SCHÄFFER and others (1997) as an alternative to the heteroepitaxial hypothesis of nucleation of nacre platelets directly onto the organic scaffolding (WEINER & TRAUB, 1980, 1981). SCHÄFFER and others (1997) observed nanopores (5–50 nm in diameter) in the decalcified interlamellar membranes of the gastropod *Haliotis rufescens* SWAINSON, 1822, and proposed that a new platelet would initiate as an offshoot of an underlying platelet through the nanopores, with no need for a new nucleation event each time a platelet is formed. The existence of mineral bridges was reinforced when several authors (DIMASI & SARIKAYA, 2004; METZLER & others, 2007; GILBERT & others, 2008; OLSON, BLONSKY, & others, 2013; GRIES & others, 2009; DALBECK & others, 2006; ENGLAND & others, 2007) later showed that superposed platelets in gastropods and bivalves are strictly co-oriented (Fig. 17), which implies that they somehow

communicate. Since the early proposal of SCHÄFFER and others (1997), the discussion has focused upon the true nature of mineral bridges.

Many authors have illustrated what may be mineral bridges in SEM and TEM images (SONG & BAI, 2001, 2003; SONG, ZHANG, & BAI, 2002; SU & others, 2002; SONG, SOH, & BAI, 2004; ROUSSEAU & others, 2005; BARTHELAT, COMI, & ESPINOSA, 2006; VELÁZQUEZ-CASTILLO & others, 2006; LIN, CHEN, & MEYERS, 2008; MEYERS & others, 2008; ESPINOSA & others, 2009; FENGZHANG & others, 2009; LI & HUANG, 2009; SARUWATARI & others, 2009). Width ranges of 36–54 nm (SONG, SOH, & BAI, 2004) and 25–55 nm (GRIES & others, 2009) have been observed. A few authors (GRIES & others, 2009; SARUWATARI & others, 2009) have shown that the crystal lattice of the two superposed tablets is apparently continuous across the mineral bridge (Fig. 26.1). Nevertheless, TEM tomography in the abalone *Haliotis laevigata* DONOVAN, 1808, has shown that what seemed to be true mineral connections are but the end of a continuum that initiates with hillocks (or nanoasperities;

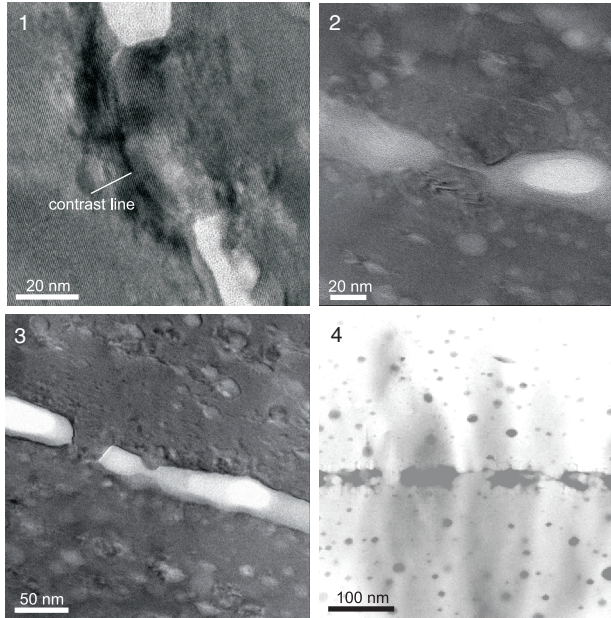


FIG. 26. Hillocks between superposed nacre platelets of *Pinctada margaritifera* (LINNAEUS, 1758). 1–3, TEM views showing several degrees of development of hillocks protruding from superposed plates; in some, the hillocks even connect with an apparent continuity of the crystal lattice (particularly in views 1, 3) (new). 4, STEM view illustrates opposing hillocks that are in contact, but not continuous across (adapted from Checa, Cartwright, & Willinger, 2011).

BARTHELAT & others, 2006) that protrude slightly from both tablets and which clearly do not connect (GRIES & others, 2009) (Fig. 26.2–26.3). Additionally, the seemingly continuous connections seen under TEM are, in fact, invariably discontinuous when seen under STEM (CHECA, CARTWRIGHT, & WILLINGER, 2011) (Fig. 26.4). The interlamellar boundaries between tablets are densely studded with purported mineral bridges and hillocks (SONG & BAI, 2001, 2003; SONG, ZHANG, & BAI, 2002; SU & others, 2002; SONG, SOH, & BAI, 2004; LIN, CHEN, & MEYERS, 2008; FENGZHANG & others, 2009; GRIES & others, 2009; LI & HUANG, 2009; SARUWATARI & others, 2009), such that a 3D estimate from their TEM or SEM views would imply hundreds of mineral bridges for a single platelet. The precise calculations of SONG, SOH, and BAI (2004) yielded 1600 mineral bridges per platelet. This number is evidently not possible, since each platelet produces at most three filial platelets, which can be seen in some bivalves.

Alternatively, CHECA and others (2009) and CHECA, CARTWRIGHT, and WILLINGER (2011) reported large bridges (150–200 nm in diameter) in the nacre of gastropods and the cephalopod *Nautilus*, which are strictly aligned with the axes of the columns of tablets. These bridges run across similarly sized circular holes in the interlamellar membrane. In bivalves, where nacre usually grows in terraces, the bridges are much more irregular in shape and size (>100 nm in diameter), and the crystal lattice is continuous through them (Fig. 27.1–27.4). Discontinuities have also been revealed in 3-D reconstructions of the interlamellar membranes (Fig. 27.5). These same authors developed models for the origin of such structures. In gastropods and *Nautilus*, the growing nacre is covered and separated from the outer environment by a proteinaceous surface membrane (~100 nm thick), and it has been observed that the tablets begin to grow within this surface membrane, before the corresponding interlamellar membrane

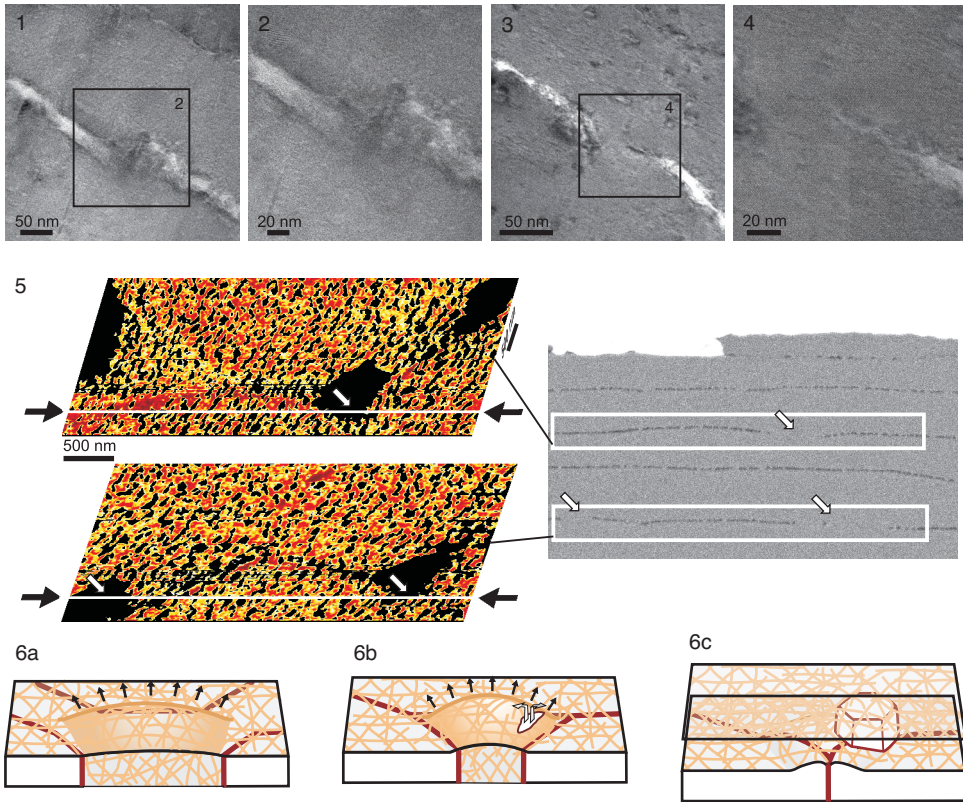


FIG. 27. 1–4, Mineral bridges in *Pinctada margaritifera* (LINNAEUS, 1758); 2, 4, close-up views of outlined areas in views 1 and 3, respectively; note that crystal lattice is continuous in all. 5, 3-D reconstruction of the interlamellar membranes in *P. margaritifera*; reconstruction was made by repeatedly slicing and imaging a small volume of nacre (right photograph) by means of FIB-SEM; white arrows indicate position of interruptions in both the sectioned and the reconstructed interlamellar membranes. 6, Diagram of the mineral bridge formation in bivalves; as the platelets grow, the volume between them is progressively reduced; with calcification, the concentration of organic molecules in the restricted compartment also increases, raising the osmotic pressure and, thus, causing an increasing bulging of the interlamellar membrane (6a, 6b), until the membrane tears (6b) and releases the osmotic pressure; the first platelet to reach the tear produces a new platelet, which emerges to the next lamella (6c) (all adapted from Checa, Cartwright, & Willinger, 2011; copyright © 2011, with permission from Elsevier).

detaches from it. When a new interlamellar membrane detaches from the surface membrane, it extends from the periphery of the central axis outwards. In this way, a continuous, central mineralized axis is formed, so that superimposed nacre tablets are crystallographically continuous across it. However, in bivalves, the mechanism is not so clear. CHECA, CARTWRIGHT, and WILLINGER (2011) hypothesized that pores form during an advanced stage of tablet growth by rupture of the interlamellar membrane due to osmotic pressure. When the compart-

ment between growing tablets becomes reduced, it is progressively isolated from the surrounding extrapallial fluid, particularly since the overlying interlamellar membrane also acts as a lid. In such a closed space, as crystallization proceeds, the concentration of organic molecules must increase. This is possible if the interlamellar membrane is semipermeable, with the flux of water and calcium carbonate ions or nanoclusters being allowed through (SCHÄFFER & others, 1997), while organic molecules are not. The increasing concentration of organic

molecules in the isolated compartment must cause an osmotic pressure difference across the interlamellar membrane, with the pressure being bigger on the isolated compartment side. The difference in the osmotic pressure across the membrane leads to its bowing upwards, and, eventually, to its rupture (Fig. 27.6). The tablet that first reaches the hole will grow to the interlamellar level above and produce a filial tablet. Such a process can be reproduced at the contacts of a single tablet with several of its neighbors, so that, by chance, a single tablet may produce not just one (as in gastropods), but from zero to three filial tablets. The free-floating organic molecules at the interlamellar spaces are finally trapped at the junctions between tablets, forming typical intertabular membranes. Upward bowing and downward bending of the interlamellar membrane (upon subsequent release of the osmotic pressure) is noted in slices through areas supposedly close to the mineral bridges (CHECA, CARTWRIGHT, & WILLINGER, 2011, fig. 9). This mechanism explains why, despite the fact that the number of filial tablets is variable, the average number of tablets remains constant across the lamellae, and why pores form preferentially at the edges of tablets.

### INDUCTURAL DEPOSITS

Inductural deposits, or inductura, are calcareous shell layers or elements of shell sculpture that are deposited exterior to the periostracum by a temporary or more persistent, outward reflection of the outer mantle fold. Inductura are common in certain gastropod groups, such as the Cypraeidae, but they are rarely seen in the Bivalvia. Inductural spines are cemented to the exterior of the periostracum in the cardiid *Ctenocardia virgo* (REEVE, 1845 in 1844–1845), and smooth, flat inductura are deposited over the entire exterior of the shell in some Late Cretaceous cardiids, such as *Protocardia (Pachycardium) stantoni* (WADE, 1926) (SCHNEIDER & CARTER, 2001; CARTER & others, 2012, p. 78). Inductural deposits in

the Bivalvia show microstructures typical of the normal outer and middle shell layers—that is, the cited examples are mostly finely prismatic and crossed lamellar (SCHNEIDER & CARTER, 2001).

The formation of an inductural deposit have never been observed *in vivo*. However, the prismatic/crossed-lamellar microstructure and the lack of a periostracal covering suggests that only the outer surface of the outer mantle fold is involved. This indicates that bivalves are capable of secreting normal shell-layer microstructures without the periostracum sealing off the margin of the biomineralization compartment.

### ADVENTITIOUS MINERALIZED STRUCTURES

Adventitious structures include and accessory plates, callums, calcareous tubes, and calcareous boring linings. Accessory shell plates and callums are largely restricted to the Pholadoidea, Gastrochaenoidea, and the family Corbulidae in Myoidea. Accessory shell plates generally include a medial, unpaired hypoplax, mesoplax, metaplax, and/or protoplax in Pholadoidea; a medial, unpaired protoplax in rare Gastrochaenoidea (e.g., Jurassic *Carterochaena* FÜRSICH, PALMER, & GOODYEAR, 1994); paired or only right-valve siphonoplaxes in Pholadoidea; and siphonal plates in some Corbulidae (for definitions and illustrations, see CARTER & others, 2012). As far as presently known, mineralized accessory shell plates are invariably aragonitic (CARTER, 1980b). The siphonoplax in the pholad *Jouannetia cumingii* (G. B. SOWERBY II, 1849) is present only on the right valve, where it appears to be a spiked extension of normal shell secretion (MORTON, 1986). The hypoplax and metaplax are both joined to the margins of the valves by periostracum, so they probably represent extensions of normal shell secretion. The mesoplax in Pholadidae and Teredinidae originates ventral to an externally shifted anterior adductor muscle, and it protects its posterior, outer surface from abrasion. The protoplax covers the more

anterior portion of an outwardly shifted anterior adductor muscle, and it varies from calcareous to entirely periostracal, and from one piece to longitudinally divided. In *Pholas campechiensis* Gmelin, 1791 in 1791–1793, the protoplax consists of an outer layer of well-defined crossed lamellae; a thin, middle layer of irregular simple prisms; and a thick, inner layer of coarsely textured, irregular, complex crossed lamellae, much like the normal shell valves (Joe Carter, 2015, personal communication). Siphonal plates in the Corbulidae are formed on the inner surface of a thick periostracum on the posterior end of the left valve, and they fit into a rostrate projection from the posterior margin of the right valve. Other than by periostracum, the siphonal plates are not attached to the shell (YONGE, 1946). They are presumably aragonitic, but their microstructure is yet unstudied. In summary, accessory shell plates appear to be extensions of normal shell secretion beyond the original shell margins, and they tend to replicate its shell microstructures.

Calcareous tubes and boring linings in the *Bivalvia* typically show irregularly prismatic microstructures that suggest less-direct mantle control than accessory shell plates. The pholadoidean callum is a more or less smooth wall, or left and right walls, closing or partially closing a pedal gape at sexual maturity. The callum may also cover the entire dorsal regions of the shell (TURNER, 1969; MORTON, 1986; CARTER & others, 2012, p. 28, fig. 24, 48–49). In some cases, the left and right halves of the callum do not meet, and they are joined by a periostracal fold with a minute pore remaining between them. In other cases, a left callum overlaps a right one to allow rocking of the shell valves about a dorsoventral axis, as, for example, in *Jouannetia cumingii* (G. B. SOWERBY II, 1849) (MORTON, 1986). Callums vary from mostly periostracal to mostly calcium carbonate (TURNER, 1969), and they have an aragonitic, irregular, simple prismatic microstructure (CARTER, 1980b; MORTON, 1986). The callum is separated from the

exposed mantle tissues by periostracum, so its mineralizing fluids are presumably extruded through the pedal mantle aperture from pallial glands positioned within the mantle cavity (MORTON, 1986).

The adventitious calcareous tube protecting the siphons in gastrochaenids is clearly secreted by the siphonal epithelium (CARTER, 1978; MORTON, PEHARDA, & PETRIĆ, 2011). MORTON, PEHARDA, and PETRIĆ (2011) suggested that the source of the mineralizing fluid is glands in the internal, posteroventral regions of the mantle cavity, presumably exiting, volcano-like, from the aperture of the incurrent siphon. This is unlikely, because *in vivo* observations of siphon-tube mineralization in this family indicate that it begins as small patches on the lateral surface of the siphons, not at their tips (Joe Carter, 2015, personal communication). The source of these mineralizing solutions must be the siphonal epithelium itself. For the more anterior parts of calcareous tubes and calcareous boring linings, secretion in gastrochaenids is probably accomplished by glands in a reflected middle mantle fold or by the exposed outer surface of the largely fused, inner mantle fold. Anterior boring lining secretion in gastrochaenids without a strongly reflected middle mantle fold has been observed *in vivo* by CARTER (1978, p. 44). Repair of a broken boring was initiated by inflation of the anteroventral inner mantle fold and secretion of an adherent mucous sheet. As this initial mucous sheet became mineralized, additional mucous sheets were secreted to extend its coverage. In gastrochaenids incapable of rotating in their tube or boring, such as *Cucurbitula* GOULD, 1861, a greatly extended middle mantle fold must also be involved in tube and boring lining secretion. Thus, tube and boring lining secretion in at least gastrochaenids is accomplished by all exposed mantle tissues. We can only surmise that similar mechanisms are involved in other boring and/or calcareous tube-dwelling bivalves, such as the Clavagelloidea.

## ACKNOWLEDGMENTS

We are indebted to several colleagues who provided original material for the illustrations: John Taylor, Natural History Museum, London (Fig. 8.1–8.3); Alejandro Rodríguez-Navarro, Department of Petrology and Mineralogy, University of Granada (original data for Fig. 13.2); P. U. P. A. Gilbert, Department of Chemistry, University of Madison, Wisconsin (Fig. 17.3–17.5); Taiga Okumura (Department of Earth and Planetary Sciences, University of Tokyo (Fig. 18.3, 18.5, 20.1–20.3); Alain Baronnet, Centre Interdisciplinaire de Nanoscience, Université de Marseille, France (Fig. 22.1–22.2); Fabio Nudelman, School of Chemistry, The University of Edinburgh (Fig. 22.3–22.4). José Luis Rueda and Jorge Baro, both from the Instituto Español de Oceanografía, provided material from their campaigns (Life+ Indemares and RECALA, respectively). The manuscript greatly benefited from comments and additions by Prof. Joseph G. Carter (Department of Geological Sciences, University of North Carolina at Chapel Hill). The authors received funding from projects CGL2010-20748-CO2-01/02 and CGL2013-48247-P of the Spanish Ministerio de Ciencia e Innovación, and RNM6433 of the Andalusian Consejería de Innovación Ciencia y Tecnología, as well as from the Research Groups RNM363 and RNM0141 (latter institution).

## REFERENCES

- Adams, Arthur, & L. A. Reeve. 1848–1850. The Zoology of the Voyage of H.M.S. Samarang: Under the command of Captain Sir Edward Belcher C.B., F.R.A.S., F.G.S., During the Years 1843–1846. Parts I–III. Reeve, Benham, & Reeve. London.
- Addadi, Lia, J. Moradian, E. Shay, N. G. Maroudas, & S. Weiner. 1987. A chemical model for the co-operation of sulfates and carboxylates in calcite crystal nucleation: Relevance to biomineralization. *Proceedings of the National Academy of Sciences of the United States of America* 84:2732–2736.
- Addadi, Lia, S. Raz, & S. Weiner. 2003. Taking advantage of disorder: Amorphous calcium carbonate and its roles in biomineralization. *Advanced Materials* 15:959–970.
- Addadi, Lia, & S. Weiner. 1985. Interactions between acidic proteins and crystals: Stereochemical requirements in biomineralization. *Proceedings of the National Academy of Sciences of the United States of America* 82:4110–4414.
- Akiva-Tal, Anat, S. Kababya, Y. S. Balazs, L. Glazer, A. Berman, A. Sagi, & A. Schmidt. 2011. In situ molecular NMR picture of bioavailable calcium stabilized as amorphous CaCO<sub>3</sub> biomineral in crayfish gastroliths. *Proceedings of the National Academy of Sciences of the United States of America* 108:14763–14768.
- Aller, R. C. 1974. Prefabrication of the shell ornamentation in the bivalve *Laternula*. *Lethaia* 7:43–56.
- Angas G. F. 1868. On a new genus and some new species of marine Mollusca from Port Jackson, New South Wales. *Proceedings of the Zoological Society of London* 1867(3):908–911, pl. 44.
- Ansell, A. D. 1961. The functional morphology of the British species of Veneracea (Eulamellibranchia). *Journal of the Marine Biological Association of the United Kingdom* 41:489–515.
- Barnes, D.W. 1823. On the genera *Unio* and *Alasmodontia*: With introductory remarks. *American Journal of Science and Arts* 6(1–2):107–127; 258–280, 13 pl.
- Baronnet, Alain, J.-P. Cuif, Yannicke Dauphin, Bastien Farre, & Julius Nouet. 2008. Crystallization of biogenic Ca-carbonate within organo-mineral micro-domains: Structure of the calcite prisms of the pelecypod *Pinctada margaritifera* (Mollusca) at the submicron to nanometre ranges. *Mineralogical Magazine* 72:617–626.
- Barthelat, François, Chun-Ming Li, Claudia Comi, & H. D. Espinosa. 2006. Mechanical properties of nacre constituents and their impact on mechanical performance. *Journal of Materials Research* 21:1977–1986.
- Bayerlein, Bernd, Paul Zaslansky, Yannicke Dauphin, Alexander Rack, Peter Fratzl, & Igor Zlotnikov. 2014. Self-similar mesostructure evolution of the growing mollusc shell reminiscent of thermodynamically driven grain growth. *Nature Materials* 13:1102–1107.
- Beedham, Gordon E. 1958a. Observations on the mantle of the Lamellibranchia. *Quarterly Journal of Microscopical Science* 3:181–197.
- Beedham, G. E. 1958b. Observations on the non-calcareous component of the shell of the Lamellibranchia. *Quarterly Journal of Microscopical Science* 3:341–358.
- Beedham, G. E., & Gareth Owen. 1965. The mantle and shell of *Solemya parkinsoni* (Protobranchia: Bivalvia). *Proceedings of the Zoological Society of London* 145:405–430.
- Behrens, Gesa, L. T. Kuhn, Rick Ubig, & A. H. Heuer. 1995. Raman spectra of vateritic calcium carbonate. *Spectroscopy Letters* 28:983–995.
- Belcher, A. M., X. H. Wu, R. J. Christensen, P. K. Hansma, G. D. Stucky, & D. E. Morse. 1996. Control of crystal phase switching and orientation by soluble mollusc-shell proteins. *Nature* 381:56–58.
- Beniash, Elia, Lia Addadi, & Stephen Weiner. 1999. Cellular control over spicule formation in sea urchin embryos: A structural approach. *Journal of Structural Biology* 125:50–62.

- Beniash, Elia, Joanna Aizenberg, Lia Addadi, & Stephen Weiner. 1997. Amorphous calcium carbonate transforms into calcite during sea-urchin larval spicule growth. *Proceedings of the Royal Society of London (Series B)* 264:461–465.
- Bernard, F. R. 1976. Living Chamidae of the eastern Pacific (Bivalvia, Heterodonta). *Natural History Museum of Los Angeles County, Contributions in Science* 278:1–43.
- Berman, Amir, J. Hanson, L. Leiserowitz, T. F. Koetzle, S. Weiner, & L. Addadi. 1993. Biological control of crystal texture: A widespread strategy for adapting crystal properties to function. *Science* 259:776–779.
- Bers, A. V., Fradry D'Souza, J. W. Klijnstra, P. R. Willemsen, & Martin Wahl. 2006. Chemical defence in mussels: Antifouling effect of crude extracts of the periostracum of the blue mussel *Mytilus edulis*. *Biofouling* 22:251–259.
- Bevelander, Gerrit, & H. Nakahara. 1967. An electron microscope study of the formation of the periostracum of *Macrocallista maculata*. *Calcified Tissue Research* 1:55–67.
- Bevelander, Gerrit, & H. Nakahara. 1969. An electron microscope study of the formation of the nacreous layer in the shell of certain bivalve molluscs. *Calcified Tissue Research* 3:84–92.
- Bottjer, D. J., & J. G. Carter. 1980. Functional and phylogenetic significance of projecting periostracal structures in the Bivalvia (Mollusca). *Journal of Paleontology* 54:200–216.
- Bouligand, Yves. 1972. Twisted fibrous arrangements in biological materials and cholesteric mesophases. *Tissue & Cell* 4:189–217.
- Braithwaite, C. J. R., J. D. Taylor, & E. A. Glover. 2000. Marine carbonate cements, biofilms, biomineralization and skeletogenesis: Some bivalves do it all. *Journal of Sedimentary Research* 70:1129–1138.
- Bronn, H. G. 1831. *Übersicht der Fossilien Ueberreste in den tertiären subappenninischen Gebirgen. Italiens Tertiär-Gebilde und deren organische Einschlüsse*. Heidelberg. xii + 176 p., 1 pl.
- Brown, Thomas. 1827. *Illustrations of the Conchology of Great Britain and Ireland*. Drawn from Nature. W. H. Lizars and D. Lizars & S. Highley. Edinburgh & London, 144 p., 52 pl.
- Bruet, B. J. F., H. J. Qi, M. C. Boyce, R. Panas, K. Tai, L. Frick, & C. Ortiz. 2005. Nanoscale morphology and indentation of individual nacre tablets from the gastropod mollusc *Trochus niloticus*. *Journal of Materials Research* 20:2400–2419.
- Bubel, Andreas. 1973. An electron-microscope study of periostracum formation in some marine bivalves. I. The origin of the periostracum. *Marine Biology* 20:213–221.
- Callil, C. T., & M. C. D. Mansur. 2005. Ultrastructural analysis of the shells of *Anodontites trapesialis* (Lamarck) and *Anodontites elongatus* (Swainson) (Mollusca, Bivalvia, Etherioidea) from the Mato Grosso Pantanal Region, Brazil. *Revista Brasileira de Zoologia* 22:724–734.
- Carriker, M. R., & R. E. Palmer. 1979. Ultrastructural morphogenesis of prodissoconch and early dissoconch valves of the oyster *Crassostrea virginica*. *Proceedings of the National Shellfisheries Association* 69:102–128.
- Carter, J. G. 1978. Ecology and evolution of the Gastrochaenacea (Mollusca, Bivalvia) with notes on the evolution of the endolithic habitat. *Bulletin of the Peabody Museum of Natural History* 41:1–92.
- Carter, J. G. 1980a. Environmental and biological controls of bivalve shell mineralogy and microstructure. *In* D. C. Rhoads, & R. A. Lutz, eds., *Skeletal Growth of Aquatic Organisms*, Chapter 2. Plenum. New York. p. 69–113.
- Carter, J. G. 1980b. Selected mineralogical data for the Bivalvia. *In* D. C. Rhoads & R. A. Lutz, eds., *Skeletal Growth of Aquatic Organisms*, Appendix 2, Part A. Plenum. New York. p. 627–643.
- Carter, J. G. 1990. Evolutionary significance of shell microstructures in the Palaeotaxodonta, Pteriomorpha and Isofilibranchia (Bivalvia: Mollusca). *In* J. G. Carter, ed., *Skeletal Biomineralization: Patterns, Processes and Evolutionary Trends*, Vol. 2. Van Nostrand Reinhold. New York. p. 135–296.
- Carter, J. G., & R. C. Aller. 1975. Calcification in the bivalve periostracum. *Lethaia* 8:315–320.
- Carter, J. G., K. Bandel, V. de Buffrenil, S. Carlson, J. Castanet, J. Dalingwater, H. Francillon-Vieillot, J. Geraudie, F. J. Meunier, H. Mutvei, A. de Riquelès, J. Y. Sire, A. Smith, J. Wendt, A. Williams, & L. Zylberberg. 1990. Glossary of Skeletal Biomineralization. *In* J. G. Carter, ed., *Skeletal Biomineralization: Patterns, Processes and Evolutionary Trends*, Vol. 1. Van Nostrand Reinhold. New York. p. 337–352.
- Carter, J. G., Enriqueta Barrera, & M. J. S. Tevesz. 1998. Thermal potentiation and mineralogical evolution in the Bivalvia (Mollusca). *Journal of Paleontology* 72(6):991–1010.
- Carter, J. G., P. J. Harries, Nikolaus Malchus, A. F. Sartori, L. C. Anderson, Rüdiger Bieler, A. E. Bogan, E. V. Coan, J. C. W. Cope, S. M. Cragg, J. R. García-March, Jørgen Hylleberg, Patricia Kelley, Karl Kleemann, Jiří Kříž, Christopher McRoberts, P. M. Mikkelsen, John Pojeta, P. W. Skelton, Ilya Tëmkin, Thomas Yancey, & Alexandra Zieritz. 2012. Part N, Revised, Volume 1, Chapter 31: Illustrated Glossary of the Bivalvia. *Treatise Online* 48:1–209, 327 fig. Revised per *Treatise* style.
- Carter, J. G., R. A. Lutz, M. J. S. Tevesz. 1990. Shell microstructural data for the Bivalvia. Part VI. Orders Modiomorphoidea and Mytiloidea. *In* J. G. Carter, ed., *Skeletal Biomineralization: Patterns Processes and Evolutionary Trends*, Vol. 1. Van Nostrand Reinhold. New York. p. 391–411.
- Cartwright, J. H. E., & A. G. Checa. 2007. The dynamics of nacre self-assembly. *Journal of the Royal Society Interface* 4:491–504.
- Cartwright, J. H. E., A. G. Checa, Bruno Escribano, & C. I. Sainz-Díaz. 2009. Spiral and target patterns in bivalve nacre manifest a natural excitable medium from layer growth of a biological liquid crystal. *Proceedings of the National Academy of Sciences of the United States of America* 106:10499–10504.
- Cartwright, J. H. E., A. G. Checa, Bruno Escribano, & C. I. Sainz-Díaz. 2012a. Crystal growth as an

- excitable medium. *Philosophical Transactions of the Royal Society A* 370:2866–2876.
- Cartwright, J. H. E., A. G. Checa, J. D. Gale, Denis Gebauer, & C. I. Sainz-Díaz. 2012b. Calcium carbonate polymorphism and its role in biomineralization: How many amorphous calcium carbonates are there? *Angewandte Chemie International Edition* 51:2–13.
- Castilho, Fernanda, J. Machado, M. L. Reis, & C. Sá. 1989. Ultrastructural study of the embryonic and larval shell of *Anodonta cygnea*. *Canadian Journal of Zoology* 67:1659–1664.
- Chateigner Daniel, C. Hedegaard, & H.-R. Wenk. 2000. Mollusc shell microstructures and crystallographic textures. *Journal of Structural Geology* 22:1723–1735.
- Chateigner, Daniel, S. Ouhenia, C. Krauss, C. Hedegaard, O. Gil, M. Morales, L. Lutterotti, M. Rousseau, & E. Lopez. 2010. Voyaging around nacre with the X-ray shuttle: From bio-mineralisation to prosthetics via mollusc phylogeny. *Materials Science and Engineering A* 528:37–51.
- Checa, A. G. 2000a. Remote biomineralization in divaricate ribs of *Strigilla* and *Solecurtus* (Tellinoidea: Bivalvia). *Journal of Molluscan Studies* 66:457–466.
- Checa, A. G. 2000b. A new model for periostracum and shell formation in Unionidae (Bivalvia, Mollusca). *Tissue & Cell* 32:405–416.
- Checa, A. G., J. T. Bonarski, M. G. Willinger, Marek Faryna, Katarzyna Berent, Bogusz Kania, Alicia González-Segura, C. M. Pina, Jan Pospiech, & Adam Morawiec. 2013. Crystallographic orientation inhomogeneity and crystal splitting in biogenic calcite. *Journal of the Royal Society Interface* 10:20130425.
- Checa, A. G., J. H. E. Cartwright, Isabel Sánchez-Almazo, J. P. Andrade, & Francisco Ruiz-Raya. 2015. The cuttlefish *Sepia officinalis* (Sepiidae, Cephalopoda) constructs cuttlebone from a liquid-crystal precursor. *Scientific Reports* 5:11513.
- Checa, A. G., J. H. E. Cartwright, & M. G. Willinger. 2009. The key role of the surface membrane in why gastropod nacre grows in towers. *Proceedings of the National Academy of Sciences of the United States of America* 106:38–43.
- Checa, A. G., J. H. E. Cartwright, & M. G. Willinger. 2011. Mineral bridges in nacre. *Journal of Structural Biology* 176:330–339.
- Checa, A. G., F. J. Esteban-Delgado, & A. B. Rodríguez-Navarro. 2007. Crystallographic structure of the foliated calcite of bivalves. *Journal of Structural Biology* 157:393–402.
- Checa, A. G., & E. M. Harper. 2010. Spikey bivalves: Intra-periostracal crystal growth in anomalodesmatans. *The Biological Bulletin* 219:231–248.
- Checa, A. G., & E. M. Harper. 2014. Periostracal mineralization in the gastrochaenid bivalve *Spengleria*. *Acta Zoologica* 95:196–208. First published online December 20, 2012; issue published March 18, 2014.
- Checa, A. G., Elena Macías-Sánchez, E. M. Harper, & J. H. E. Cartwright. 2016. Organic membranes determine the pattern of the columnar prismatic layer of mollusc shells. *Proceedings of the Royal Society B* 283:20160032.
- Checa, A. G., Harry Mutvei, A. J. Osuna-Mascaró, J. T. Bonarski, Marek Faryna, Katarzyna Berent, C. M. Pina, Marthe Rousseau, & Elena Macías-Sánchez. 2013. Crystallographic control on the substructure of nacre tablets. *Journal of Structural Biology* 183:368–376.
- Checa, A. G., Takashi Okamoto, & Joaquín Ramírez. 2006. Organisation pattern of nacre in Pteriidae (Bivalvia: Mollusca) explained by crystal competition. *Proceedings of the Royal Society B* 273:1329–1337.
- Checa, A. G., C. M. Pina, A. J. Osuna-Mascaró, A. B. Rodríguez-Navarro, & E. M. Harper. 2014. Crystal-line organization of the fibrous prismatic calcitic layer of the Mediterranean mussel *Mytilus galloprovincialis*. *European Journal of Mineralogy* 26:495–505.
- Checa, A. G., & Alejandro Rodríguez-Navarro. 2001. Geometrical and crystallographic constraints determine the self-organization of shell microstructures in Unionidae (Bivalvia: Mollusca). *Proceedings of the Royal Society B* 268:771–778.
- Checa, A. G., & Alejandro Rodríguez-Navarro. 2005. Self-organisation of nacre in the shells of Pterioidea (Bivalvia: Mollusca). *Biomaterials* 26:1071–1079.
- Checa, A. G., A. B. Rodríguez-Navarro, & F. J. Esteban-Delgado. 2005. The nature and formation of calcitic columnar prismatic shell layers in pteriomorphian bivalves. *Biomaterials* 26:6404–6414.
- Checa, A. G., Joaquín Ramírez-Rico, Alicia González-Segura, & Antonio Sánchez-Navas. 2009. Nacre and false nacre (foliated aragonite) in extant monoplacophorans (=Tryblidiida: Mollusca). *Naturwissenschaften* 96:111–122.
- Checa, A. G., Carmen Salas, E. M. Harper, & J. D. Bueno-Pérez. 2014. Early stage biomineralization in the periostracum of the ‘living fossil’ bivalve *Neotrigonia*. *PLoS ONE* 9(2):e90033. DOI:10.1371/journal.pone.0090033.
- Checa, A. G., Antonio Sánchez-Navas, & A. B. Rodríguez-Navarro. 2009. Crystal growth in the foliated aragonite of monoplacophorans (Mollusca). *Crystal Growth & Design* 9:4574–4580.
- Chernov, A. A. 2003. Protein crystals and their growth. *Journal of Structural Biology* 142:3–21.
- Chinzei, Kiyotaka, & Adolf Seilacher. 1993. Remote biomineralization. I: Fill skeletons in vesicular oyster shells. *Neues Jahrbuch für Geologie und Paläontologie Abhandlungen* 190:349–361.
- Cölfen, Helmut, & Markus Antonietti. 2005. Mesocrystals: Inorganic superstructures made by highly parallel crystallization and controlled alignment. *Angewandte Chemie International Edition* 44:5576–5591.
- Conrad, T. A. 1837. Description of new marine shells, from Upper California. Collected by Thomas Nuttall, Esq. *Journal of the Academy of Natural Sciences, Philadelphia* 7:227–268.
- Cosel R. von, T. Comtet, & E. M. Krylova. 1999. *Bathymodiulus* (Bivalvia: Mytilidae) from hydrothermal vents on the Azores triple junction and the Logatchev hydrothermal field. *The Veliger* 42(3): 218–248.

- Cossmann, Maurice. 1912. Essais de paléonchologie comparée. Part 9. Published by Author. Paris. 248 p., 4 pl.
- Crenshaw, M. A. 1972. The inorganic composition of molluscan extrapallial fluid. *The Biological Bulletin* 143:506–512.
- Cuif, J.-P., Yannicke Dauphin, Gernot Nehrke, Julius Nouet, & Alberto Pérez-Huerta. 2012. Layered growth and crystallization in calcareous biominerals: Impact of structural and chemical evidence on two major concepts in invertebrate biomineralization studies. *Minerals* 2:11–39.
- Cusack, Maggie, & Andy Freer. 2008. Biomineralization: Elemental and organic influence in carbonate systems. *Chemical Reviews* 108:4433–4454.
- Cuvier, G. L. C. F. D. 1798. *Tableau Élémentaire de l'Histoire Naturelle des Animaux*. Baudouin. Paris. xvi + 710 p., 14 pl.
- Dalbeck, Paul, Jennifer England, Maggie Cusack, M. R. Lee, & A. E. Fallick. 2006. Crystallography and chemistry of the calcium carbonate polymorph switch in *M. edulis* shells. *European Journal of Mineralogy* 18(5):601–609.
- Dall, W. H. 1902. Synopsis of the family Veneridae and of the North American recent species. *Proceedings of the United States National Museum* 26:335–412.
- Dauphin, Yannicke. 2001. Nanostructures de la nacre des tests de céphalopodes actuels. *Paläontologische Zeitschrift* 75:113–122.
- Dauphin, Yannicke. 2006. Structure and composition of the septal nacreous layer of *Nautilus macromphalus* L. (Mollusca, Cephalopoda). *Zoology* 109:85–95.
- Dauphin, Yannicke. 2008. The nanostructural unity of mollusk shells. *Mineralogical Magazine* 72:243–246.
- Dauphin, Yannicke, & Elise Dufour. 2008. Nanostructures of the aragonitic otolith of cod (*Gadus morhua*). *Micron* 39:891–896.
- Dautzenberg, Philippe. 1929. Mollusques testacés marins de Madagascar. *Faune des Colonies Françaises* (Paris) 3:321–636, pl. 4–7.
- Dillaman, Richard, Stephanie Hequembourg, & Mark Gay. 2005. Early pattern of calcification in the dorsal carapace of the blue crab, *Callinectes sapidus*. *Journal of Morphology* 263:356–374.
- Dillwyn, L. W. 1817. *A Descriptive Catalogue of Recent Shells, Arranged According to the Linnean Method; with Particular Attention to the Synonymy*. 2 vol. John and Arthur Arch. London. xii + p. 1–580 (vol. 1); p. 581–1092 + 29 p. (vol. 2).
- DiMasi, Elaine, & Mehmet Sarikaya. 2004. Synchrotron X-ray microbeam diffraction from abalone shell. *Journal of Materials Research* 19:1471–1476.
- Donovan, Edouard. 1808. *Conchology, Plate VI*. In Abraham Rees, ed., 1802–1820, *The Cyclopædia; or, Universal Dictionary of Arts, Sciences, and Literature*. Plates Vol. V. Natural History. Longman, Hurst, Rees, Orme and Brown, London.
- Dunachie, J. F. 1963. The periostracum of *Mytilus edulis*. *Transactions of the Royal Society of Edinburgh* 65:383–411.
- Dunker, Wilhelm. 1880. Die Gattung *Avicula* in Abbildungen nach der Natur mit Beschreibungen. In H. C. Küster, ed., *Systematisches Conchylien*: Cabinet von Martini und Chemnitz. Vol. 7, Part 3. Bauer und Raspe. Nürnberg. p. 69–84, pl. 25–27.
- Duplat Denis, M. Puisségur, Laurent Bédouet, Marthe Rousseau, H. Boulzaguët, Christian Milet, Daniel Sellos, Alain Van Wormhoudt, & Evelyne Lopez. 2006. Identification of calconectin, a calcium-binding protein specifically expressed by the mantle of *Pinctada margaritifera*. *FEBS Letters* 580:2435–2441.
- England, Jennifer, Maggie Cusack, Paul Dalbeck, & Alberto Pérez-Huerta. 2007. Comparison of the crystallographic structure of semi nacre and nacre by electron backscatter diffraction. *Crystal Growth & Design* 7:307–310.
- Erben, H. K. 1972. Über die Bildung und das Wachstum von Perlmutter. *Biomineralization* 4:15–46.
- Espinosa, H. D., J. E. Rim, François Barthelat, & M. J. Buehler. 2009. Merger of structure and material in nacre and bone: Perspectives on *de novo* biomimetic materials. *Progress in Materials Science* 54:1059–1100.
- Esteban-Delgado, F. J., E. M. Harper, A. G. Checa, & A. B. Rodríguez-Navarro. 2008. Origin and expansion of foliated microstructure in pteriormorph bivalves. *Biological Bulletin* 214(2):153–165.
- Falini, Giuseppe, Shira Albeck, Steve Weiner, & Lia Addadi. 1996. Control of aragonite or calcite polymorphism by mollusk shell macromolecules. *Science* 271:67–69.
- Feng, Q. L., G. Pu, Y. Pei, F. Z. Cui, H. D. Li, & T. N. Kim. 2000. Polymorph and morphology of calcium carbonate crystals induced by proteins extracted from mollusk shell. *Journal of Crystal Growth* 216:459–465.
- Fengzhang Ren, Xindi Wan, Zhanhong Ma, & Juanhua Su. 2009. Study on microstructure and thermodynamics of nacre in mussel shell. *Materials Chemistry and Physics* 114:367–370.
- Field, I. A. 1922. Biology and economic value of the sea mussel *Mytilus edulis*. *Bulletin of the United States Bureau of Fisheries* 38:127–259.
- Freer, Andy, Daniel Greenwood, Peter Chung, C. L. Pannell, & Maggie Cusack. 2010. Aragonite prismatic interface in freshwater mussels *Anodonta anatina* (Linnaeus, 1758) and *Anodonta cygnea* (L. 1758). *Crystal Growth & Design* 10:344–347.
- Fürsich, F. T., T. J. Palmer, & K. L. Goodyear. 1994. Growth and disintegration of bivalve-dominated patch reefs in the Upper Jurassic of southern England. *Palaeontology* 37(1):131–171, 7 pl.
- García-Gasca, S. A., & F. García-Domínguez. 1995. Histología comparada del manto marginal y paleal de las almejas *Megapitaria aurantiaca* (Sowerby, 1831) y *M. squalida* (Sowerby, 1835) (Bivalvia: Veneridae). *Anales de la Escuela Nacional de Ciencias Biológicas de México* 40:173–181.
- Gebauer, Denis, Antje Völkel, & Helmut Cölfen. 2008. Stable prenucleation calcium carbonate clusters. *Science* 322:1819–1822.
- Gilbert, P. U. P. A., R. A. Metzler, Dong Zhou, Andreas Scholl, Andrew Doran, Anthony Young, Martin Kunz, Nobumichi Tamura, & S. N. Coppersmith. 2008. Gradual ordering in red abalone

- nacre. *Journal of the American Chemical Society* 130:17519–17527.
- Gilbert, P. U. P. A., & F. H. Wilt. 2011. Chapter 7, Molecular aspects of biomineralization of the echinoderm endoskeleton. In W. E. G. Müller, ed., *Molecular Biomineralization: Aquatic Organisms Forming Extraordinary Materials*. Springer. New York. p. 199–223.
- Glover, E. A., & J. D. Taylor. 2010. Needles and pins: Acicular crystalline periostracal calcification in venerid bivalves (Bivalvia: Veneridae). *Journal of Molluscan Studies* 76:157–179.
- Gmelin, J. F. 1791–1793. Tome I, Pars VI (Vermes). In C. A. Linnaeus & J. F. Gmelin, 1788–1793, *Systema Naturae per Regna Tria Naturae, Secundum Classes, Ordines, Genera, Species, cum Characteribus, Differentiis, Synonymis, Locis*. 13th edition, Aucta, Reformata. 3 vol. Georg Emanuel Beer. Lipsiae. 2 + p. 3021–3910. Two printings: first by Beer, Lipsiae (Leipzig) has printed date of 1790; second by J. B. Delamollière, Lugduni (Lyon) is dated post 1790, and commonly cited as 1791. Tome I, Pars 7, Index to 1–3, p. 3911–4120 (Lipsiae, 1792; Lugduni, post 1792?). Second printing 1789–1796, by J. B. Delamollière, Lugduni; the two printings are not identical; Tome III (1793) was suppressed by ICZN Opinion 296, 1954, for nomenclatorial purposes.
- Gould, A. A. 1850. Molluscs from the South Pacific (United States Exploring Expedition). *Proceedings of the Boston Society of Natural History* 3:343–348.
- Gould, A.A. 1861. Descriptions of shells collected by the North Pacific exploring expedition. *Proceedings of the Boston Society of Natural History* 8:14–40.
- Gower, L. B. 2008. Biomimetic model systems for investigating the amorphous precursor pathway and its role in biomineralization. *Chemical Reviews* 108:4551–4627.
- Gray, J. E. 1825. Conchological observations, being an attempt to fix the study of conchology on a firm basis. *The Zoological Journal* 1:204–223.
- Gray, J. E. 1833. Some observations on the economy of molluscous animals, and on the structure of their shells. *Philosophical Transactions of the Royal Society of London* 123:771–819.
- Gray, J. E. 1842. *Synopsis of the Contents of the British Museum*. 44th ed. British Museum. London. iv + 308 p.
- Grégoire, C. 1974. On the organic and mineral components of the shells of the Aetheriidae. *Revue de Zoologie Africaine* 88:847–896.
- Gries, Katharina, Roland Kröger, Christian Kübel, Marco Schowalter, Monika Fritz, & Andreas Rosenauer. 2009. Correlation of the orientation of stacked aragonite platelets in nacre and their connection via mineral bridges. *Ultramicroscopy* 109:230–236.
- Habe, Tadashige. 1958. Report on the Mollusca chiefly collected by the S. S. Sōyō-Marū of the Imperial Fisheries Experimental Station on the continental shelf bordering Japan during the years 1922–1930. Part 3. Lamellibranchia (1). Seto Marine Biological Laboratory, Publications 6(3)241–280, pl. 11–13. Published by Kyoto University.
- Habe, Tadashige. 1961. Coloured Illustrations of the Shells of Japan. II. Hoikusha. Osaka. xii + 183 + 42 p. (Appendix), 66 pl. Version 1 of 21.
- Hare, P. E. 1963. Amino acids in the proteins from aragonite and calcite in the shells of *Mytilus californianus*. *Science* 139:216–217.
- Hare, P. E., & P. H. Abelson. 1965. Amino acid composition of some calcified proteins. *Carnegie Institution of Washington Year Book* 64:223–232.
- Harper, E. M. 1997. The molluscan periostracum: An important constraint in bivalve evolution. *Palaeontology* 40:71–98.
- Harper, E. M., A. G. Checa, & A. B. Rodríguez-Navarro. 2009. Organization and mode of secretion of the granular prismatic microstructure of *Entodesma navicula* (Bivalvia: Mollusca) *Acta Zoologica* 90:132–141.
- Hasse, Bernd, Helmut Ehrenberg, J. C. Marxen, Wilhelm Becker, & Matthias Epple. 2000. Calcium carbonate modifications in the mineralized shell of the freshwater snail *Biomphalaria glabrata*. *Chemistry—A European Journal* 6:3679–3685.
- Hedegaard, Claus, & H. R. Wenk. 1998. Microstructure and texture patterns of mollusc shells. *Journal of Molluscan Studies* 64:133–136.
- Hedley, Charles. 1902. Studies on Australian Mollusca. Part VI. Proceedings of the Linnean Society of New South Wales 27:7–29, pl. 1–3.
- Hedley, Charles. 1906. The Mollusca of Mast Head Reef, Capricorn Group, Queensland. Part I. Proceedings of the Linnean Society of New South Wales 31:453–479.
- Holten, H. S. 1802. *Enumeratio Systematica Conchyliorum beat J. H. Chemnitzii quondam Ecclesiae Zebaothi Havniae Pastoris, Plurim Societum Sodialis p. p. quae Publica Auctione Venduntur die 7me Decembris Ano Pres. Copenhagen*. K. H. Scidelini. vi + 88 p.
- Hillman, R. E. 1961. Formation of the periostracum in *Mercenaria mercenaria*. *Science* 134:1754–1755.
- Huang, Zaiwang, & Xiadong Li. 2012. Order-disorder transition of aragonite nanoparticles in nacre. *Physical Review Letters* 109:025501.
- Jackson, D. J., Carmel McDougall, Kathryn Green, Fiona Simpson, Gert Wörheide, & B. M. Degnan. 2006. A rapidly evolving secretome builds and patterns a sea shell. *BMC Biology* 4:40.
- Jackson, D. J., Carmel McDougall, Ben Woodcroft, Patrick Moase, R. A. Rose, Michael Kube, Richard Reinhardt, D. S. Rokhsar, Caroline Montagnani, Caroline Joubert, David Piquemal, & B. M. Degnan. 2010. Parallel evolution of nacre building gene sets in molluscs. *Molecular Biology and Evolution* 27:591–608.
- Jacob, D. E., A. L. Soldati, R. Wirth, J. Huth, U. Wehrmeister, & W. Hofmeister. 2008. Nanostructure, composition and mechanisms of bivalve shell growth. *Geochimica et Cosmochimica Acta* 72:5401–5415.
- Jacob, D. E., R. Wirth, A. L. Soldati, U. Wehrmeister, & A. Schreiber. 2011. Amorphous calcium carbonate in the shells of adult *Unionoida*. *Journal of Structural Biology* 173(2):241–249.
- Jameson, H. L. 1901. On the identity and distribution of the Mother of Pearl Oysters with a revision of the

- subgenus *Margaritifera*. Proceedings of the Zoological Society of London 1: 372–394.
- Jay, J. C. 1857. Report on the shells collected by the Japan Expedition, under the command of Commodore M. C. Perry, U.S.N., together with a list of Japan shells. In F. L. Hawks, ed. Narrative of the Expedition of an American Squadron to the China Seas and Japan: Performed in the years 1852, 1853, and 1854, Under the Command of Commodore M.C. Perry, United States Navy, by Order of the Government of the United States. Vol. 2: With Illustrations. Senate Printer. Washington, D.C. p. 289–297, pl. 1–5.
- Joubert, Caroline, David Piquemal, Benjamin Marie, Laurent Manchon, Fabien Pierrat, Isabelle Zanel-la-Cléon, Nathalie Cochennec-Laureau, Yannick Gueguen, & Caroline Montagnani. 2010 Transcriptome and proteome analysis of *Pinctada margaritifera* calcifying mantle and shell: Focus on biomineralization. BMC Genomics 11:613.
- Kádár, Enikő, & Valentina Costa. 2006. First report on the micro-essential metal concentrations in bivalve shells from deep-sea hydrothermal vents. Journal of Sea Research 56:37–44.
- Kádár, Enikő, Isabel Guerra-Tschuschke, & Antonio Checa. 2008. Post-capture hyperbaric simulations to study the mechanism of shell regeneration of the deep-sea hydrothermal vent mussel *Bathymodiolus azoricus* (Bivalvia: Mytilidae). Journal of Experimental Marine Biology and Ecology 364:80–90.
- Kamhi, S. R. 1963. On the structure of vaterite,  $\text{CaCO}_3$ . Acta Crystallographica 16:770–772.
- Kawaguti, Siro, & N. Ikemoto. 1962. Electron microscopy on the mantle of a bivalve gastropod. Biological Journal of Okayama University 8:1–20.
- Kawakami, K., & Gonpachiro Yasuzumi. 1964. Electron microscope studies on the mantle of the pearl oyster *Pinctada martensii* Dunker. Preliminary report: The fine structure of the periostracum fixed with permanganate. Journal of Electron Microscopy 13:119–123.
- Kessel, Erwin. 1944. Über Periostracum-Bildung. Zeitschrift für Morphologie und Ökologie der Tiere 40:348–360.
- Killian, C. E., R. A. Metzler, Y. U. T. Gong, I. C. Olson, Joanna Aizenberg, Yael Politi, F. H. Wilt, Andreas Scholl, Anthony Young, Andrew Doran, Martin Kunz, Nobumichi Tamura, S. N. Coppersmith, & P. U. P. A. Gilbert. 2009. Mechanism of calcite co-orientation in the sea urchin tooth. Journal of the American Chemical Society 131:18404–18409.
- Kléman, Maurice. 1989. Defects in liquid crystals. Reports on Progress in Physics 52:555–654.
- King, P. P., & W. J. Broderip. 1832. Description of the Cirrhipeda, Conchifera and Mollusca, in a collection formed by the officers of H.M.S. Adventure and Beagle employed between the years 1826 and 1830 in surveying the southern coasts of South America, including the Straits of Magalhaens and the coast of Tierra del Fuego. Zoological Journal 5:332–349.
- Kobayashi, Iwao. 1971. Internal shell microstructure of recent bivalvian molluscs. Science Reports of Niigata University, Series E, Geology and Mineralogy 2:27–50.
- Kobayashi, Shinjiro. 1964a. Studies in shell formation. X. A study of the proteins of the extrapallial fluid in some molluscan species. The Biological Bulletin 126:414–422.
- Kobayashi, Shinjiro. 1964b. Calcification in fish and shellfish. II. A paper electrophoretic study on the acid mucopolysaccharides and PAS-positive materials of the extrapallial fluid in some molluscan species. Bulletin of the Japanese Society of Scientific Fisheries 30:893–907.
- Kono, Makiko, Nakanobu Hayashi, & Tetsuro Samata. 2000. Molecular mechanism of the nacreous layer formation in *Pinctada maxima*. Biochemical and Biophysical Research Communications 269:213–218.
- Kouchinsky, A. V. 1999. Shell microstructures of the Early Cambrian *Anabarella* and *Watsonella* as new evidence on the origin of the Rostroconchia. Lethaia 32:173–180.
- Kudo, Miki, Jun Kameda, Kazuko Saruwatari, Noriaki Ozaki, Keiju Okano, Hiromichi Nagasawa, & Toshihiro Kogure. 2010. Microtexture of larval shell of oyster, *Crassostrea nippona*: A FIB-TEM study. Journal of Structural Biology 169:1–5.
- Lakshminarayanan Rajamani, Emma Ooi Chi-Jin, Xian Jun Loh, R. Manjunatha Kini, & Suresh Valiyaveetil. 2005. Purification and characterization of a vaterite-inducing peptide, pelovaterin, from the eggshells of *Pelodiscus sinensis* (Chinese soft-shelled turtle). Biomacromolecules 6:1429–1437.
- Lamarck, J. B. P. A. de Monet. 1799. Prodrome d'une nouvelle classification des coquilles, comprenant une rédaction appropriée des caractères génériques, et l'établissement d'un grand nombre de genres nouveaux. Memoires de la Société d'Histoire Naturelle de Paris 1:63–91.
- Lamarck, J. B. P. A. de Monet. 1804. Sur un nouvelle espèce de trigone, et sur une nouvelle d'huître, découverts dans le voyage du capitaine Baudin. Muséum Nationale d'Histoire Naturelle, Annales 4:351–359 + pl. 67.
- Lamarck, J. B. P. A. de Monet. 1807. Sur la division des mollusques acéphalés conchylières, et sur un nouveau genre de coquille appartenant à cete division. Annales du Muséum National d'Histoire Naturelle. 10:389–408, pl. 29–32.
- Lamarck, J. B. P. A. de Monet. 1818–1822. Histoire Naturelle des Animaux sans Vertèbres. 1st Edition. 7 vol. Verdrière. Paris. Vol. 5, 612 p. (1818); vol. 6, part 1, 232 p. (1819); vol. 6, part 2 (1822); vol. 7, 711 p. (1822).
- Lamprell, K. L., & T. Whitehead. 1990. Eight new marine bivalves from Australia (Mollusca, Bivalvia). Malacological Society of Australia, Journal 11:33–52.
- Leach, W. E. 1814–1817. The Zoological Miscellany; Being Descriptions of New, or Interesting Animals; Illustrated with Coloured Figures. 3 vol. E. Nodder & Son. London. 144 p., 60 pl. (vol 1, 1814) 154 + 6 p., pl. 61–120 (vol. 2, 1815); 151 p., pl. 121–149 (vol. 3, 1817).
- Levi-Kalisman, Yael, Giuseppe Falini, Lia Afddadi, & Steve Weiner. 2001. Structure of the nacreous organic matrix of a bivalve mollusk shell examined in the

- hydrated state using cryo-TEM. *Journal of Structural Biology* 135:8–17.
- Li, Hanying, Huolin L. Xin, M. E. Kunitake, E. C. Keene, D. A. Muller, & L. A. Stroff. 2011. Calcite prisms from mollusk shells (*Atrina rigida*): Swiss-cheese-like organic–inorganic single-crystal composites. *Advanced Functional Materials* 21:2028–2034.
- Li, Xiaodong, Wei-Che Chang, Yuh J. Chao, Rizhi Wang, & Ming Chang. 2004. Nanoscale structural and mechanical characterization of a natural nanocomposite material: The shell of red abalone. *Nano Letters* 4:613–617.
- Li, Xiaodong, & Zaiwang Huang. 2009. Unveiling the formation mechanism of pseudo-single crystal aragonite platelets in nacre. *Physical Review Letters* 102:075502.
- Li, Xiaodong, Zhi-Hui Xu, & Rizhi Wang. 2006. In situ observation of nanograin rotation and deformation in nacre. *Nano Letters* 6:2301–2304.
- Lightfoot, John. 1786. *A Catalogue of the Portland Museum, Lately the Property of the Duchess Dowager of Portland, Deceased*. Skinner & Co. London. viii + 194 p.
- Lin, Albert Yu-M., Po-Yu Chen, & M. A. Meyers. 2008. The growth of nacre in the abalone shell. *Acta Biomaterialia* 4:131–138.
- Linnaeus, C. A. 1758. *Systema Naturae per Regna Tria Naturae, Secundum Classes, Ordines, Genera, Species, cum Characteribus, Differentiis, Synonymis, Locis*. 10th ed., Reformata, 2 vol. Laurentii Salvii. Holmiae (Stockholm) & Lipsiae (Leipzig). 4 + 823 + 1 errata p. (vol. 1, 1758); 4 + 560 p. (vol. 2, 1759). Vol. 1–2 paged continuously: p. 1–823 (vol. 1), p. 825–1384 (vol. 2). A photographic facsimile of vol. 1, 10th edition, *Regnum Animale*, was published in 1956, by order of the Trustees British Museum (Natural History), printed by Unwin Brothers Ltd., London.
- Linnaeus, C. A. 1766–1768. *Systema Naturae per Regna Tria Naturae, Secundum Classes, Ordines, Genera, Species, cum Characteribus, Differentiis, Synonymis, Locis*. 12th ed., Reformata. 3 vol. Laurentii Salvii. Stockholm. 3 vol., 3 pl. (folded). Vol. 1 in 2 parts: part 1 (p. 1–532) published 1766, part 2 (“Vermes Testacea,” p. 533–1328) published 1767. Vol. 2 includes *Mantissa plantarum, Generum editionis VI, et Specierum editionis II*, published 1767. Vol. 3, *Regnum Lapideum*, 1768.
- Liu, Xiaojun, & Jiale Li. 2013. Formation of the prismatic layer in the freshwater bivalve *Hyriopsis cumingii*: The feedback of crystal growth on organic matrix. *Acta Zoologica* 96:30–36. First published online September 30, 2013; vol. 96(1) published January 2015.
- Lopes-Lima, Manuel, Susana Freitas, Liliana Pereira, Eugenia Gouveia, Mariana Hinzmann, Antonio Checa, & Jorge Machado. 2012. Ionic regulation and shell mineralization in the bivalve *Anodonta cygnea* (swan mussel) following heavy-metal exposure. *Canadian Journal of Zoology* 90:267–283.
- Lorens, R. B., & M. L. Bender. 1980. The impact of solution chemistry on *Mytilus edulis* calcite and aragonite. *Geochimica et Cosmochimica Acta* 44(9):1265–1278.
- Lowenstam, H. A. 1981. Minerals formed by organisms. *Science* 211:1126–1131.
- Lowenstam, H. A., & Stephen Weiner. 1989. *On Biomineralization*. Oxford University Press. New York. 324 p.
- Ma, H. Y., & I.-S. Lee. 2006. Characterization of vaterite in low quality freshwater-cultured pearls. *Materials Science and Engineering C* 26:721–723.
- Ma, Y. R., S. Weiner, & L. Addadi. 2007. Mineral deposition and crystal growth in the continuously forming teeth of sea urchins. *Advanced Functional Materials* 17:2693–2700.
- Mann, Stephen. 1983. Mineralization in biological systems. *Structure and Bonding* 54:125–174.
- Mann, Stephen. 1988. Molecular recognition in biomineralization. *Nature* 332:119–124.
- Marin, Frédéric, Gilles Luquet, Benjamin Marie, & D. Medakovic. 2008. Molluscan shell proteins: Primary structure, origin, and evolution. *Current Topics in Developmental Biology* 80:209–276.
- Markich, S. J., R. A. Jeffree, & P. T. Burke. 2002. Freshwater bivalve shells as archival indicators of metal pollution from a copper-uranium mine in tropical northern Australia. *Environmental Science & Technology* 36(5):821–32.
- Marxen, J. C., Wilhelm Becker, Doreen Finke, Bernd Hasse, & Matthias Epple. 2003. Early mineralization in *Biomphalaria glabrata*: Microscopic and structural results. *Journal of Molluscan Studies* 69:113–121.
- Medakovic, Davorin, M. Hrs-Brenko, S. Popović, & B. Gržeta. 1989. X-ray diffraction study of the first larval shell of *Ostrea edulis*. *Marine Biology* 101:205–209.
- Meek, F. B. 1876. A Report on the Invertebrate Cretaceous and Tertiary Fossils of the Upper Missouri Country. In F. V. Hayden, ed., *Report of the United States Geological Survey of the Territories*. Vol. 9. Government Printing Office. Washington, D.C. lxiv + 629 p., 45 pl.
- Meenakshi, V. R., P. E. Hare, N. Watabe, & K. M. Wilbur. 1969. The chemical composition of the periostracum of the molluscan shell. *Comparative Biochemistry and Physiology* 29:611–620.
- Meldrum, F. C., & S. T. Hyde. 2001. Morphological influence of magnesium and organic additives on the precipitation of calcite. *Journal of Crystal Growth* 231:544–558.
- Metzler, R. A., Mike Abrecht, R. M. Olabisi, Daniel Ariosa, J. J. Christopher, B. H. Frazer, S. N. Coppersmith, & P. U. P. A. Gilbert. 2007. Architecture of columnar nacre, and implications for its formation mechanism. *Physical Review Letters* 98:268102.
- Meyers, M. A., Albert Yu-Min Lin, Po-Yu Chen, & Julie Muyco. 2008. Mechanical strength of abalone nacre: Role of the soft organic layer. *Journal of the Mechanical Behavior of Biomedical Materials* 1:76–85.
- Misogianes, M. J., & N. D. Chasteen. 1979. A chemical and spectral characterization of the extrapallial fluid of *Mytilus edulis*. *Analytical Biochemistry* 100:324–334

- Montagu, George. 1803. Testacea Britannica or Natural History of British Shells, Marine, Land, and Fresh-Water, Including the Most Minute: Systematically Arranged and Embellished with Figures. 2 vol. J. White. London. xxxvii + 291 p. (vol. 1); 293–606 p. (vol. 2).
- Moor, Beatrice. 1983 Organogenesis. In N. H. Verdonk, J. A. M van den Biggelaar, & A. S. Tompa, eds., The Mollusca: Development, Vol. 3. Academic Press. New York. p. 123–177.
- Morton, Brian. 1986. The biology and functional morphology of the coral-boring *Jouannetia cumingii* (Bivalvia: Pholadacea). Journal of Zoology, London (A) 208(3):339–366, 2 pl.
- Morton, Brian, Melita Peharda, & Mirela Petrić. 2011. Functional morphology of *Rocellaria dubia* (Bivalvia: Gastrochaenidae) with new interpretations of crypt formation and adventitious tube construction, and a discussion of evolution within the family. Biological Journal of the Linnean Society 104(4):786–804.
- Mount, A. S., A. P. Wheeler, R. P. Paradkar, & D. Snider. 2004. Haemocyte-mediated shell mineralization in the Eastern oyster. Science 304:297–300.
- Müller, O. F. 1773–1774. Vermium Terrestrium et Fluviatilium, seu Animalium Infusorium, Helminthicorum et Testaceorum, non Marinarum, Succincta Historia, & c. Heineck & Faber. Havniae & Lipsiae. 2 vol. [xxx] + 135 p. (vol. 1, 1773); 72 + [viii] p. (vol. 1, 1774); xxxvi + 214 + [x] (vol. 2, 1774).
- Mullins, W. W. 1956. Two-dimensional motion of idealized grain boundaries. Journal of Applied Physics 27:900–904.
- Mutvei, Harry. 1978. Ultrastructural characteristics of the nacre in some gastropods. Zoologica Scripta 7:287–296.
- Nakahara, Hiroshi. 1991. Nacre formation in bivalve and gastropod mollusks. In Shoichi Suga & Hiroshi Nakahara, eds., Mechanisms and Phylogeny of Mineralization in Biological Systems. Springer. Berlin. p. 343–350.
- Nakahara, Hiroshi, & Gerrit Bevelander. 1971. The formation and growth of the prismatic layer of *Pinctada radiata*. Calcified Tissue Research 7:31–45.
- Nassif, Nadine, Nadine Pinna, Nicole Gehrke, Markus Antonietti, Christian Jäger, & Helmut Cölfen. 2005. Amorphous layer around aragonite platelets in nacre. Proceedings of the National Academy of Sciences of the United States of America 102:12653–12655.
- Neff, J. M. 1972a. Ultrastructural studies on periostracum formation in the hard shelled clam *Mercenaria mercenaria* (L). Tissue & Cell 4:311–326.
- Neff, J. M. 1972b. Ultrastructure of the outer epithelium of the mantle in the clam *Mercenaria mercenaria* in relation to calcification of the shell. Tissue & Cell 4:591–600.
- Nehrke, Gernot, Harald Pognier, Dorothee Wilhelms-Dick, Thomas Brey, & Doris Abele. 2012. Coexistence of three calcium carbonate polymorphs in the shell of the Antarctic clam *Laternula elliptica*. Geochemistry, Geophysics, Geosystems 13:Q05014. DOI:10.1029/2011GC003996.
- Neumann, John von. 1952. Discussion: Shape of metal grains. In C. Herring, ed., Metal Interfaces. American Society of Metals. Cleveland, Ohio. p. 108–110.
- Neville, A. C. 1993. Biology of Fibrous Composites. Cambridge University Press. Cambridge, UK. 226 p.
- Nouet Julius, Alain Baronnet, & Lauren Howard. 2012. Crystallization in organo-mineral micro-domains in the crossed-lamellar layer of *Nerita undata* (Gastropoda, Neritopsina). Micron 43:456–462.
- Nudelman, Fabio, Hong H. Chen, H. A. Goldberg, Steve Weiner, & Lia Addadi. 2007. Lessons from biomineralization: Comparing the growth strategies of mollusc shell prismatic and nacreous layers in *Atrina rigida*. Faraday Discussions 136:9–25.
- Ockelmann, K. W. 1958. The zoology of east Greenland. 4. Marine Lamellibranchiata. Meddelelser om Grønland 122:1–256.
- Ockelmann, K.W. 1983. Descriptions of mytilid species and definition of the Dacrydiinae n. subfam. (Mytilacea—Bivalvia). Ophelia 22:81–123.
- Okumura, Taiga, Michio Suzuki, Hiromichi Nagasawa, & Toshihiro Kogure. 2010. Characteristics of biogenic calcite in the prismatic layer of a pearl oyster, *Pinctada fucata*. Micron 41:821–826.
- Okumura, Taiga, Michio Suzuki, Hiromichi Nagasawa, & Toshihiro Kogure. 2012. Microstructural variation of biogenic calcite with intracrystalline organic macromolecules. Crystal Growth & Design 12:224–230.
- Okumura, Taiga, M. Suzuki, Michio Suzuki, Hiromichi Nagasawa, & Toshihiro Kogure. 2013. Microstructural control of calcite via incorporation of intracrystalline organic molecules in shells. Journal of Crystal Growth 381:114–120.
- Oliver, P. G., C. F. Rodrigues, & M. R. Cunha. 2011. Chemosymbiotic bivalves from the mud volcanoes of the Gulf of Cadiz, NE Atlantic, with descriptions of new species of Solemyidae, Lucinidae and Vesicommyidae. Zookeys 113:1–38.
- Olson, I. C., A. Z. Blonsky, Nobumichi Tamura, Martin Kunz, Boaz Pokroy, C. P. Romao, M. A. White, & P. U. P. A. Gilbert. 2013. Crystal nucleation and near-epitaxial growth in nacre. Journal of Structural Biology 184:454–463.
- Olson, I. C., Reinhard Kozdon, J. W. Valley, & P. U. P. A. Gilbert. 2012. Mollusk shell nacre ultrastructure correlates with environmental temperature and pressure. Journal of the American Chemical Society 134:7351–7358.
- Olson, I. C., R. A. Metzler, Nobumichi Tamura, Martin Kunz, C. E. Killian, & P. U. P. A. Gilbert. 2013. Crystal lattice tilting in prismatic calcite. Journal of Structural Biology 183:180–190.
- Osuna-Mascaró, A. J., Teresa Cruz-Bustos, Frédéric Marin, & A. G. Checa. 2015. Ultrastructure of the interlamellar membranes of the nacre of the bivalve *Pteria hirsundo*, determined by immunolabelling. PLoS ONE 10:e0122934.
- Paillard, Christine, & M. Le Pennec. 1993. Ultrastructural studies of the mantle and the periostracal lamina in the manila clam, *Ruditapes philippinarum*. Tissue & Cell 25:183–194.
- Pereira-Mourtiés, Lucilia, M.-J. Almeida, Cristina Ribeiro, Jean Peduzzi, Michel Barthélemy, Christian

- Milet, & Evelyne Lopez. 2002. Soluble silk-like organic matrix in the nacreous layer of the bivalve *Pinctada maxima*: A new insight in the biomineralization field. *European Journal of Biochemistry* 269:4994–5003.
- Petit, Henri. 1981. Survol de la minéralisation chez les Unionidae. *Haliotis* 11:181–195.
- Petit, Henri, W. L. Davis, & R. G. Jones. 1978. Morphological studies on the mantle of the fresh-water mussel *Amblema* (Unionidae): Scanning electron microscopy. *Tissue & Cell* 10:619–627.
- Petit, Henri, W. L. Davis, & R. G. Jones. 1979. Morphological studies on the periostracum of the fresh-water mussel *Amblema* (Unionidae): Light microscopy, transmission electron microscopy, and scanning electron microscopy. *Tissue & Cell* 11:633–642.
- Petit, Henri, W. L. Davis, & R. G. Jones. 1980. A scanning electron microscopy study of the inorganic and organic matrices comprising the mature shell of *Amblema*, a fresh-water mollusc. *Tissue & Cell* 12:581–593.
- Petit, Henri, W. L. Davis, R. G. Jones, & H. K. Hagler. 1980. Morphological studies on the calcification process in the fresh-water mussel *Amblema*. *Tissue & Cell* 12:13–28.
- Pfeiffer, Carl. 1825. *Naturgeschichte Deutscher Land und Süßwasser Mollusken*. Zweite Abtheilung. Landes-Industrie-Comptoir. Weimar. vi + 40 p., 8 pl.
- Philippi, R. A. 1844. Nachtrag zum zweiten Bande der *Enumeratio Molluscorum Siciliae*. *Zeitschrift für Malakozoologie* 1:100–112.
- Pichon, B. P., P. H. H. Bomans, P. M. Frederik, & N. A. J. M. Sommerdijk. 2008. A quasi-time resolved cryo-TEM study of the nucleation of calcium carbonate under Langmuir monolayers. *Journal of the American Chemical Society* 130:4034–4040.
- Pietrzak, J. E., J. M. Bates, & R. M. Scott. 1973. Constituents of unionid extrapallial fluid. I. Electrophoretic and immunological studies of protein components. *The Biological Bulletin* 144:391–399.
- Pokroy, Boaz, M. Kapon, F. Marin, N. Adir, & E. Zolotoyabko. 2007. Protein-induced, previously unidentified twin form of calcite. *Proceedings of the National Academy of Sciences of the United States of America* 104:7337–7341.
- Politi, Yael, Talmon Arad, Eugenia Klein, Steve Weiner, & Lia Addadi. 2004. Sea urchin spine calcite forms via a transient amorphous calcium carbonate phase. *Science* 306:1161–1164.
- Politi, Yael, Y. Levi-Kalishman, S. Raz, F. Wilt, L. Addadi, S. Weiner, & I. Sagi. 2006. Structural characterization of the transient calcium carbonate amorphous precursor phase in sea urchin embryos. *Advanced Functional Materials* 16:1289–1298.
- Politi, Yael, R. A. Metzler, Mike Abrecht, Benjamin Gilbert, F. H. Wilt, Irit Sagi, Lia Addadi, Steve Weiner, & P. U. P. A. Gilbert. 2008. Transformation mechanism of amorphous calcium carbonate into calcite in the sea urchin larval spicule. *Proceedings of the National Academy of Sciences of the United States of America* 105:17362–17366.
- Pouget, E. M., P. H. H. Bomans, J. A. C. M. Goss, P. M. Frederik, Gijsbertus de With, & N. A. J. M. Sommerdijk. 2009. The initial stages of template-controlled CaCO<sub>3</sub> formation revealed by cryo-TEM. *Science* 323:1455–1458.
- Preston, H. B. 1910. Additions to the non-marine molluscan fauna of British and German East Africa and Lake Abert Edward. *Journal of Natural History (series 8)* 6(35):526–536.
- Prezant, R. S. 1979. Shell spinules of the bivalve *Lyonisia hyalina* (Bivalvia: Anomalodesmata). *Nautilus* 93:93–95.
- Przenioslo, Radosław, J. Stolarski, M. Mazur, & M. Brunelli. 2008. Hierarchically structured scleractinian coral biocrystals. *Journal of Structural Biology* 161:74–82.
- Radha, A. V., T. Z. Forbes, C. E. Killian, P. U. P. A. Gilbert, & Alexandra Navrotsky. 2010. Transformation and crystallization energetics of synthetic and biogenic amorphous calcium carbonate. *Proceedings of the National Academy of Sciences of the United States of America* 107:16438–16443.
- Raith, Andrea, W. T. Perkins, N. J. G. Pearce, & T. E. Jeffries. 1996. Environmental monitoring on shellfish using UV laser ablation ICP-MS. *Fresenius' Journal of Analytical Chemistry* 355:789–792.
- Raz, Sefi, P. Hamilton, F. Wilt, Steve Weiner, & Lia Addadi. 2003. The transient phase of amorphous calcium carbonate in sea urchin larval spicules: the involvement of proteins and magnesium ions in its formation and stabilization. *Advanced Functional Materials* 13:480–486.
- Raz, Sefi, O. Testeniére, A. Hecker, Steve Weiner, & G. Luquet. 2002. Stable amorphous calcium carbonate is the main component of the calcium storage structures of the crustacean *Orchestia cavimana*. *The Biological Bulletin* 203:269–274.
- Reeve, L. A. 1842. Monograph of *Crassatella*, a genus of Acepulous Mollusks (Family Mactracea). *Proceedings of the Zoological Society of London* 10:42–46.
- Reeve, L. A. 1844–1845. Monograph of the genus *Cardium*. In L. A. Reeve, ed., *Conchologia Iconica; or, Illustrations of the Shells of Molluscos Animals*. Vol. 2. L. A. Reeve & Co. London. 22 pl. Unnumbered pages contain captions for the plates; plates published separately: pl. 1–4 (October, 1844), pl. 5–8 (November, 1844), pl. 9–12 (December, 1844), pl. 13–16 (January, 1845), pl. 17–22 (March 1845).
- Reeve, L. A. 1860–1863. Monograph of the genus *Anatina*. In L. A. Reeve, ed., *Conchologia Iconica; or, Illustrations of the Shells of Molluscos Animals*. Vol. 14. L. A. Reeve & Co. London. 20 [unnumbered] p., 4 pl. + 1 p. index + erratum. Plate 2 published December, 1860; pl. 1, 3–4 published February, 1863; unnumbered pages are captions for the plates.
- Richardson, C. A., D. J. Crisp, & N. W. Runham. 1981. Factors influencing shell deposition during a tidal cycle in the intertidal bivalve *Cerastoderma edule*. *Journal of the Marine Biological Association of the United Kingdom* 61:465–476.
- Richardson, C. A., N. W. Runham, & D. J. Crisp. 1981. A histological and ultrastructural study of the cells of the mantle edge of a marine bivalve, *Cerastoderma edule*. *Tissue & Cell* 13:715–730.

- Röding, P. F. 1798. Museum Boltenianum sive Catalogus Cimeliorum e Tribus Regnis Naturae quae olim Collegerat Joa. Fried. Bolten M. D. p. d. Pars Secunda Continens Conchylia sive Testacea Univalvia, Bivalvia et Multivalvia. Johan. Christi. Trappii, Hamburgi. viii + 199 p. In German.
- Rodríguez-Navarro, A. B., Antonio Checa, M.-G. Willinger, Raúl Bolmaro, & Jan Bonarski. 2012. Crystallographic relationships in the crossed lamellar microstructure of the shell of the gastropod *Conus marmoreus*. *Acta Biomaterialia* 8:830–835.
- Rousseau, Marthe, Evelyne Lopez, Phillipe Stempflié, Marcel Brendlé, Loïc Franke, Alain Guette, Roger Naslain, & Xavier Bourrat. 2005. Multiscale structure of sheet nacre. *Biomaterials* 26:6254–6262.
- Salas, Carmen, P. Marina, A. G. Checa, & J. L. Rueda. 2012. The periostracum of *Digitaria digitaria* (Bivalvia: Astartidae): Formation and structure. *Journal of Molluscan Studies* 78:34–43.
- Saleuddin, A. S. M. 1965. The mode of life and functional anatomy of *Astarte* spp. (Eulamellibranchia). *Journal of Molluscan Studies* 36:229–257.
- Saleuddin, A. S. M. 1974. An electron microscopic study of the formation and structure of the periostracum in *Astarte* (Bivalvia). *Canadian Journal of Zoology* 52:1463–1471.
- Saleuddin, A. S. M., & H. P. Petit. 1983. The mode of formation and the structure of the periostracum. In A. S. M. Saleuddin & K. M. Wilbur, eds., *The Mollusca, Physiology, Vol. 4, Part 1*. Academic Press. New York. p. 199–234.
- Sars, G. O. 1872. On some remarkable forms of animal life from the great deeps off the Norwegian coast. I. Partly from the posthumous manuscripts of the late Professor Dr. Michael Sars. Christiania. Brøgger & Christie. viii + 82 p., 6 pl.
- Saruwatari, Kazuko, Tomoyuki Matsui, Hiroki Mukai, Hiromichi Nagasawa, & Toshihiro Kogure. 2009. Nucleation and growth of aragonite crystals at the growth front of nacre in pearl oyster, *Pinctada fucata*. *Biomaterials* 30:3028–3034.
- Savazzi, Enrico, & Takenori Sasaki. 2013. Observations on land-snail shells in near-ultraviolet, visible and near-infrared radiation. *Journal of Molluscan Studies* 79:95–111.
- Say, Thomas. 1818. Description of a new genus of fresh water bivalve shells. *Journal of the Academy of Natural Sciences of Philadelphia* 1(2):459–460.
- Say, Thomas. 1822. An account of some of the marine shells of the United States. *Academy of Natural Sciences of Philadelphia, Journal* (series 1) 2(2):221–325. Published in several parts: p. 221–224 (June), p. 225–248 (July), p. 257–276 (August); p. 302–320 (September); p. 321–325 (November).
- Schäffer, T. E., Cristian Ionescu-Zanetti, Roger Proksch, Monika Fritz, D. A. Walters, Nils Almquist, C. M. Zaremba, A. M. Belcher, B. L. Smith, G. D. Stucky, D. E. Morse, & P. K. Hansma. 1997. Does abalone nacre form by heteroepitaxial nucleation or by growth through mineral bridges? *Chemistry of Materials* 9:1731–1740.
- Schmidt, W. J. 1922. Über den Aufbau der Schale von *Nucula*. *Archiv für Mikroskopische Anatomie* 96:171–181.
- Schmidt, W. J. 1924a. Bau und bildung der Perlmuttermasse. *Zoologische Jahrbücher, Abteilung für Anatomie und Ontogenie* 96:1–148.
- Schmidt, W. J. 1924b. Die Bausteine des Tierkörpers in polarisiertem Lichte. Verlag F. Cohen. Bonn. xi + 528 p.
- Schneider, J. A., & J. G. Carter. 2001. Evolution and phylogenetic significance of cardioidean shell microstructure (Mollusca, Bivalvia). *Journal of Paleontology* 75(3):607–643.
- Seki, Haruo. 1934. Description of *Ostrea nippona* n. sp. with remarks on *Ostrea circumpecta* Pilsbry. *Venus* (Japanese Journal of Malacology) 5:275–284.
- Sethmann, Ingo, Ruth Hinrichs, Gert Wöhrheide, & Andrew Putnis. 2006. Nano-cluster composite structure of calcitic sponge spicules: A case study of basic characteristics of biominerals. *Journal of Inorganic Biochemistry* 100:88–96.
- Seto, Jong, Yurong Ma, S. A. Davis, Fiona Meldrum, Aurelien Gourrier, Yi-yeou Kim, Uwe Schilde, Michael Sztucki, Manfred Burghammer, Sergey Maltsev, Christian Jäger, & Helmut Cölfen. 2012. Structure-property relationships of a biological mesocrystal in the adult sea urchin spine. *Proceedings of the National Academy of Sciences of the United States of America* 109:3699–3704.
- Smith, E. A. 1874. Mollusca. In John Richardson & J. E. Gray, eds., *The Zoology of the Voyage of H.M.S. Terror, under the Command of Captain Sir James Clark Ross, During the Years 1839 to 1843*. By the Authority of the Lords Commissioners of the Admiralty. Vol. 2, Reptiles, Fishes, Crustacea, Insects, Mollusca. E. W. Janson. London. p. 1–7, pl. 1–4. Larger work published 1844–1875; each section paginated separately and with plates numbered separately.
- Song Fan & Bai Yilong. 2001. Mineral bridges in nacre and its effects. *Acta Mechanica Sinica* 17:251–257.
- Song, Fan, & Y. L. Bai. 2003. Effects of nanostructures on the fracture strength of the interfaces in nacre. *Journal of Materials Research* 18:1741–1744.
- Song, Fan, A. K. Soh, & Y. L. Bai. 2004. Structural and mechanical properties of the organic matrix layers of nacre. *Biomaterials* 24:3623–3631.
- Song, Fan, X. H. Zhang, & Y. L. Bai. 2002. Microstructure and characteristics in the organic matrix layers of nacre. *Journal of Materials Research* 17:1567–1570.
- Song, Rui-Qi, & Helmut Cölfen. 2010. Mesocrystal-ordered nanoparticle superstructures. *Advanced Materials* 22:1301–1330.
- Sowerby, G. B., I., & G. B. Sowerby II. 1832–1841. *The Conchological Illustrations; or coloured Figures of All the Hitherto Unfigured Recent Shells*. Sowerby. London. 200 pl. in 200 parts, each with its own text, paginated separately, and usually also reissued in 1841.
- Sowerby, G. B. II. 1849. Monograph of the Genus *Triumphalia*. In G. B. Sowerby II, ed., *Thesaurus Conchyliorum, Vol. 2*. Sowerby. London. p. 500–503, pl. 106.
- Sowerby, James, & J. de C. Sowerby. 1812–1846. *The Mineral Conchology of Great Britain; or Coloured Figures and Description of those Remains of Testaceous Animals or Shells Which Have Been Preserved*

- at Various Times and Depths in the Earth. 7 vol. B. Meredith. London. 1353 p., 648 pl. Published in 113 parts in 7 volumes. James Sowerby published parts 1–66, 1812–1822; his son, James de Carle Sowerby, completed parts 67–113, 1823–1846.
- Spann, Nicole, E. M. Harper, & D. C. Aldridge. 2010. The unusual mineral vaterite in shells of the freshwater bivalve *Corbicula fluminea* from the UK. *Naturwissenschaften* 97:743–751.
- Stanley, S. M. 2006. Influence of seawater chemistry on biomineralization throughout phanerozoic time: Paleontological and experimental evidence. *Palaeogeography, Palaeoclimatology, Palaeoecology* 232:214–236.
- Stanley, S. M., & L. A. Hardie. 1998. Secular oscillations in the carbonate mineralogy of reef-building and sediment-producing organisms driven by tectonically forced shifts in seawater chemistry. *Palaeogeography, Palaeoclimatology, Palaeoecology* 144:3–19.
- Stenzel, H. B. 1964. Oysters: Composition of the larval shell. *Science* 145:155–156.
- Su, Xiao-wei, A. M. Belcher, C. M. Zarella, D. E. Morse, G. D. Stucky, & A. H. Heuer. 2002. Structural and microstructural characterization of the growth lines and prismatic microarchitecture in red abalone shell and the microstructures of abalone “flat pearls.” *Chemistry of Materials* 14:3106–3117.
- Swainson, William. 1822. *Zoological Illustrations, or, Original Figures and Descriptions of New, Rare, or Interesting Animals, Selected Chiefly from the Classes of Ornithology, Entomology, and Conchology, and Arranged on the Principles of Cuvier and Other Modern Zoologists*. Vol. 2. Baldwin, Cradock, and Joe & W. Wood. London & Strand. pl. 84–134.
- Taylor, J. D., E. A. Glover, & C. J. R. Braithwaite. 1999. Bivalves with ‘concrete overcoats,’ *Granicorium* and *Samarangia*. *Acta Zoologica* 80:285–300.
- Taylor, J. D., E. A. Glover, M. Peharda, G. Bigatti, & A. Ball. 2004. Extraordinary flexible shell sculpture: the structure and formation of calcified periostracal lamellae in *Lucina pensylvanica* (Bivalvia: Lucinidae). *Malacologia* 46:277–294.
- Taylor, J. D., E. A. Glover, & S. T. Williams. 2005. Another bloody bivalve: Anatomy and relationships of *Eucrasatella donacina* from south western Australia (Mollusca: Bivalvia: Crassatellidae). *In* F. E. Wells, D. I. Walker, & G. E. Kendrick, eds., *The Marine Flora and Fauna of Esperance*. West Australian Museum. Perth. p. 261–288.
- Tevesz, M. J., & J. G. Carter. 1980. Environmental relationships of shell form and structure of unionacian bivalves. *In* D. C. Rhoads & R. A. Lutz, eds., *Skeletal Growth of Aquatic Organisms*. Plenum. New York. p. 295–322.
- Towe, K. M., & H. A. Lowenstam. 1967. Ultrastructure and development of iron mineralization in the radular teeth of *Cryptochiton stelleri* (Mollusca). *Journal of Ultrastructural Research* 17:1–13.
- Tryon, G. W. 1861. Synopsis of the Recent species of Gastrochaenidae, a family of Acepalous Mollusca. *Proceedings of the Academy of Natural Sciences of Philadelphia* 13:465–494.
- Turner, R. D. 1969. Superfamily Pholadacea. *In* R. C. Moore & Curt Teichert, eds., *Treatise on Invertebrate Paleontology*, Part N, Bivalvia, Mollusca 6, Vol. 2. The Geological Society of America & The University of Kansas Press. Boulder, Colorado & Lawrence, Kansas. p. 702–742.
- Tsuji, Tadashi. 1960. Studies on the mechanism of shell and pearl formation in Mollusca. *Journal of the Faculty of Fisheries, Prefectural University of Mie* 5:1–70.
- Ubukata, Takao. 1994. Architectural constraints of the morphogenesis of prismatic structures in Bivalvia. *Palaeontology* 37:241–261.
- Vecht, A., & T. G. Ireland. 2000. The role of vaterite and aragonite in the formation of pseudo-biogenic carbonate structures: Implications for Martian exobiology. *Geochimica et Cosmochimica Acta* 64:2719–2725.
- Velázquez-Castillo, R. R., Jose Reyes-Gasga, D. I. García-Gutiérrez, & M. José-Yacamán. 2006. Crystal structure characterization of nautilus shell at different length scales. *Biomaterials* 27:4508–4517.
- Wada, Kôji. 1960. Crystal growth of the inner shell surface of *Pinctada martensii* (Dunker) I. *Journal of Electron Microscopy (Tokyo)* 9:21–23.
- Wada, Kôji. 1961. Crystal growth of molluscan shells. *Bulletin of the National Pearl Research Laboratory of Japan* 7:703–828.
- Wada, Kôji. 1968. Electron microscopic observations of the formation of the periostracum of *Pinctada fucata*. *Bulletin of the National Pearl Research Laboratory* 13:1540–1560.
- Wada, Kôji. 1972. Nucleation and growth of aragonite crystals in the nacre of some bivalve molluscs. *Biomineralization* 6:141–159.
- Wada, Kôji, & T. Fujinuki. 1976. Biomineralization in bivalve molluscs with emphasis on the chemical composition of the extrapallial fluid. *In* Norimitsu Watabe & K. M. Wilbur, eds., *Mechanisms of Mineralization in the Invertebrates and Plants*. University of South Carolina Press. Columbia, South Carolina. p. 175–190.
- Wade, Bruce. 1926. *The fauna of the Ripley Formation on Coon Creek, Tennessee*. United States Geological Survey Professional Paper 137:1–272, 72 pl.
- Waite, H. J., A. S. M. Saleuddin, & S. O. Andersen. 1979. Periostracin: A soluble precursor of sclerotized periostracum in *Mytilus edulis* L. *Journal of Comparative Physiology* 130:301–307.
- Waller, T. R. 1980. Scanning electron microscopy of shell and mantle in the order Arcoida (Mollusca: Bivalvia). *Smithsonian Contributions to Zoology* 313:1–58.
- Waller, T. R. 1981. Functional morphology and development of veliger larvae of the European oyster, *Ostrea edulis* Linné. *Smithsonian Contributions to Zoology* 328:1–70.
- Waller, T. R. 1983. Dahllite in the periostracum of *Litobphaga nigra* (Mollusca: Bivalvia) and its taxonomic and functional implications. *American Malacological Bulletin* 1:101.
- Wang, Jianwei, & Udo Becker. 2009. Structure and carbonate orientation of vaterite (CaCO<sub>3</sub>). *American Mineralogist* 94:380–386.

- Wang, Sheng-nan, Xiao-Hui Yan, Rizhi Wang, Da-Hui Yu, & Xiao-Xiang Wang. 2013. A microstructural study of individual nacre tablet of *Pinctada maxima*. *Journal of Structural Biology* 183:404–411.
- Watabe, Norimitsu. 1984. Shell. In J. Bereiter-Hahn, A. G. Matolsty, & K. S. Richards, eds., *Biology of the Integument: Invertebrates*. Vol. 1. Springer-Verlag Berlin. Heidelberg. p. 448–485.
- Watabe, Norimitsu. 1988. Shell structure. In E. R. Trueman & M. R. Clarke, eds., *The Mollusca*, Vol. 11, Form and Function. Academic Press. New York. p. 69–104.
- Wehrmeister, Ursula, D. E. Jacob, A. L. Soldati, T. Häger, & W. Hofmeister. 2007. Vaterite in freshwater cultured pearls from China and Japan. *The Journal of Gemmology* 31:269–276.
- Weiner, Steve, & Lia Addadi. 1997. Design strategies in mineralized biological materials. *Journal of Materials Chemistry* 7:689–702.
- Weiner, Steve, & Lia Addadi. 2011. Crystallization pathways in biomineralization. *Annual Review of Materials Research* 41:21–40.
- Weiner, Steve, Julia Mahamid, Yael Politi, Yurong Ma, & Lia Addadi. 2009. Overview of the amorphous precursor phase strategy in biomineralization. *Frontiers of Materials Science in China* 3:104–108.
- Weiner, Steve, & Wolfie Traub. 1980. X-ray diffraction study of the insoluble organic matrix of mollusk shells. *FEBS Letters* 111:311–316.
- Weiner, Steve, & Wolfie Traub. 1981. Structural aspects of recognition and assembly. In M. Balaban, J. L. Sussman, Wolfie Traub, & A. Yonath, eds., *Biological Macromolecules*, Vol. 1. Balaban ISS. Rehovot & Philadelphia. p. 467–482.
- Weiner, Steve, & Wolfie Traub. 1984. Macromolecules in mollusk shells and their functions in biomineralization. *Philosophical Transactions of the Royal Society of London (series B)* 304:425–434.
- Weiner, Steve, Wolfie Traub, & H. A. Lowenstam. 1983. Organic matrix in calcified exoskeletons. In P. Westbroek & E. W. de Jong, eds., *Biomineralization and Biological Metal Accumulation*. Reidel Publishing Company. Dordrecht. p. 205–224.
- Weiss, I. M., & Veronika Schönitzer. 2006. The distribution of chitin in larval shells of the bivalve mollusk *Mytilus galloprovincialis*. *Journal of Structural Biology* 153:264–277.
- Weiss, I. M., Noreen Tuross, Lia Addadi, & Steve Weiner. 2002. Mollusk larval shell formation: Amorphous calcium carbonate is a precursor for aragonite. *Journal of Experimental Zoology* 293:478–491.
- Wilbur, K. M. 1964. Shell formation and regeneration. In K. M. Wilbur & C. M. Yonge, eds., *Physiology of Mollusca*, Vol. 1. Academic Press. New York. p. 243–282.
- Wilbur, K. M., & A. S. M. Saleuddin. 1983. Shell formation. In A. S. M. Saleuddin & K. M. Wilbur, eds., *The Mollusca*, Vol. 4, Physiology, Part 1. Academic Press. New York. p. 235–287.
- Wilbur, K. M., & K. Simkiss. 1968. Calcified shells. In M. Florkin & E. H. Stotz, eds., *Comprehensive Biochemistry*, Vol. 26A. Elsevier. New York. p. 229–295.
- Wilt, F. H. 2002. Biomineralization of the spicules of sea urchin embryos. *Zoological Science* 19:253–261.
- Winckworth, R. A. 1930. Notes on nomenclature. *Proceedings of the Malacological Society of London* 19(1):14–16.
- Wise, S. W. 1970. Microarchitecture and mode of formation of nacre (mother of pearl) in pelecypods, gastropods and cephalopods. *Eclogae Geologicae Helveticae* 63:775–797.
- Wolf, S. E., Ingo Lieberwirth, Filipe Natalio, J. F. Bardeau, Nicolas Delorme, Franziska Emmerling, Raul Barrea, Michael Kappl, & Frédéric Marin. 2012. Merging models of biomineralisation with concepts of nonclassical crystallisation: Is a liquid amorphous precursor involved in the formation of the prismatic layer of the Mediterranean fan mussel *Pinna nobilis*? *Faraday Discussions* 159:433–448.
- Yonge, C. M.. 1946. On the habits and adaptations of *Aloidis (Corbula) gibba*. *Marine Biological Association of the United Kingdom, Journal* 26(3):358–376.
- Yonge, C. M. 1957. Mantle fusion in the Lamelli-branchia. *Publicazione della Stazione Zoologica di Napoli* 29:151–171.
- Zhang, Gangsheng, & Xiaodong Li. 2012. Uncovering aragonite nanoparticle self-assembly in nacre: A natural armor. *Crystal Growth & Design* 12:4306–4310.
- Ziegler, Andreas. 1994. Ultrastructure and electron spectroscopic diffraction analysis of the sternal calcium deposits of *Porcellio scaber* Latr. (Isopoda, Crustacea). *Journal of Structural Biology* 112:110–116.
- Ziegler, Andreas, Helge Fabritius, & Monica Hagedorn. 2005. Microscopical and functional aspects of calcium-transport and deposition in terrestrial isopods. *Micron* 36:137–153.
- Zieritz, Alexandra, A. G. Checa, D. C. Aldridge, & E. M. Harper. 2011. Variability, function and phylogenetic significance of periostracal microprojections in unionid bivalves (Mollusca). *Journal of Zoological Systematics and Evolutionary Research* 49:6–15.